UNIVERSITÀ DEGLI STUDI DI MILANO

Facoltà di Scienze e Tecnologie
Laurea Magistrale in Fisica

Optimal control for long-range interacting quantum systems in the spin-wave approximation

Tesi di Laurea Magistrale di:
Pietro Torta
Matricola n° 898409

Relatore interno:
Prof. Sergio Caracciolo

Relatore esterno:
Prof. Alessandro Silva

Correlatore esterno:
Prof. Andrea Gambassi

Anno Accademico 2018/2019

Codice PACS
03.65.Sq
05.30.-d
02.30.Yy

Outline

My thesis is in the context of quantum optimal control, applied to quantum many-body systems. In particular, we consider quantum spin systems with long-range interactions.

The problem of quantum optimal control can be formulated in a concise way: consider a quantum system (few- or many-body) with Hamiltonian H, in an initial state $|\psi_0\rangle$, and suppose that we want to evolve it to the target state $|\psi_{\text{tar}}\rangle$. In order to do so, we couple the system to one or more time-dependent external fields $\Gamma_j(t)$, which enter in the Hamiltonian as an interaction term: $H'(t) = H + V\big(\{\Gamma_j(t)\}\big)$. The goal is to find the functional form of the control fields, so that the system evolves to the target state $|\psi_{\text{tar}}\rangle$ at some finite time $t = T$, or asymptotically as $t \to \infty$.

In most cases it is not feasible to exactly reach the target state, so the problem is recast into the extremization of a figure of merit $\mathcal{M}$, encoding some relevant information about the target state.

The ability to prepare quantum systems in a desired state is of primary importance for many tasks, such as to realize quantum gates, perform quantum information or communication protocols, or to control the initial condition of an experiment.

Recent years have witnessed a formidable progress in the experimental realization of artificial controllable quantum systems, with a decisive role played by ultracold atoms and cavity/circuit QED. Alongside with an enhanced theoretical understanding of quantum physics, in particular quantum computation and information [1], this paves the way to the realization of quantum technologies, such as quantum simulators and quantum computers.

Beside the intrinsic scientific and technological interest of artificial quantum systems, these serve as unprecedented tools to simulate condensed matter physics in a highly-controlled setup, and to unveil unexplored features of nature, for instance engineering novel phases of matter.

In a nutshell, on one side quantum simulators gave access to direct experimental investigation of quantum many-body dynamics in a controlled and tunable

way; on the other side, the characterization and control of quantum dynamics is crucial in any realistic implementation of quantum technologies, for instance in the transfer of quantum information.

It is meaningful to mention that control theory is a wide and fast-growing mathematical field, whose scope and questions are not necessarily related to (quantum) physics. Nevertheless, several concepts and methods of control theory have been borrowed and further developed in diverse areas of classical and quantum physics.

Only recently, however, has control theory been applied to quantum many-body systems. In fact, while a plethora of methods exist to study control problems, only few of them are powerful and versatile enough to cope with their complexity.

After this short introduction, my thesis is organized as follows.

1. In the first chapter we formulate the quantum optimal control problem for a generic Hamiltonian. Moreover, we review a successful algorithm to control quantum many-body systems.

2. In the second chapter we introduce the Lipkin-Meshkov-Glick (LMG) model, which is a paradigmatic system with long-range interactions. We explain how, in the thermodynamic limit, it can be mapped to a classical Hamiltonian with one collective degree of freedom.

3. In the third chapter we address the optimal control problem for the LMG model in the thermodynamic limit. We give a possible analytical solution and we study the problem with a complementary numerical approach. We find a minimal time below which the target state cannot be reached.

4. In the fourth chapter we review the time-dependent spin-wave expansion, a recently developed method, useful to assess the impact of small perturbations on both equilibrium and dynamical properties of the LMG model [2], [3].

5. In the fifth chapter we study the robustness of the optimal (or sub-optimal) protocols to quantum fluctuations, which are described in terms of the spin-wave expansion.

6. Finally, in the sixth chapter, we suggest some possible directions for further investigation.

The main original contributions of the thesis are in the third and in the fifth chapters.

The part dedicated to the spin-wave theory is somewhat detailed, and it contains a few additions with respect to the original works. Hopefully, it could serve as an introductive pedagogical exposition, useful for further studies and developments.

Contents

Notation and conventions

For the sake of clarity, notation and conventions are explained when introduced in the text. Here we only state the following, which are adopted throughout the thesis.

- As customary, we set $\hbar = 1$. Accordingly, time is measured in inverse units of energy.
- We shall always assume our system to be at zero absolute temperature $T = 0$ (unless otherwise stated). This implies that *equilibrium* is a synonym for *ground state*.
- The identity symbol is $a \equiv b$.
- The expression $a \coloneqq b$ means that a is defined in terms of b.
- Generic vectors are usually denoted as $(\vec{a}, \vec{b}, \dots)$. The only exception are vectors identifying direct space and Fourier space lattice sites, which are indicated in boldface $(\mathbf{r}, \mathbf{k}, \dots)$, since they mostly compare as subscripts.

Chapter 1

Quantum optimal control

In this chapter we explain the quantum optimal control scenario, briefly formulated in the outline. In section 1.2 we review a successful numerical method to control quantum many-body systems, which is also a valid tool for optimal control problems arising in different contexts.

1.1 Formulation of the problem

Consider a quantum system with Hamiltonian H, acting on a finite dimensional Hilbert space $\mathbb{C}^N$. Suppose at time $t = 0$ the system is prepared in a pure state $|\psi_0\rangle$, and that we aim to drive it to a target state $|\psi_{\text{tar}}\rangle$ in some time T.

Normally, the deterministic time evolution generated by H does not evolve $|\psi_0\rangle$ in $|\psi_{\text{tar}}\rangle$ for any value of T. The strategy to gain control over quantum dynamics is to couple the system to one or more external control fields $\Gamma_j(t)$, whose time dependence is experimentally tunable. The complete Hamiltonian now reads

$$H'(t) = H + V\big(\{\Gamma_j(t)\}\big), \tag{1.1}$$

where V describes the coupling of the system to the control fields. In addition, some experimental constraints are often present on the latters, and can usually be expressed in the form $\mathcal{C}_\alpha(\{\Gamma_j\}) = 0$.

As already mentioned in the introduction, complete control on a quantum system can only be achieved in idealized cases, so the control problem is reformulated as the minimization of a proper figure of merit (or cost function) $\mathcal{M}$, that embodies the desired properties of $|\psi_{\text{tar}}\rangle$.

The target time T can either be set to a fixed value, or be an additional parameter to be chosen in order to minimize $\mathcal{M}$; in this thesis we shall always

consider it to be fixed[1]. Importantly, the whole evolution should be performed faster than the system's decoherence time, due to the always present interactions with the environment.

On the other hand, it is quite natural to ask whether the control problem could be solved for arbitrary short times T. The answer is generally negative, and is deeply connected to the existence of quantum speed limits, which set a minimal time T_{QSL} for the evolution of a quantum system in its Hilbert space [4]. The value of T_{QSL} depends on the initial and target states, as well as on the nature of the driving fields. The important relation between quantum optimal control and quantum speed limits was firstly discussed in [5].

The problem of quantum optimal control is thus well defined: one should solve the Schrödinger equation

$$i\frac{d}{dt}\left|\psi(t)\right\rangle = H'(t)\left|\psi(t)\right\rangle \tag{1.2}$$

with the initial condition $|\psi_0\rangle$ and concurrently minimize the cost function $\mathcal{M}$, while satisfying possible constraints on the driving fields $\mathcal{C}_\alpha(\{\Gamma_j\}) = 0$. From a mathematical standpoint, this amounts to a functional minimization of $\mathcal{M}$ with respect to the set of control fields $\Gamma_j(t)$.

In most typical cases, this figure of merit only depends on the set of driving fields through the final state $|\psi_T\rangle$, reached at the end of the evolution (see the following examples). The specific choice of T is physically crucial, both to avoid decoherence effects and to satisfy the bounds of quantum speed limits.

In order to be more concrete and gain some physical insight, let us mention a few common situations.

1. If the target state is known with certainty, one usually tries to minimize the infidelity between the final state and the target. For pure states this is given by

$$\mathcal{M}(T) \equiv \mathcal{I}(T) = 1 - |\langle\psi_{\mathrm{tar}}|\psi(T)\rangle|^2 \equiv 1 - |\langle\psi_{\mathrm{tar}}|U(T)\psi_0\rangle|^2, \tag{1.3}$$

   indicating with $U(t)$ the time-evolution operator generated by $H'(t)$.

2. The target is quite often the ground state of some problem Hamiltonian H_{p}, sometimes coinciding with the final-time Hamiltonian $H'(T)$. If the ground state is unknown, the cost function is given by the average energy

$$\mathcal{M}(T) \equiv E_p(T) = \langle\psi(T)|H_{\mathrm{p}}|\psi(T)\rangle\,. \tag{1.4}$$

[1] This is the common choice in quantum control, in particular for quantum many-body systems. We remark that considering T as an additional parameter would make the problem significantly, and often unnecessarily, more complex.

If, on the contrary, the ground state is known, also the final infidelity can be a valid choice for $\mathcal{M}(\mathcal{T})$.

In a more general framework, the figure of merit could be some property that different states can satisfy: for instance in a bipartite (or multipartite) system, one could set as a target the production of maximally entangled (or factorized) states. Even more generally, one could try to model the system's interactions with the environment and use as a figure of merit the Von Neumann entropy, or the purity, of the final marginal state of the system.

As customary in Physics, with high generality come important practical issues. In this respect, we mention that the *forward* problem of calculating the evolution of a quantum system initialized in $|\psi_0\rangle$, under assigned control fields $\Gamma_j(t)$, is linear in the initial state. In contrast, the *inverse* problem of finding the control fields $\Gamma_j(t)$ to approach a target state $|\psi_{\text{tar}}\rangle$ is highly nonlinear, since the final state $|\psi(T)\rangle$ depends on the whole functional form of the fields, usually in a very intricate way.

Despite these difficulties, quantum optimal control has found application in a number of physical problems; a non-exhaustive list includes rotational, vibrational, and electronic excitation in molecules, atomic physics and solid-state electron dynamics [6]. Properly tailored laser pulses or low-frequency electric or magnetic fields are usually the driving fields exploited for achieving control over those systems.

As already anticipated in the introduction, quantum many-body systems complexity hinders a straightforward application of most control methods. However, in recent years remarkable progress has been made in this direction, and some effective methods to control many-body systems have been proposed. In the following section we give a concise review of one possible approach.

1.2 The CRAB algorithm

In this section we describe a simple but effective strategy, known as Chopped RAndom Basis (CRAB) technique, developed in [7]. This method has been effectively used to control the dynamics of quantum many-body systems in a number of interesting problems, see for instance [8], [9].

The versatility of the CRAB method comes from recasting the intricate mathematical problem of a *functional* minimization into a multi-variable *function* minimization, to be performed in a subspace of the initial functional space, and which can be worked out numerically with suitable methods.

The starting point is a guess solution $\Gamma_j^0(t)$ for the control fields, motivated

by plausible arguments or physical intuition about the concrete problem. Customary choices are linear or exponential ramps. One then looks for the best possible correction, expanded in a *truncated* functional basis.

In concrete, the usual choice is a multiplicative correction of the form

$$\Gamma_j(t) = \Gamma_j^0(t)\, c_j(t), \tag{1.5}$$

where the functions $c_j(t)$ are expanded in a truncated Fourier space as

$$c_j(t) = b(t) \left[1 + \sum_{k=1}^{N_j} A_k \sin(\omega_k t) + B_k \cos(\omega_k t) \right], \tag{1.6}$$

with $b(t)$ enforcing boundary conditions on the control fields (if necessary).

In the previous expression, N_j is the number of harmonics exploited to expand the correction $c_j(t)$, $\{A_k, B_k\}$ is the set of expansion coefficients, and ω_k the corresponding frequencies.

The problem is thus reduced to the minimization of a multi-variable cost function $\mathcal{M}(\{A_k, B_k\})$, whereas the frequencies ω_k are fixed before the minimization.

Beside truncating the functional basis, the other prescription of the CRAB algorithm is to *randomize* the parameters labeling the basis functions; for the Fourier basis this can be done by choosing $\omega_k = 2\pi k(1 + r_k)/T$, with r_k random numbers uniformly distributed in $[0, 1]$.

One should note that the randomization breaks the orthonormality of the basis function, but this is of no concern since the basis has already been truncated. However, it is natural to ask why such a strategy should be adopted. The underlying motivation is that it permits to enlarge the subspace of functions explored by the algorithm, without any additional free parameter.

In other terms, instead of running the minimization algorithm n times starting from different initial points $\{A_k, B_k\}_{k=1}^N$ and for some fixed values of ω_k, it is generally more effective to run it n times from the same initial point, but with different randomized frequencies ω_k [7].

Nevertheless, the randomization is by no means a compulsory ingredient: if there is some physical motivation for the choice of frequencies, or for a sufficiently simple problem, one can simply set the ω_k to fixed values.

Let us give some final remarks on the CRAB algorithm.

1. The choice of a truncated Fourier basis is usually made, mainly due to the possible physical interpretation of the frequencies ω_k. However, also other function bases may be considered.

2. The minimization problem of the multivariable function $\mathcal{M}(A_k, B_k)$ can in principle be arbitrarily hard to solve, and in general the solution could be only a local minimum (corresponding to sub-optimal driving fields). Direct search methods[2] are usually a safe and effective choice, since they can perform well also in the case of complicate optimization landscapes.

In conclusion, let us point out that in this framework the problem of local minima is not necessarily relevant. In fact, one has already restricted an infinite dimensional functional space to a finite dimensional subspace, which depends on the arbitrary choice of the basis, on the truncation and on the (possible) randomization.

The honest admission here is that in this framework the *optimality* of the solution for the driving fields $\Gamma_j(t)$ is to be intended in a broad generalized sense, as a possibly sub-optimal solution in a restricted research space. On the other hand, this approach simplifies a problem that would otherwise be intractable, and is one of few effective tools to control many body-quantum systems.

The success of the CRAB optimization is due to its straightforward adaptability to different situations; for example different figures of merit and constraints can be easily considered without any major modification to the algorithm.

In this respect, let us note that there is nothing inherently quantum about CRAB, which can be equally well adopted for classical control problems.

[2]Direct search methods are a class of heuristic optimization methods, whose implementation does not require the evaluation of gradients. As a result, they can be used also for cost functions that are not continuous or differentiable in the set of free parameters.

Chapter 2

The Lipkin-Meshkov-Glick (LMG) model

In this chapter we review the Lipkin-Meshkov-Glick model, introduced a few decades ago in the context of nuclear physics [10]. After a brief introduction to quantum spin lattice models in section 2.1, we describe in detail the thermodynamic limit of the LMG model in section 2.2, showing explicitly how it can be mapped to a *classical* Hamiltonian system with one degree of freedom. This result is exploited in order to study the equilibrium and dynamical properties of the LMG model in the thermodynamic limit, in section 2.3.

2.1 Introduction to the model

In this thesis we refer to a general class of models with quantum s-spins on a lattice, subject to ferromagnetic interactions and coupled to a possibly time-dependent transverse magnetic field. The Hamiltonian reads

$$H = -\sum_{\mathbf{r},\mathbf{r}'} J_{|\mathbf{r}-\mathbf{r}'|}\, \sigma^x_{\mathbf{r}} \sigma^x_{\mathbf{r}'} - g(t) \sum_{\mathbf{r}} \sigma^z_{\mathbf{r}}, \tag{2.1}$$

where the sums run over the lattice sites $\{\mathbf{r}\}$ and we defined the normalized spin operators $\sigma^\alpha_{\mathbf{r}} = S^\alpha_{\mathbf{r}}/s$, along the $\alpha = x, y, z$ direction. These operators represent a straightforward generalization of the standard Pauli matrices for $s = 1/2$. We shall consider ferromagnetic couplings J_r depending only on the distance $r = |\mathbf{r} - \mathbf{r}'|$ between two sites.

Note that in the absence of an external field, i.e. if $g(t) = 0$, the Hamiltonian (2.1) is immediately diagonalizable in the basis of eigenvectors of the operators $\{\sigma^x_{\mathbf{r}}\}$, and no interesting quantum effects are expected, since all operators in it commute. In the opposite limit where the ferromagnetic coupling J_r is negligible,

for instance in the case of a very strong constant field g, the Hamiltonian (2.1) reduces to the trivial problem of a collection of localized spins in an external magnetic field.

The many-body Hamiltonian (2.1) in its full generality is an extremely complex non-integrable system. However, there are some qualitative features that are worth mentioning, which hold true for general ferromagnetic interactions J_r (short- or long-range) [11].

In the first place, the system in the thermodynamic limit ($N \to \infty$) is expected to have an equilibrium (zero-temperature) quantum phase transition at a finite $g = g_{\rm cr}$. For $g > g_{\rm cr}$ the system is expected to be in an unique paramagnetic ground state, with vanishing order parameter $\langle \sigma^x \rangle = 0$, while for $g < g_{\rm cr}$ there are two degenerate ferromagnetic ground states with finite magnetization $\langle \sigma^x \rangle_\pm = \pm m \neq 0$. The latters are characterized by the breaking of the $\mathbb{Z}_2$-symmetry of the Hamiltonian, which is $\sigma^x_{\mathbf{r}} \to -\sigma^x_{\mathbf{r}}$, $\sigma^y_{\mathbf{r}} \to -\sigma^y_{\mathbf{r}}$, $\sigma^z_{\mathbf{r}} \to \sigma^z_{\mathbf{r}}$.

Solving for the spectrum of a generic instance of the Hamiltonian (2.1), with a constant external field g, is already a formidable numerical task (especially in dimensionality $d > 1$, or even for long $d = 1$ spin chains). Exact solutions exist, but are limited to simple (yet non-trivial) classes of systems.

In light of this, it is manifestly inconceivable to exactly control numerically (with a classical computer) a generic quantum many-body system's dynamics with Hamiltonian (2.1) by manipulating a time-dependent $g(t)$, so as to drive the system to a target state $|\psi_{\rm tar}\rangle$ in a fixed time T.

Therefore, we firstly focus on one of the simplest instances of this class of models, by choosing $J_r = \lambda/N$, corresponding to the fully-connected transverse field Ising magnet

$$H = -\frac{\lambda}{N} \sum_{i,j=1}^{N} \sigma^x_i \sigma^x_j - g \sum_{i=1}^{N} \sigma^z_i, \tag{2.2}$$

where each of the N spins interacts with all the others with the same ferromagnetic coupling strength, $\lambda/N > 0$[1]. The $1/N$ scaling of the ferromagnetic coupling is necessary in order to make the energy extensive in the thermodynamic limit. The $\mathbb{Z}_2$ symmetry of the model Hamiltonian in Eq. (2.2) now reads $\sigma^x_i \to -\sigma^x_i$, $\sigma^y_i \to -\sigma^y_i$, $\sigma^z_i \to \sigma^z_i$, and is spontaneously broken for small values of the external field g, corresponding to a ferromagnetic phase, as described in the following section.

This model is equivalent to the Lipkin-Meshkov-Glick (LMG) model. As

[1] Note that also unphysical self-interactions are present in the model, precisely the terms corresponding to $i = j$ in the first sum. This is not of much concern, since self-interaction terms are negligible, if compared to the $i \neq j$ terms, in the thermodynamic limit $N \to \infty$.

already mentioned, in the context of statistical physics, it mainly serves as a simple but non-trivial framework in order to study long-range interactions physics [12]. Obviously, the LMG model is not supposed to accurately describe by itself any realistic condensed matter system. Interestingly, however, some direct experimental realizations of the LMG model have recently been proposed. A remarkable implementation was realized in circuit QED, with an array of superconducting qubits[2] coupled to a quantized cavity mode that serves as a "quantum bus", inducing the long-range interactions between the qubits [13].

In order to study the LMG model (2.2) it is convenient to introduce the Fourier components operators, defined as

$$\tilde{\sigma}_k^\alpha = \sum_{j=1}^{N} e^{-ikj} \sigma_j^\alpha, \tag{2.3}$$

where k varies over the reciprocal lattice sites $k = 2\pi n/N$ for $n = -N/2 + 1, \ldots, N/2$.[3] These Fourier operators are completely delocalized with respect to the lattice sites, but often convenient to study lattice models. The LMG model Hamiltonian in Eq. (2.2) can be immediately rewritten as

$$H = -\frac{\lambda}{N}(\tilde{\sigma}_{k=0}^x)^2 - g\,\tilde{\sigma}_{k=0}^z, \tag{2.4}$$

which depends only on the total spin components $\tilde{\sigma}_{k=0}^\alpha = \sum_{i=1}^N \sigma_i^\alpha$ (Fourier components with zero momentum $k = 0$). All the other operators $\tilde{\sigma}_{k\neq 0}^\alpha$, which describe the spatial fluctuations of the spins in Fourier space, do not contribute to its dynamical properties.

The full Hilbert space has dimension $(2s+1)^N$, but the Hamiltonian H commutes with the total spin operator $\left|\vec{J}\right|^2 = s^2\left|\vec{\tilde{\sigma}}_{k=0}\right|^2$, so it can be diagonalized separately in each sector of fixed total spin magnitude $j(j+1)$, where $j = 0, 1, \ldots, Ns$ or $j = 1/2, 3/2, \ldots, Ns$ (depending on Ns being integer or half integer respectively). The dynamics of the LMG model is therefore constrained to the $(2j+1)$-dimensional subspace generated by the states $\{|j, j_z\rangle\}$, where j is the conserved total angular momentum and $-j \leq j_z \leq j$ are the possible projections along the z-axis. This is an enormous simplification, since the relevant subspace dimension scales at most linearly with the number of spins N, rather than exponentially.

In the particular case of $s = 1/2$, an additional symmetry prevents the dynamical coupling of states having a different parity in the number of spins

[2] A major advantage of considering superconducting qubits, rather than ultracold atoms, is the absence of particle motion.

[3] The Fourier operators $\{\tilde{\sigma}_k^\alpha\}$ are defined as a unitary transformation (after normalization) applied to the set of $\{\sigma_j^\alpha\}$ [compare with the inverse transformation in Eq. (4.37)].

pointing in the magnetic field direction, since the Hamiltonian commutes with the product of Pauli matrices $\prod_j \sigma_j^z$.

It can be shown that the ground state of the Hamiltonian belongs to the subspace with maximal total spin, corresponding to the quantum number $j = Ns$.

The LMG model with Hamiltonian (2.4) exhibits a remarkably simple behavior if we consider the thermodynamic limit $N \to \infty$, as can be better understood introducing the rescaled operators ($\alpha = x, y, z$)

$$\mathcal{S}^\alpha := \frac{\tilde{\sigma}^\alpha_{k=0}}{N} \equiv \frac{J^\alpha}{Ns}, \tag{2.5}$$

and focusing on the reduced Hamiltonian

$$\mathcal{H} := \frac{H}{N} = -\lambda\,(\mathcal{S}^x)^2 - g\,\mathcal{S}^z. \tag{2.6}$$

In this limit, the equilibrium (ground state) and dynamical properties of the LMG model become essentially *classical*.

This fact can be understood by considering the commutation relations of the operators $\mathcal{S}^\alpha$:

$$\left[\mathcal{S}^\alpha, \mathcal{S}^\beta\right] = \frac{1}{Ns} i\epsilon^{\alpha\beta\gamma}\mathcal{S}^\gamma, \tag{2.7}$$

which imply that the effective Planck's constant $\hbar_{\text{eff}} := 1/(Ns)$ vanishes for $N \to \infty$. This observation formally means that the thermodynamic limit of the system coincides with its semiclassical limit, which can be carried out as an expansion in powers of $\hbar_{\text{eff}}$ of the Schrödinger equation.

In the thermodynamic limit the spectrum of $\left|\vec{\mathcal{S}}\right|$ becomes dense in the interval $[0, 1]$, independently on Ns being integer or half integer. In fact, the eigenvalues of the operator $\left|\vec{\mathcal{S}}\right|$ can be expanded to the first order in $\hbar_{\text{eff}}$ yielding

$$\frac{\sqrt{j(j+1)}}{Ns} = \rho + \frac{\hbar_{\text{eff}}}{2} + \mathcal{O}(\hbar^2_{\text{eff}}), \tag{2.8}$$

with

$$\rho := \frac{j}{Ns} \tag{2.9}$$

becoming a continuous variable in $[0, 1]$ in the thermodynamic limit.

If we ignore all corrections in $\hbar_{\text{eff}}$, considering the plain thermodynamic limit $N \to \infty$, the intuition may suggest that the system is completely described by the classical reduced Hamiltonian

$$\mathcal{H}_{\text{cl}}(\vec{s}) = -\lambda(s^x)^2 - gs^z, \tag{2.10}$$

where $\vec{s}$ is now a classical (continuous) spin, its phase space being the surface of a sphere of *fixed* radius $0 < \rho \leq 1$[4]. This intuition is indeed correct: both the ground state and the off-equilibrium coherent quantum dynamics of the LMG model (as $N \to \infty$) are described by the classical Hamiltonian in Eq. (2.10).

Since this is a central result for the following chapters of the thesis, we will analyze it in more detail in the following section.

2.2 LMG model in the thermodynamic limit

In the last section we anticipated that the LMG model in the $N \to \infty$ limit is described by the classical Hamiltonian in Eq. (2.10). This statement can be rephrased in more formal terms, as follows.

Regarding the equilibrium properties (at $T = 0$) of the system, the ground state expectation values $\langle \mathcal{S}^\alpha \rangle$ are given by the minimum point of $\mathcal{H}_{\rm cl}$ on the sphere with radius $\rho = 1$, with vanishingly small quantum fluctuations around this average.

In the context of quantum control we are particularly interested in the off-equilibrium dynamics of the model. Assuming the initial condition to be a spin coherent state in the maximal spin sector $j = Ns$, it can be proven that the off-equilibrium coherent quantum dynamics of the averages $\langle \mathcal{S}^\alpha(t) \rangle$, possibly driven by a time-dependent field $g(t)$, is given by the corresponding classical trajectory on the sphere.

These classical trajectories are governed by $\mathcal{H}_{\rm cl}$ in Eq. (2.10), via the equations of motion

$$\dot{s}^\alpha = \{s^\alpha, \mathcal{H}_{\rm cl}\}, \tag{2.11}$$

where the spin Poisson brackets are defined as $\{s^\alpha, s^\beta\} \coloneqq \varepsilon^{\alpha\beta\gamma} s^\gamma$ and time is rescaled by the *single quantum spin* value s[5].

There is a number of different ways to understand these concepts, at various levels of mathematical rigor and technical complexity, see e.g. [14] and references therein.

Probably the most direct way to obtain these results is to write down the

[4] As stated above, the ground state belongs to the maximal total spin sector, which is identified with $\rho = 1$ in the thermodynamic limit.

[5] From here onwards, time is always intended to be rescaled as $t' = t/s$.

Heisenberg equations of motion for the Heisenberg operators $\mathcal{S}_H^\alpha$, which read

$$\begin{cases} \dot{\mathcal{S}}_H^x = g\,\mathcal{S}_H^y \\ \dot{\mathcal{S}}_H^y = -g\,\mathcal{S}_H^x + \lambda(\mathcal{S}_H^x\mathcal{S}_H^z + \mathcal{S}_H^z\mathcal{S}_H^x) \\ \dot{\mathcal{S}}_H^z = -\lambda(\mathcal{S}_H^x\mathcal{S}_H^y + \mathcal{S}_H^y\mathcal{S}_H^x), \end{cases} \tag{2.12}$$

where time is rescaled as mentioned above. These equations yield an exact description of the quantum dynamics for any value of N.

However, in the limit $N \to \infty$, the commutators for $\mathcal{S}^\alpha$, written in Eq. (2.7), are $\mathcal{O}(\hbar_{\text{eff}})$ and can therefore be neglected. By making use of this observation and considering the expectation values in some state, we obtain

$$\begin{cases} \frac{d}{dt}\langle\mathcal{S}^x\rangle = g\,\langle\mathcal{S}^y\rangle \\ \frac{d}{dt}\langle\mathcal{S}^y\rangle = -g\,\langle\mathcal{S}^x\rangle + 2\lambda\,\langle\mathcal{S}^x\mathcal{S}^z\rangle \\ \frac{d}{dt}\langle\mathcal{S}^z\rangle = -2\lambda\,\langle\mathcal{S}^x\mathcal{S}^y\rangle\,, \end{cases} \tag{2.13}$$

where we neglected $\mathcal{O}(\hbar_{\text{eff}})$ corrections due to operator ordering. If we further neglect correlations as in $\langle\mathcal{S}^\alpha\mathcal{S}^\beta\rangle \approx \langle\mathcal{S}^\alpha\rangle\langle\mathcal{S}^\beta\rangle$, which corresponds to a mean-field approximation, we end up with

$$\begin{cases} \frac{d}{dt}\langle\mathcal{S}^x\rangle = g\,\langle\mathcal{S}^y\rangle \\ \frac{d}{dt}\langle\mathcal{S}^y\rangle = -g\,\langle\mathcal{S}^x\rangle + 2\lambda\,\langle\mathcal{S}^x\rangle\langle\mathcal{S}^z\rangle \\ \frac{d}{dt}\langle\mathcal{S}^z\rangle = -2\lambda\,\langle\mathcal{S}^x\rangle\langle\mathcal{S}^y\rangle\,. \end{cases} \tag{2.14}$$

These equations coincide with the classical equations of motion [see Eq. (2.11)], upon substitution of the quantum averages with the classical spin components, i.e. $\langle\mathcal{S}^\alpha\rangle \to s^\alpha$. This is verified explicitly in the following section.

It should be noted that, while the approximation of neglecting operator ordering is under control in the thermodynamic limit, for a generic time-evolving state the approximation $\langle\mathcal{S}^\alpha\mathcal{S}^\beta\rangle \approx \langle\mathcal{S}^\alpha\rangle\langle\mathcal{S}^\beta\rangle$ is not valid.

However, this approximation is correct for a spin coherent state, up to $\mathcal{O}(\hbar_{\text{eff}})$ corrections. Spin coherent states are briefly reviewed in appendix A, and in particular Eq. (A.9) proves the previous statement[6].

In fact, as mentioned in the beginning of this section, the classical Hamiltonian describes the coherent quantum evolution of an initial spin coherent state; it does *not* describe the generic incoherent evolution of any initial quantum state.

Spin coherent states have a well defined semiclassical limit[7], since they can be mapped to phase space points with vanishingly small spin fluctuations. In

[6] We are considering the maximal spin sector $j = Ns$, therefore the neglected terms in Eq. (A.9) are $\mathcal{O}(\hbar_{\text{eff}})$.

[7] Recall that the semiclassical limit coincides with the thermodynamic limit, for the LMG model.

fact, by recalling the definition of $\mathcal{S}^\alpha$ in Eq. (2.5), the property of coherent states in Eq. (A.5) can be rewritten as

$$\begin{cases} \langle\theta,\phi|\mathcal{S}^x|\theta,\phi\rangle = \sin\theta\cos\phi \\ \langle\theta,\phi|\mathcal{S}^y|\theta,\phi\rangle = \sin\theta\sin\phi \\ \langle\theta,\phi|\mathcal{S}^z|\theta,\phi\rangle = \cos\theta. \end{cases} \tag{2.15}$$

Moreover, spin fluctuations in transverse directions vanish as

$$(\Delta\tilde{J}^x)^2 = (\Delta\tilde{J}^y)^2 = \frac{1}{2Ns} = \mathcal{O}(\hbar_{\text{eff}}), \tag{2.16}$$

where $\tilde{J}^x$ and $\tilde{J}^y$ are spin projections on an orthonormal basis in the plane orthogonal to $\vec{n} = (\sin\theta\cos\phi, \sin\theta\sin\phi, \cos\theta)$ [compare with Eq (A.8)].

In the thermodynamic limit, transverse spin fluctuations are identically zero, thus the system's dynamics remains coherent at all times and is fully described by Eq. (2.14). If we consider large but finite values of N, i.e. we include finite-size effects, the initial coherent state is described as a localized wave packet with center in $\langle\theta,\phi|\vec{\mathcal{S}}|\theta,\phi\rangle$ and isotropic transverse spreading given by Eq. (2.16). Moreover, as briefly mentioned in appendix A, in the large N limit spin coherent states become equivalent to harmonic oscillator coherent states.

In the case of large but finite N, the initial coherent state first undergo a coherent dynamics, described by the evolution of its averages, behaving as a well-defined wave packet. However, this picture holds only up to some characteristic time scale, which diverges with the system size; after this time the coherent wave packet delocalizes and its evolution is no more captured by Eq. (2.14).

In appendix A we mention that for the Zeeman Hamiltonian, coherent states evolve coherently at all times, for any finite N; the Zeeman Hamiltonian, which describes simple spin precession, corresponds to the limit $\lambda = 0$ of the LMG model. In the general case, in the presence of a competition between ferromagnetic ordering and the external field, decoherence effects are to be expected, as finite size corrections.

The time for which the semiclassical picture breaks down is usually called the Ehrenfest time t_{Ehr}, and it is defined as the time scale at which the wave packet spreading becomes of $\mathcal{O}(1)$.

The Ehrenfest time is shown to depend on the qualitative features of the classical dynamics of $\langle\vec{\mathcal{S}}\rangle \to \vec{s}$: It can be shown with general arguments [15] that, for regular dynamics in integrable systems, $t_{\text{Ehr}} \sim \hbar_{\text{eff}}^{-1/2} \sim \sqrt{N}$. In the case of chaotic or unstable dynamics (e.g. on a separatrix of the classical phase space), spreading is predicted to occur at shorter time scales, of order $t_{\text{Ehr}} \sim \log N$.

In the following, we shall consider only coherent dynamics of the initial spin coherent state. This is clearly related to the choice of the target time T for the

optimal control, or equivalently to the choice of the system size N: we will assume such values to satisfy the condition

$$T \ll t_{\mathrm{Ehr}}. \tag{2.17}$$

Up to this point, we proved the initial statement regarding coherent quantum dynamics. Let us now briefly motivate the analogous statement, concerning the ground state properties of the LMG model in the thermodynamic limit. A natural question that arises is whether, in the large N limit, the ground state of the LMG model can be approximately described with a localized spin coherent state.

The problem is somewhat subtle, as it was recently pointed out in [16], with remarkable clarity. The reason is that the $\mathbb{Z}_2$ symmetry of the Hamiltonian, which is invariant under $\sigma_i^x \to -\sigma_i^x$, $\sigma_i^y \to -\sigma_i^y$, $\sigma_i^z \to \sigma_i^z$, implies that, for any finite value of N, exact eigenstates of the Hamiltonian should be invariant under this transformation. In particular, any exact eigenstate must satisfy the condition

$$\langle \mathcal{S}^x \rangle = \langle \mathcal{S}^y \rangle = 0. \tag{2.18}$$

However, the only spin coherent state with this property is clearly the highest weight state $|j, j_z = j\rangle$. This is in fact the ground state for strong values of the external field g, i.e. in the symmetric phase.

Spontaneous symmetry breaking occurs rigorously only in the thermodynamic limit, implying that any localized spin coherent state, which does not satisfy Eq. (2.18), does not yield, in principle, a valid description of the ground state for finite N.

However, one can prove that, for large values of N, a mean-field variational approach restricted to the spin coherent state system gives an approximate description for the ground state, which is correct up to $\mathcal{O}(\hbar_{\mathrm{eff}})$. Let us briefly sketch this procedure.

Following the general variational approach scheme, one tries to minimize the variational energy

$$E_{\mathrm{var}} = \langle \theta, \phi | \mathcal{H} | \theta, \phi \rangle \,, \tag{2.19}$$

with the reduced Hamiltonian $\mathcal{H}$ defined in Eq. (2.6). The free parameters for the minimization are given by the angles θ, ϕ that characterize a spin coherent state.

The fact that spin coherent states represent a reasonable ansatz for mean-field states, can be better appreciated in the case of N spins $s = 1/2$, where the usual expression for spin coherent states [see Eq. (A.1)] can be equivalently rewritten as

$$|\theta, \phi\rangle = \bigotimes_{j=1}^{N} \cos\frac{\theta}{2} |\uparrow\rangle_j + \sin\frac{\theta}{2} e^{i\phi} |\downarrow\rangle_j \,, \tag{2.20}$$

where the kets $|\uparrow\rangle_j$ and $|\downarrow\rangle_j$ are the eigenstates of operator σ_j^z with eigenvalues $+1, -1$ respectively. In light of the previous expression, it appears that a spin coherent state is composed of the tensor product of N single qubit states, all with the same orientation in the Bloch sphere. Since all the single spins 1/2 are pointing in the same direction, this is a valid choice for a mean-field state.

The variational energy in Eq. (2.19) is readily evaluated by making use of Eqs. (A.5) and (A.9)

$$E_{\text{var}} = -\lambda \langle \mathcal{S}^x \rangle^2 - g \langle \mathcal{S}^z \rangle + \mathcal{O}(\hbar_{\text{eff}}). \tag{2.21}$$

It is then clear that the solution to the variational problem is found with a minimization of the classical Hamiltonian in Eq. (2.10) in classical phase space.

The previous argument formalizes the intuitive idea that, while true spontaneous symmetry breaking formally occurs only in the thermodynamic limit, in the case of large but finite N there should exist some localized states, with vanishingly small energy above the exact symmetric ground state. These states do not respect the $\mathbb{Z}_2$ symmetry, and reduce to the symmetry-broken ground states of the ferromagnetic phase when $N \to \infty$.

Remarkably, in reference [16], it is shown that a tiny perturbation or fluctuation (which is finite instead of infinitesimal) can break the symmetry of the exact ground state for finite large values of N, and map it to a localized state, which is close to the corresponding mean-field coherent state.

2.3 The equivalent classical model

Relying on the results presented in the previous section, we now describe the ground state and off-equilibrium dynamical properties of the LMG model in the thermodynamic limit, by studying the equivalent classical system with Hamiltonian (2.10).

2.3.1 Equilibrium properties and equilibrium critical point

In the following, we analyze the equilibrium properties of the classical system described by the Hamiltonian

$$\mathcal{H}_{\text{cl}}(\vec{s}) = -\lambda (s^x)^2 - g s^z, \tag{2.22}$$

with constant external field g. As illustrated in the previous section, the classical minimum will yield the ground state properties of the LMG model in the thermodynamic limit.

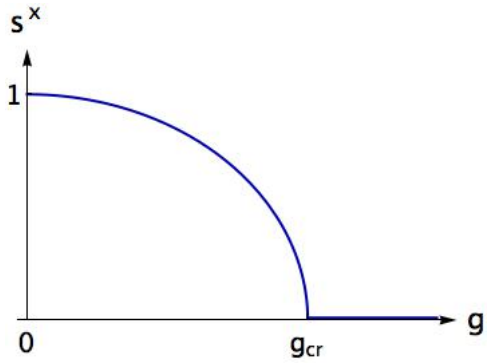

Figure 2.1: Equilibrium order parameter $\langle \mathcal{S}^x \rangle \to s^x$ of the LMG model in the thermodynamic limit, as a function of the constant positive field g ($\rho = 1$). Only the positive magnetization branch is shown. The critical exponent is 1/2, corresponding to a square root singularity at the quantum critical point $g_{\rm cr} = 2\lambda$.

The minimization of $\mathcal{H}_{cl}$ has to be carried out over the phase space, which, as already mentioned, is a sphere of (fixed) radius ρ.

The classical minimum is easily found with an unconstrained minimization in the usual spherical coordinates θ and ϕ, and the result depends qualitatively on $|g|$ being larger or smaller than a critical value $g_{\rm cr} = 2\lambda\rho$.

If $|g| > g_{\rm cr}$ the minimum point is $\vec{s} = \mathrm{sgn}(g)\rho\,(0, 0, 1)$, with (negative) energy $\mathcal{E}_> = -|g|\rho$ and zero magnetization s^x, corresponding to the paramagnetic phase of the quantum many-body LMG model in the thermodynamic limit.

In contrast, for $|g| < g_{\rm cr}$, the paramagnetic minimum becomes an unstable saddle point and bifurcates into two degenerate minima corresponding to the ferromagnetic phase. As could be predicted from symmetry arguments, this minima lie in the xz-plane and have opposite finite values of the magnetization: precisely they are located in $(\theta^*, 0)$, (θ^*, π) with

$$\cos(\theta^*) = \frac{g}{g_{\rm cr}}. \tag{2.23}$$

Accordingly, the value of the magnetization is

$$s^x = \pm\rho \sin\theta^* = \pm\rho\sqrt{1 - (g/g_{\rm cr})^2}, \tag{2.24}$$

[see Fig. 2.1], while $s^y = 0$, $s^z = \rho\,(g/g_{\rm cr})$ and the two minima have the same energy

$$\mathcal{E}_< = -\lambda\rho^2 - \frac{g^2}{4\lambda}. \tag{2.25}$$

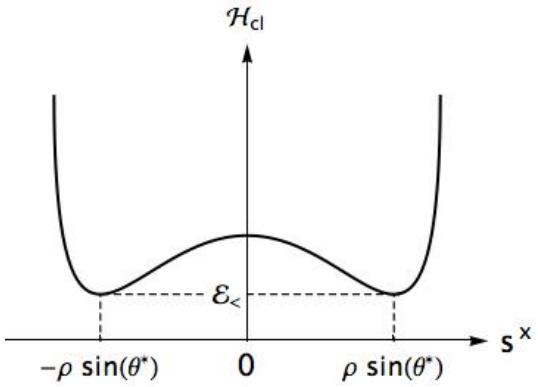

Figure 2.2: Double-well classical energy landscape in the half-plane $s^y \equiv 0$, $s^z > 0$, where the two symmetric ferromagnetic minima [given by Eq. (2.23)] are located if $0 < g < g_{\rm cr}$. In the thermodynamic limit, the depth of the two wells diverges proportionally to N. This implies that the quantum tunneling of a coherent localized wave packet from one well to the other is suppressed. Finite size quantum tunneling effects occur over an exponentially long time scale, and can be safely ignored in our framework. We remark that the coherent dynamics of the system is *not* confined in this half-plane.

As explained in the previous section, the mean field ground state is a spin coherent state in the maximal total spin sector (i.e. for $\rho = 1$), which is characterized by the classical minimum angles (θ^*, ϕ^*),

Finally, a schematic physical picture of the ferromagnetic phase is given in Fig. 2.2.

2.3.2 Dynamical properties

We now turn to the classical dynamics generated by the Hamiltonian (2.22), which is governed by the equations of motion

$$\dot{s}^\alpha = \left\{ s^\alpha, \mathcal{H}_{\rm cl}(\vec{s}) \right\}, \tag{2.26}$$

where the curly braces indicate Poisson brackets.

As promised in the previous section, we verify explicitly that upon the substitution $\langle \mathcal{S}^\alpha \rangle \to s^\alpha$, they coincide with the equations (2.14), which describe the coherent evolution of localized wave packets.

The classical equations can be recast into an explicit form exploiting the standard Poisson brackets of a classical spin

$$\left\{ s^\alpha, s^\beta \right\} = \epsilon^{\alpha\beta\gamma} s^\gamma, \tag{2.27}$$

and the following general property, valid for any (analytic) function of the spin components:

$$\{f(\vec{s}), g(\vec{s})\} = \sum_{\alpha,\beta=x,y,z} \frac{\partial f}{\partial s^\alpha} \frac{\partial f}{\partial s^\beta} \left\{s^\alpha, s^\beta\right\} = \sum_{\alpha,\beta=x,y,z} \frac{\partial f}{\partial s^\alpha} \frac{\partial f}{\partial s^\beta} \epsilon^{\alpha\beta\gamma} s^\gamma. \tag{2.28}$$

The equation above, in the particular case $f(\vec{s}) = s^\alpha$ and $g(\vec{s}) = H(\vec{s})$, yields the generic equations of motion for a classical spin

$$\dot{s}^\alpha = \epsilon^{\alpha\beta\gamma} \frac{\partial H}{\partial s^\beta} s^\gamma, \tag{2.29}$$

which may be rewritten in a compact vector notatation

$$\dot{\vec{s}} = \nabla H \times \vec{s}. \tag{2.30}$$

In the specific case of the Hamiltonian in Eq. (2.22), the result is the following system of coupled non-linear ODEs

$$\begin{cases} \dot{s}^x = g s^y \\ \dot{s}^y = -g s^x + 2\lambda s^x s^z \\ \dot{s}^z = -2\lambda s^x s^y, \end{cases} \tag{2.31}$$

which are indeed identical to those in Eq. (2.14).

While a direct numerical solution of these equations is straightforward, it is convenient to exploit the two evident constants of motion, precisely the total spin $(s^x)^2 + (s^y)^2 + (s^z)^2 = \rho^2$ and the energy (the Hamiltonian is time-independent). Therefore, the system can actually be integrated analytically.

As a first step, it is convenient to describe the system with a pair of canonical coordinates Q and P, satisfying canonical Poisson brackets $\{Q, P\} = 1$. This can be done by identifying $P \coloneqq s^z$ with the canonical momentum and $Q \coloneqq \phi$ with the conjugated coordinate. In fact, one can always rewrite the other spin components as

$$\begin{cases} s^x = \sqrt{\rho^2 - P^2} \cos Q \\ s^y = \sqrt{\rho^2 - P^2} \sin Q, \end{cases} \tag{2.32}$$

in terms of the coordinates $-1 \leq P \leq 1$ and $Q \in \mathbb{R}$, which enters in the equations only modulo 2π. The fact that the latters are actually canonical variables is easily checked with a direct calculation, using the definition of the azimuth angle $Q = \arctan(s^y/s^x) + c$, where c is a constant equal to 0 in the first quadrant, equal to π in the second and third quadrants and equal to 2π in the fourth[8]. Regardless of the constant, one can verify that

$$\{Q, P\} = \frac{\partial Q}{\partial s^y} s^x - \frac{\partial Q}{\partial s^x} s^y = 1. \tag{2.33}$$

[8]We assumed that $0 \leq Q < 2\pi$, and the standard range $(-\pi/2, \pi/2)$ for the $\arctan(\cdot)$.

The Hamiltonian in Eq. (2.22) can be expressed in terms of these canonical variables as[9]

$$\mathcal{H}_{\rm cl}(s^z,\phi) = -\lambda(\rho^2 - (s^z)^2)\cos^2\phi - gs^z, \tag{2.34}$$

which is the Hamiltonian of a dynamical system with one degree of freedom ($P \equiv s^z, Q \equiv \phi$), just *not* in the usual form of a quadratic kinetic term plus a potential depending on Q. The equations of motion are now canonical Hamilton equations and read

$$\begin{cases} \dot{s}^z = -2\lambda(\rho^2 - (s^z)^2)\cos\phi\sin\phi \\ \dot{\phi} = 2\lambda s^z\cos^2\phi - g. \end{cases} \tag{2.35}$$

Let us now take advantage of the time-translational invariance and write down the energy conservation

$$\mathcal{H}_{\rm cl}(s^z,\phi) = -\lambda(\rho^2 - (s^z)^2)\cos^2\phi - gs^z \equiv \mathcal{E}. \tag{2.36}$$

One thus obtains an explicit expression for

$$s^z(\phi) = \frac{g \pm \left[g^2 + 4\lambda^2\rho^2\cos^4\phi + 4\lambda\,\mathcal{E}\cos^2\phi\right]^{1/2}}{2\lambda\cos^2\phi}, \tag{2.37}$$

along a generic solution of the equations of motion (2.35). By substitution of this result in the second Hamilton equation, one finds a closed differential equation

$$\dot{\phi} = \pm\left[g^2 + 4\lambda^2\rho^2\cos^4\phi + 4\lambda\,\mathcal{E}\cos^2\phi\right]^{1/2}, \tag{2.38}$$

which is formally solved by separation of variables as

$$\int \frac{d\phi}{\left[g^2 + 4\lambda^2\rho^2\cos^4\phi + 4\lambda\,\mathcal{E}\cos^2\phi\right]^{1/2}} = \pm\int_0^t dt'. \tag{2.39}$$

The integral at the l.h.s. of the previous equation can be recast into the standard form

$$\int \frac{du}{\left[au^4 + bu^2 + c\right]^{1/2}}, \tag{2.40}$$

where we used the substitution $u = \tan\phi$ and defined the constants

$$\begin{cases} a = g^2 \\ b = 2g^2 + 4\lambda\,\mathcal{E} \\ c = g^2 + 4\lambda^2\rho^2 + 4\lambda\,\mathcal{E}\ . \end{cases} \tag{2.41}$$

[9]Having well understood that s^z, ϕ are conjugated canonical variables, we drop the notation with P, Q, in order to avoid later confusion with canonical coordinates describing quantum fluctuations.

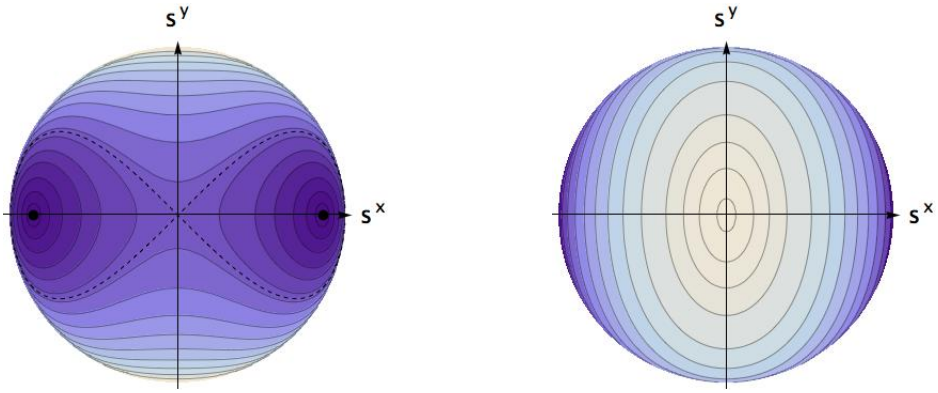

(a) Ferromagnetic portrait for $s^z > 0$. **(b)** Ferromagnetic portrait for $s^z < 0$.

Figure 2.3: Schematic phase portrait of the ferromagnetic behavior, in the hemispheres $s^z > 0$ and $s^z < 0$ viewed from the north and south poles respectively. In the left panel the separatrix is shown (dotted line) and the stable equilibrium points (energy minima) are represented with a black dot. In both panels darker colors indicate lower energy.

This integral can be solved in terms of a Jacobi elliptic function [17].

However, the exact solution is quite unpractical and unnecessary for our scopes. A better physical insight is given by a qualitative study of the constant energy trajectories defined analytically in Eq. (2.37), while for the actual motion we can resort to a trivial numerical integration of Eq. (2.38), with suitable initial conditions.

A qualitative analysis of the energy contours is more natural using the Cartesian coordinates s^α rather than the canonical variables, so let us refer to the initial Hamiltonian in Eq. (2.22).

As a preliminary observation, note that the Hamilton equations in (2.35) are invariant under the inversion of the field $g \to -g$, if one also reflects the conjugated coordinates $s^z \to -s^z$ and $\phi \to -\phi$. This implies that the dynamical properties for a given value of the field g_0, or for $-g_0$, are the same up to these reflections. We shall thus focus on $g > 0$, and treat separately the hemispheres $s^z > 0$ and $s^z < 0$ for graphical convenience.

The phase portrait for the ferromagnetic behavior of our classical system is reported in Fig. 2.3. The most interesting features are displayed in the hemisphere $s^z > 0$. Firstly, the ferromagnetic energy minima are represented with a black dot, while the other unstable equilibrium points are the saddle point $\vec{s} = (0, 0, \rho)$ and the opposite maximum point $\vec{s} = (0, 0, -\rho)$. Qualitatively different trajectories are set apart by the separatrix (dotted line), which passes through the saddle point in $\vec{s} = (0, 0, \rho)$ and therefore has energy $\mathcal{E} = -g\rho$. The separatrix is actually

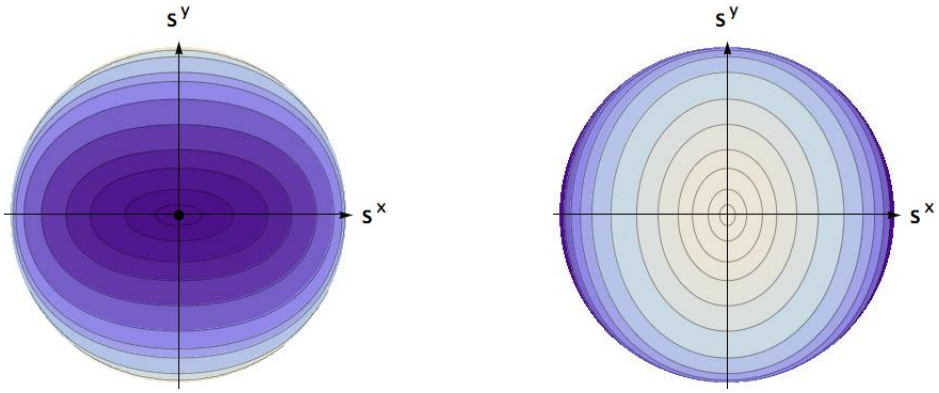

(a) Paramagnetic portrait for $s^z > 0$. **(b)** Paramagnetic portrait for $s^z < 0$.

Figure 2.4: Schematic phase portrait of the paramagnetic behavior, in the hemispheres $s^z > 0$ and $s^z < 0$ viewed from the north and south poles respectively. In the left panel the stable equilibrium point (energy minimum) is represented with a black dot. In both panels darker colors indicate lower energy.

composed of three independent solutions of the Hamilton equations, including the saddle point itself, reachable only in the infinite time limit.

One can get a qualitative picture thanks to the color scale in figure: contour plots progressively further from the minima and approaching the maximum $\vec{s} = (0, 0, -\rho)$ correspond to higher values of energy, as evidenced by lighter colors.

The phase portrait for the paramagnetic behavior is shown in Fig. 2.4. The point $\vec{s} = (0, 0, \rho)$ is now the energy minimum, while the energy maximum is still in $\vec{s} = (0, 0, -\rho)$. The solutions are all qualitatively the same, reminiscent of the simple spin precession around the z-axis characterizing the motion in the limit $g \gg \lambda$.

Let us remark for the sake of completeness that the energy in the hemisphere $s^z > 0$ is negative definite, therefore all the contours entering in this region certainly correspond to negative energies, while in the other hemisphere $s^z < 0$ also null or positive energy solutions are present. However, in this framework there is not any physical meaning in the energy sign, and one can freely translate the energy of an additive constant.

In conclusion, it is instructive to point out the dynamics for the simple limit cases $|g| \gg \lambda$ and $|g| \ll \lambda$, which are better understood looking back at the equations for s^α in Eqs. (2.31). In the first limit s^z becomes a constant of motion and, as already mentioned, the system precedes around the z-axis with angular frequency equal to g, independently from the initial condition. Precisely, it is easy to check that the rotation is CW for $g > 0$ and CCW for $g < 0$ (looking

from the positive direction of s^z).

In the second limit s^x becomes a constant of motion and the ferromagnetic solutions tend to occupy all the phase portrait describing precession around the x-axis with angular frequency $2\lambda|s^x|$. The paramagnetic solutions are shrinked in a phase space region with vanishing area, corresponding to the infinite-period orbit for $s^x = 0$.

Accordingly with the simplicity of the motion, in these limit cases the integral in Eq. (2.40) assumes an elementary form and can be readily evaluated in terms of inverse trigonometric functions.

2.3.3 Dynamical critical point

In this section we concisely review a possible definition of *dynamical* phase transition and outline the dynamical critical properties of our model, which are of some interest for the later discussion, regarding control of the LMG dynamics.

Dynamical phase transitions in fully-connected models were extensively studied in [14], while some significant insight beyond mean field was recently presented in [2], [3].

Let us generalize the previous Hamiltonian by considering time-dependent external fields

$$\mathcal{H}_{\mathrm{cl}}(\vec{s}) = -\lambda(s^x)^2 - g(t)s^z. \tag{2.42}$$

The standard definition of non-equilibrium order parameter is given by

$$\overline{s^x} = \lim_{T\to\infty} \frac{1}{T} \int_0^T dt\, s^x(t), \tag{2.43}$$

which is the infinite-time average of the magnetization. In the case of a system at equilibrium, this non-equilibrium order parameter reduces to the usual time-independent magnetization.

One can identify a parametric family of protocols to drive the system out of an equilibrium initial condition, which is accomplished by varying in time an external field $g(t)$, with the expression of the field depending on a set of free parameters.

If, by slowly varying one of these free parameters, one observes a singularity in the non-equilibrium order parameter, then the point of singularity is referred to as a *dynamical critical point* and the system is said to undergo a dynamical phase transition[10].

[10] As for the usual equilibrium phase transitions, the proper definition of critical point and different phases is valid only in the thermodynamic limit. Consequently, the classical description of the LMG model is accurate and decoherence effects are suppressed at all times.

An example of dynamical criticality in the LMG model is observed with the following protocol. Suppose that the system is prepared at time $t = 0$ in one of the ferromagnetic minima of the Hamiltonian in Eq. (2.42), with a transverse field g_0 such that $|g_0| < g_{\rm cr} \equiv 2\lambda\rho$. At $t = 0$, the system is driven out of equilibrium by a quantum quench, consisting in an external field sudden variation from the initial value g_0 to the final value g, with the transient being much shorter than the typical timescale of the system's dynamics. The subsequent dynamics is generated by the post-quench Hamiltonian $\mathcal{H}_{\rm cl}(g)$, with the initial condition given by the equilibrium ferromagnetic state of the pre-quench Hamiltonian $\mathcal{H}_{\rm cl}(g_0)$.

In this case, the only free parameter is the post-quench value of the field g. By a direct analysis of the post-quench Hamiltonian's phase portrait, one can prove that, depending on the value of g, the dynamics occurs in qualitatively different trajectories.

If the post-quench value of the field g satisfies the inequality

$$-\frac{1}{2}\big(g_{\rm cr} - g_0\big) < g < \frac{1}{2}\big(g_{\rm cr} + g_0\big), \tag{2.44}$$

the system's dynamics is constrained in the starting ferromagnetic sector of the post-quench Hamiltonian and the spin will precede around the corresponding minimum, as in the low-energy trajectories in the left panel of Fig.2.3. This behavior corresponds to the *dynamical ferromagnetic phase*, since the non-equilibrium order parameter is finite.

If on the contrary g lies outside the above interval, the system moves on a trajectory encompassing the whole phase space, and (for $|g| < g_{cr}$) encircling both the ferromagnetic minima of the post-quench Hamiltonian. This corresponds to a *dynamical paramagnetic phase*, characterized by a vanishing non-equilibrium order parameter.

Finally, in the limit cases where

$$\begin{cases} g = g_{\rm dyn} \coloneqq \dfrac{1}{2}\big(g_{\rm cr} + g_0\big), \text{ or} \\ g = \tilde{g}_{\rm dyn} \coloneqq -\dfrac{1}{2}\big(g_{\rm cr} - g_0\big) \end{cases} \tag{2.45}$$

the system moves on the classical separatrix of the post-quench Hamiltonian, located in the upper or lower hemisphere respectively. The period of the orbit diverges exponentially as $g \to g^{-}_{\rm dyn}$ or $g \to \tilde{g}^{+}_{\rm dyn}$, and the corresponding equilibrium point is only approached in the infinite-time limit.

A graphical interpretation of these different dynamical phases is given in Fig. 2.5, where for definiteness we consider pre and post-quench values of the external field such that $0 \leq g_0 < g < g_{\rm cr}$.

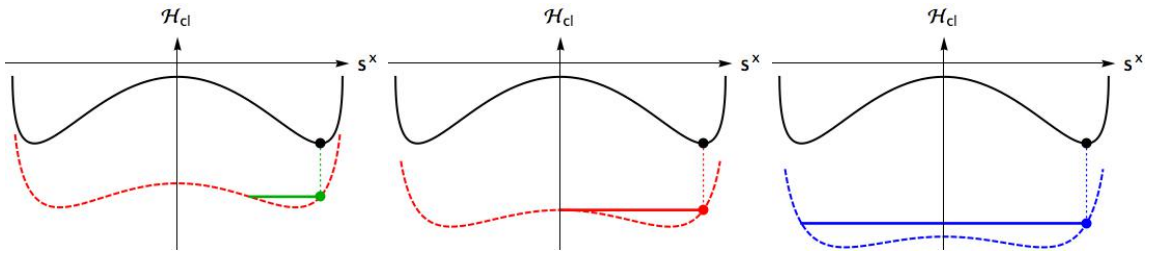

Figure 2.5: Classical energy landscapes in the half-plane $s^y \equiv 0$, $s^z > 0$, as a function of the magnetization s^x. The energy landscape of the pre-quench Hamiltonian $\mathcal{H}_{\rm cl}(g_0)$ (with $0 < g_0 < g_{\rm cr}$) is represented with a black solid line, with the system lying in a ferromagnetic minimum. The energy landscape of the post-quench Hamiltonian is displayed in a green, red or blue dashed line corresponding to increasing values of g. For a shallow quench $g_0 < g < g_{\rm dyn}$ (green) the system is in the *dynamical ferromagnetic phase*, while for a deep quench $g_{\rm dyn} < g < g_{\rm cr}$ (blue) the system is in the *dynamical paramagnetic phase*, with an orbit encircling the two post-quench minima. In the limit case $g = g_{\rm dyn}$ (red), the system moves on a branch of the separatrix, with diverging period.

In conclusion, the two dynamical critical points $g_{\rm dyn}$ and $\tilde{g}_{\rm dyn}$ separate a *dynamical ferromagnetic phase* with $\overline{\sigma^x} \neq 0$, from a *dynamical paramagnetic phase* with $\overline{\sigma^x} = 0$. In the latter, the symmetry is dynamically restored at the level of infinite-time averages. It is possible to prove with an explicit calculation that the non-equilibrium order parameter vanishes with a logarithmic singularity at the dynamical critical points, and the same type of singularity is found for the frequency of the classical orbits [3].

We remark that the equilibrium criticality and the dynamical criticality are two entirely different phenomena, with different scaling properties.

Chapter 3

Optimal control for the LMG model in the thermodynamic limit

After formulating the control problem for the LMG model in the thermodynamic limit in section 3.1, we describe a possible analytical solution in section 3.2 and illustrate a complementary numerical approach in section 3.3.

Numerical methods and direct experimental simulation are the usual ways of addressing optimal control problems for quantum systems, since analytical solutions are hardly ever feasible.

As already mentioned in the outline, only few numerical techniques of control theory are powerful and versatile enough to cope with quantum many-body systems complexity. Regarding the LMG model for finite values of N, optimal control methods [18], adiabatic evolution [19] and hybrid strategies [20] have been applied.

3.1 Formulation of the control problem

In this section we address the task of controlling the dynamics of the LMG model in the thermodynamic limit, by manipulating a time dependent transverse external field. We recall the classical Hamiltonian in canonical coordinates, given by[1]

$$\mathcal{H}_{\mathrm{cl}}(t) = -\lambda(1-(s^z)^2)\cos^2\phi - g(t)s^z. \tag{3.1}$$

In the presence of a time-dependent driving field, the energy is not conserved and thus the classical model loses its integrability.

In light of the discussion in section 2.2, the classical equations of motion generated by $\mathcal{H}_{\mathrm{cl}}(t)$ describe the quantum coherent dynamics of the initial spin-

[1] Throughout this section we shall always consider the maximal total spin sector, i.e. ρ=1.

coherent state. In the case of large but finite values of N, the initial state delocalizes on a characteristic time scale $t_{\rm Ehr}$, which diverges with the system size. As already pointed out in the previous section, we will always assume

$$T \ll t_{\rm Ehr}, \tag{3.2}$$

which allows us to neglect such decoherence effects.

The generic scenario of optimal control, in our framework, translates to: Given the initial coherent state of the system and a target coherent state (represented by points in the phase space, with vanishing spin fluctuations), determine the optimal (or a sub-optimal) protocol $g(t)$ to "reach" the target state in a fixed time T[2].

Thanks to the condition in Eq. (3.2), the final state $|\psi(T)\rangle$ is still described (to a good degree of approximation, for large but finite N) by a coherent state $|\vec{n}(T)\rangle = |\theta(T), \phi(T)\rangle$. Therefore, the fidelity with the target state is given by Eq. (A.4) and reads

$$\mathcal{F}\left(\vec{n}(T), \vec{n}_{\rm tar}\right) = |\langle \vec{n}_{\rm tar}|\vec{n}(T)\rangle|^2 = \left(\frac{1+\vec{n}_{\rm tar}\cdot\vec{n}(T)}{2}\right)^{2Ns}. \tag{3.3}$$

Accordingly, a reasonable choice for the figure of merit $\mathcal{M}$, which we shall try to minimize, is given by the non-negative quantity

$$\eta \coloneqq 1 - \vec{n}_{\rm tar}\cdot\vec{n}(T). \tag{3.4}$$

Clearly, the minimization of η is equivalent to the maximization of the fidelity; moreover, if $\eta \ll 1$, one has the relation

$$\eta \approx \frac{1}{Ns}\big|\log \mathcal{F}\left(\vec{n}_{\rm tar}, \vec{n}(T)\right)\big|. \tag{3.5}$$

We stress that the control problem formulated here is classical and consists in the control of the Hamilton equations

$$\begin{cases} \dot{s}^z = -2\lambda(1-(s^z)^2)\cos\phi\sin\phi \\ \dot{\phi} = 2\lambda s^z\cos^2\phi - g(t), \end{cases} \tag{3.6}$$

in the classical phase space.

For the sake of definiteness, we set the initial value of the external field $g(0) = 0$, so that the two symmetry-broken fully-polarized states along the x-direction correspond to the mean-field ferromagnetic ground states of the initial-time Hamiltonian $\mathcal{H}_{\rm cl}(0)$. Let us choose as initial condition for the dynamics

[2]We remark that the value of T is set a priori, and is not a free parameter of the protocol.

the spin coherent ground state with positive magnetization, given by $|\vec{n}_0\rangle = |\theta_0 = \pi/2, \phi_0 = 0\rangle$.

The target coherent state could in principle correspond to a generic point in the classical phase space. However, having fixed the x-axis by the ferromagnetic interactions, we assume to be able to set the direction of the transverse field in the ortoghonal plane. In this way we can always choose the direction of the external field, let it be z, such that the initial and final conditions both belong to the plane $s^y \equiv 0$.

The target state is then given by $|\vec{n}_{\rm tar}\rangle = |\theta_{\rm tar}, 0\rangle$ or $|\vec{n}_{\rm tar}\rangle = |\theta_{\rm tar}, \pi\rangle$, depending on whether the corresponding point in phase space was initially placed in the $s^x > 0$ or $s^x < 0$ hemisphere respectively. Let us now consider the first setting, with the initial state $|\vec{n}_0\rangle = |\theta_0 = \pi/2, 0\rangle$ and the target state $|\vec{n}_{\rm tar}\rangle = |\theta_{\rm tar}, 0\rangle$ both lying on the $\phi \equiv 0$ curve.

In addition, we choose the final value of the driving field such that the target coherent state corresponds to a mean-field ferromagnetic ground state of the final time Hamiltonian. This is accomplished by choosing $g(T) = 2\lambda \cos\theta_{\rm tar}$ [see Eq. (2.23)].

Before addressing the optimal control task, a few preliminary observations can be made, in order to gain some intuition and concurrently simplify the problem. In the first place, the points $\vec{s} = (0, 0, \pm 1)$ are stationary solutions of the Eqs. (2.31). From the uniqueness of the solution of (sufficiently good) differential equations with assigned initial conditions, it follows that it is impossible to find a protocol to exactly reach these points in a finite time.

This could be expected on physical grounds, since $\vec{s} = (0, 0, \pm 1)$ correspond to the LMG paramagnetic ground state in the thermodynamic limit, for $g > g_{\rm cr}$ and $g < -g_{\rm cr}$ respectively, while our initial condition is the ferromagnetic ground state for $g = 0$. If one tries to dynamically connect the ground states of different phases, the dynamics is severely perturbed at the quantum critical point, usually preventing the possibility of reaching the target state without the creation of defects. In the thermodynamic limit, the ferromagnetic and paramagnetic ground states are exactly mapped to phase space points, which accordingly cannot be easily connected with a finite-time protocol.

A second observation, relevant for the solution of the control problem, consists in a simple relation between the sign of $\dot{s}^z$ and the value of ϕ. Precisely, from the first equation it immediately follows that $\dot{s}^z > 0$ iff $\sin(2\phi) < 0$, which is verified in the second and fourth quadrants; on the contrary $\dot{s}^z < 0$ in the first and third quadrants. In light of this argument and for the initial condition $|\vec{n}_0\rangle = |\theta_0 = \pi/2, 0\rangle$, we expect the optimal solution to be entirely located in the first or fourth quadrant for $s^z_{\rm tar} \equiv \cos\theta_{\rm tar} < 0$ or $s^z_{\rm tar} \equiv \cos\theta_{\rm tar} > 0$ respectively.

However, as already noticed in section 2.3, the Hamilton equations (here with a time-dependent driving field, see Eqs. (3.6)) are invariant under the inversion of the field $g(t) \to -g(t)$ and concurrent reflections of the conjugated coordinates: $s^z \to -s^z$ and $\phi \to -\phi$. In light of this, we shall always consider $s^z_{\rm tar} > 0$, since any result can be immediately translated to $-s^z_{\rm tar}$, upon these reflections.

In addition, it is reasonable to ask whether the target spin coherent state could be reached in arbitrarily short times, by choosing an adequate protocol $g(t)$. It turns out that this is not the case, and there exist a minimum time $T_{\rm min}$ below which the the problem of control certainly does not admit an exact solution. This can be proven by the following simple argument.

Let us focus again on the first Hamilton equation in (3.6), which implies

$$|\dot{s}^z| = \lambda(1 - (s^z)^2)|\sin 2\phi| \leq \lambda, \tag{3.7}$$

where the last inequality follows from $|\sin 2\phi| \leq 1$ and $|s^z| \leq 1$. Accordingly, one has

$$\Big| \int_0^T dt\, \dot{s}^z \Big| \leq \int_0^T dt |\dot{s}^z| =\leq \lambda T, \tag{3.8}$$

yielding

$$T \geq \frac{|s^z_{\rm tar}|}{\lambda} \equiv \frac{|\cos\theta_{\rm tar}|}{\lambda}. \tag{3.9}$$

While this is only a lower bound on the true value of $T_{\rm min}$, it turns out to be an accurate estimate of the latter. In fact, one can calculate explicitly the exact value of $T_{\rm min}$, as we will show in section 3.3, relying on some intuition gained from numerically optimized protocols.

3.2 Double-quench protocol

In the specific case of the LMG model in the thermodynamic limit, an analytical solution to the control problem is possible at the level of the equivalent classical system, relying on the knowledge of the phase portrait for any given value of g.

The ferromagnetic phase portrait, qualitatively displayed in Fig. 3.1, suggests that it might be possible to choose a constant value of $g = \tilde{g}$, such that the initial point and the target point both lie on the same contour. If this was the case, an exact solution would be given by a double-quench protocol, consisting on two successive instantaneous quenches. The first one is at time $t = 0$, from $g(0) = 0$ to $\tilde{g}$, starting the evolution of the system along the contour connecting the initial condition to the target state; the second quench is at time $t = \tau/2$, where τ is the classical period of the selected trajectory, from the value $\tilde{g}$ to

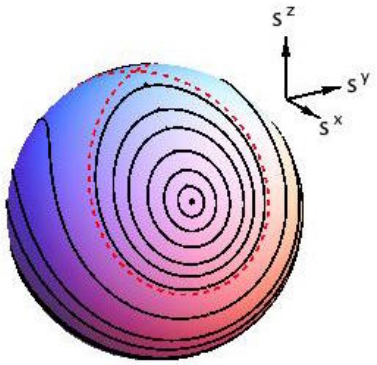

Figure 3.1: Schematic 3D representation of the phase portrait for the ferromagnetic phase, which suggests a possible analytical solution to the optimal control problem for the LMG model in the thermodynamic limit.

$g(T) = 2\lambda s^z_{\rm tar}$. The effect of the latter is to stop the dynamics at the target state, which is a minimum point of the final-time Hamiltonian $\mathcal{H}_{\rm cl}(T)$.

In the following we will show that such a $\tilde{g}$ exists for any target point, calculate its value as a function of $s^z_{\rm tar}$ and evaluate the classical period of the corresponding trajectory. We remark that this solution is valid in principle for every $T \geq \tau/2$, since the second quench stops the dynamics at the target point, but it is clearly not valid for shorter target times $T < \tau/2$. However, we anticipate that non-ideality effects arise due to the infinite steepness of the quenches, as well as if finite size effects are taken into account (this is described at the end of this section).

From the analytical expression of the contours in Eq. (2.37), one finds that the two points with $\phi = 0$ lying on the contour with energy $\mathcal{E}$ are given by

$$s^z = \frac{g \pm \left[g^2 + 4\lambda^2 + 4\lambda\,\mathcal{E}\right]^{1/2}}{2\lambda}. \tag{3.10}$$

By requiring one of these two points to be the initial condition of a fully-polarized state along x, one has $\mathcal{E} = -\lambda$ and finds

$$s^z = 0,\ \frac{g}{\lambda}\,. \tag{3.11}$$

This straightforward argument shows that for any target point ($s^z_{\rm tar} \equiv \cos\theta_{\rm tar}, 0$), one can simply choose $\tilde{g} = \lambda s^z_{\rm tar}$, finding an exact solution of the control problem. As a useful check, the value $\tilde{g}$ obviously verifies the condition in Eq. (2.44) for $g_0 = 0$, which characterizes the dynamical ferromagnetic phase.

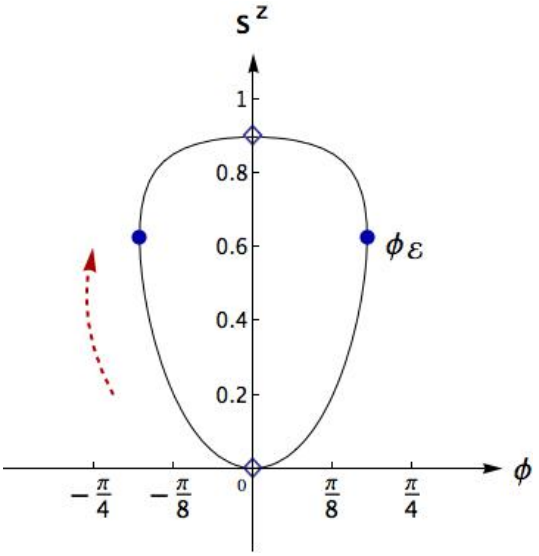

Figure 3.2: The contour connecting the initial condition with the target state $s^z_{\rm tar} = 0.9$ (both are indicated with open symbols). The latters and the turning points (see text) divide the classical orbit in four equally lasting parts. Only the left half of the orbit, lying in the fourth quadrant ($\phi < 0$), is relevant for our control problem.

The period τ of classical oscillations for a closed trajectory can be evaluated as

$$\tau = \int_{\rm contour} \frac{d\phi}{\dot\phi(\phi)} \tag{3.12}$$

with $\dot\phi(\phi)$ given by Eq. (2.38). An example is displayed in Fig.3.2, where the orbit is divided in four parts by the initial and target states (indicated with open symbols) and by the two turning points $\pm\phi_{\mathcal{E}}$ (full circles), such that $\dot\phi(\pm\phi_{\mathcal{E}}) = 0$. The red arrow indicates the direction of the motion, which is clockwise, accordingly with our previous observation on the relation between the sign of $\dot s^z$ and the value of ϕ.

By choosing the appropriate sign for $\dot\phi(\phi)$, one easily checks that all the four parts in which the orbit is divided require an equal time to be covered. This leads to

$$\tau = 4\int_0^{\phi_{\mathcal{E}}} \frac{d\phi}{\left[g^2 + 4\lambda^2\rho^2\cos^4\phi + 4\lambda\,\mathcal{E}\cos^2\phi\right]^{1/2}} \tag{3.13}$$

Moreover, an explicit calculation for the turning points yields

$$\phi_{\mathcal{E}} = \arccos\left[\sqrt{\frac{1}{2\lambda}\Big(-\mathcal{E} + \sqrt{\mathcal{E}^2 - g^2}\Big)}\right], \tag{3.14}$$

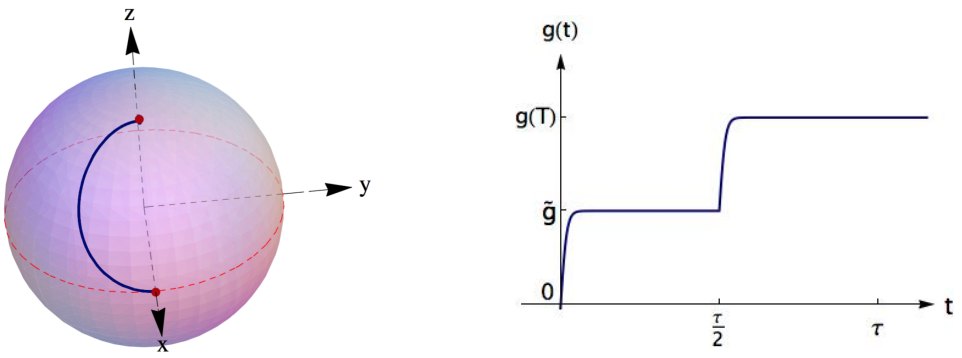

Figure 3.3: Approximate double-quench protocol for $s^z_{\rm tar} = 0.95$ and $T = 3.5\,\tau$, in the case $a = b = 10$. The initial and target points are marked with a red dot. Thanks to the steepness of the two ramps, closely resembling two ideal quenches, the system is effectively stopped at the target point. The final error is $\eta \approx 2 \times 10^{-4}$.

valid only in the ferromagnetic phase $|g| < g_{\rm cr}$ and for ferromagnetic orbits, which correspond to contours of energy $\mathcal{E}$, lying inside the range between the minimum and separatrix energies

$$-\lambda - \frac{g^2}{4\lambda} \leq \mathcal{E} \leq -|g|. \tag{3.15}$$

The corresponding value for s^z is easily checked to be

$$s^z_{\mathcal{E}} = \frac{g}{-\mathcal{E} + \sqrt{\mathcal{E}^2 - g^2}}. \tag{3.16}$$

The integral in Eq. (3.13), with the expression for $\phi_{\mathcal{E}}$ calculated in Eq. (3.14), can be evaluated numerically. One correctly verifies that $T = \tau/2$ always satisfies the lower bound in Eq. (3.9).

Let us conclude this section with two remarks. As already noted, this double-quench protocol yields an exact mathematical solution to the optimal control problem in the thermodynamic limit, which is valid only for target times $T \geq \tau/2$, leaving open the problem for $T_{\rm min} \leq T < \tau/2$. Moreover, this protocol is rather idealized, since it requires two instantaneous quenches, while any experimental realization would obviously imply non-instantaneous ramps, characterized by a finite transient.

In particular, any realistic implementation of the protocol would not drive the system to the exact target state at the exact time $\tau/2$, and therefore the second quench would not *exactly* stop the system's dynamics at the target point. As a consequence, for values of T significantly larger than $\tau/2$, the later evolution from $t = \tau/2$ to $t = T$ could result in a severe loss of control on the final state.

A possible solution to study numerically these non-idealities is to approximate the double-quench protocol with a regular function, depending on two free

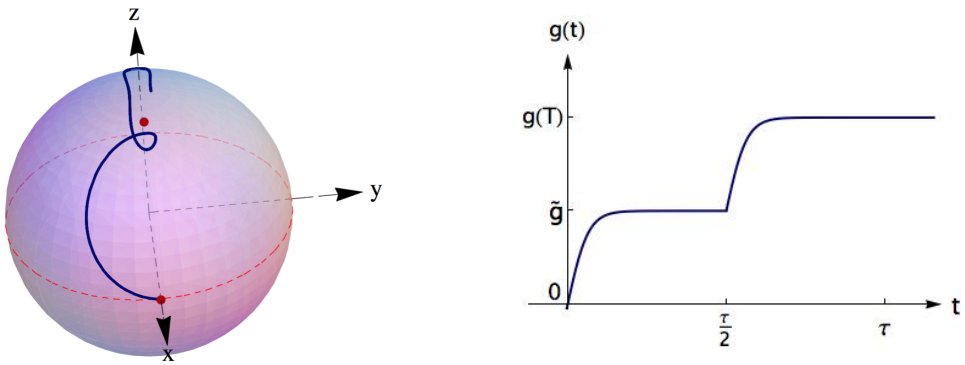

Figure 3.4: Approximate double-quench protocol for $s^z_{\text{tar}} = 0.95$ and $T = 3.5\,\tau$, in the case $a = b = 3$. The initial and target points are marked with a red dot. Note that the ramps are not steep enough, thus the protocol fails to stop the dynamics at the target point. This causes a complete loss of control over the system's dynamics for $\tau/2 < t < T$, and consequently over the final error η.

parameters that can be tuned as to vary the steepness of the two ramps. A convenient approximation for the two quenches at $t = 0$ and $t = \tau/2$ is given in terms of hyperbolic tangents

$$g(t) = \tilde{g}\tanh(a\,t) + \theta\left(t - \frac{\tau}{2}\right)(g(T) - \tilde{g})\tanh\left[b\left(t - \frac{\tau}{2}\right)\right], \tag{3.17}$$

where by increasing the values of a and b one has steeper ramps, recovering the ideal double-quench protocol in the limit $a, b \gg 1$.

This non-ideality is particularly evident when the target point is close to the point $\vec{s} = (0, 0, 1)$, as shown in Fig. 3.3 and 3.4. In both cases, we set $s^z_{\text{tar}} = 0.95$ and $T = 3.5\,\tau$; while in the first figure the ramps' steepness is set to $a = b = 10$, closely resembling the ideal double-quench protocol, in the second one we set it to $a = b = 3$. In numerical simulations we always set $\lambda = 1$, so that energies are measured in units of λ and the rescaled time $t' = t/s$ in units of λ^{-1}.[3]

As displayed in the figures, in the first case the dynamics is effectively stopped by the second quench, resulting in a small[4] error of $\eta \approx 2 \times 10^{-4}$. In contrast, in the second case the quench does not stop the dynamics, but on the contrary it makes the system evolve on a paramagnetic orbit. This clearly results in a complete loss of control over the final error η.

Another source of non-ideality arises when, instead of the rigorous thermodynamic limit, we consider large but finite values of N. In this case, the target state is an approximate mean-field ground state for the final-time Hamiltonian:

[3] As stated in the short section about notation and conventions, we always set $\hbar = 1$.

[4] We recall that the radius of the sphere is $\rho = 1$.

even if it was reached with unit fidelity at time $t = \tau/2$, the system would then undergo a further evolution until time $t = T$.

In light of the above discussion, the ideal double-quench protocol can be regarded as a stable solution only for times $T \gtrsim \tau/2$, in order to avoid later loss of control on the system, due to non-ideal ramps or finite size effects.

3.3 Numerical minimization

In this section we describe a complementary numerical approach to the optimal control task, which was formulated in section 3.1.

The minimization of the figure of merit in Eq. (3.4) is formally a functional minimization with respect to $g(t)$: even in this simplified classical setting, this is a non-trivial mathematical problem. However, we are not interested in a detailed mathematical analysis, and we use a version of the CRAB algorithm, previously described in chapter 1.

In our case the only driving field is $g(t)$, so we should start from an ansatz solution $g_0(t)$, and then apply a correction of the form

$$g(t) = g_0(t)\, c(t), \tag{3.18}$$

with the function $c(t)$ expanded in a truncated Fourier space as

$$c(t) = b(t) \left[1 + \sum_{k=1}^{N} A_k \sin(\omega_k t) + B_k \cos(\omega_k t) \right], \tag{3.19}$$

where the function $b(t)$ enforces the boundary conditions $g(0) = 0$ and $g(T) = 2\lambda s^z_{\text{tar}}$ previously discussed.

We remark that $\{A_k, B_k\}$ is the set of free parameters, while ω_k are the corresponding frequencies, whose values are fixed before the minimization. One can either choose $\omega_k = 2\pi k/T$ for each call of the minimization routine, or randomize the frequencies as $\omega_k = 2\pi k(1 + r_k)/T$, with r_k random numbers uniformly distributed in $[0, 1]$. In our case, as explained below, randomization is not necessary and we shall consider the standard harmonics. Moreover, we can simplify the standard expression in Eq. (3.19) as

$$c(t) = \left[1 + \sum_{k=1}^{N} A_k \sin(\omega_k t) \right], \tag{3.20}$$

which already satisfies the boundary conditions.

The Hamilton equations in Eq. (3.6) can be formally rewritten as

$$\begin{cases} \dot{s}^z = -2\lambda(1-(s^z)^2)\cos\phi\sin\phi \\ \dot{\phi} = 2\lambda s^z\cos^2\phi - g\big(\{A_k,B_k\};t\big), \end{cases} \tag{3.21}$$

and should be solved as a function of the free parameters $\{A_k, B_k\}$. In particular, one is interested in the final point reached at $t = T$, in order to minimize the figure of merit

$$\eta(\{A_k,B_k\}) = 1 - \vec{n}_{\rm tar}\cdot\vec{n}(\{A_k,B_k\};T). \tag{3.22}$$

As mentioned in chapter 1, it is convenient to adopt a direct search heuristic as the minimization routine. In particular, we use an algorithm known as Differential Evolution which, among other advantages, is self-organizing and requires very little input from the user [21]. Moreover, while its implementation is straightforward and requires only few lines of code, it has been shown to have comparable performances to other acclaimed direct search methods.

As a preliminary remark, in order to ease the comparison between the analytical double-quench protocol and the numerical approach discussed here, we find it natural to rescale the target time T in units of τ, where τ is the period of the orbit that connects the initial point with the target.

Regarding the ansatz solution, a reasonable choice is a linear ramp interpolating the two boundary conditions above, which is simply given by

$$g_0(t) = 2\lambda s^z_{\rm tar}\,\frac{t}{T}. \tag{3.23}$$

We observe that the linear ramp reduces to an adiabatic driving in the limit $T \gg 1/\lambda$. Consequently, for long times T, it can work reasonably well without any correction $c(t)$; on the contrary, one expects it to yield a poor solution for short values of T, thus requiring a proper correcting term. This is indeed the case, as we exemplify in Fig. 3.5, where we set $s^z_{\rm tar} = 0.9$ (corresponding to $\tau \approx 4.56$) and we compare $T/\tau = 1, 3$ and 30.

Remarkably, if one tries to evaluate a proper correction in terms of the function $c(t)$ defined in Eq. (3.20), then faces a problem similar to statistical overfitting for values $T/\tau \gtrsim 1$.

In fact, even restricting to the subspace spanned by only few free parameters $\{A_k\}$, there is in general a number of different solutions, which correspond to final values of η compatible with zero: an illustrative example is shown in Fig. 3.6 and in Fig. 3.7. In both cases we set $s^z_{\rm tar} = 0.9$, $T/\tau = 3$ and the minimization is done with respect to the free parameters $\{A_k\}_{k=1}^4$. The only difference between the two figures is the value of a random seed, which is necessary for the minimization

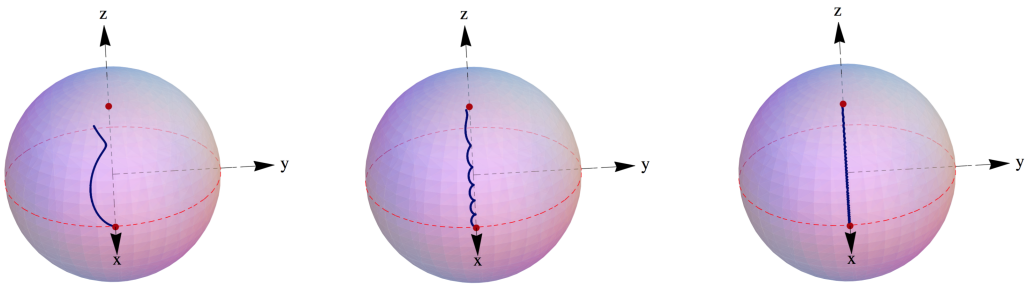

(a) $T/\tau = 1$ **(b)** $T/\tau = 3$ **(c)** $T/\tau = 30$

Figure 3.5: Comparison of classical trajectories, where the driving field $g(t)$ is given by the ansatz solution in Eq. (3.23). We set $s^z_{\rm tar} = 0.9$ and compare different values of $T/\tau = 1, 3$ and 30 from the left to right panel. The initial and target states are denoted with red points. In the left panel, the linear ramp is qualitatively not a good solution, with $\eta \approx 0.03$. In the middle panel we have $\eta \approx 9 \times 10^{-4}$, while in the right panel the final error is $\eta \approx 5 \times 10^{-5}$. In the latter case, the trajectory closely resembles an adiabatic driving.

routine. The final value of η, for both optimized protocols, is almost zero (see figures).

This hints that, if one enlarges the search space by adding more harmonics, or by randomizing the frequencies, the number of valid solutions can increase significantly.

The picture emerging from an accurate numerical analysis, carried out for different values of $s^z_{\rm tar}$ and of $T/\tau \gtrsim 1$, is that there is a plethora of possible sub-optimal solutions corresponding to values of η compatible with zero. Which solution is actually found depends on the specific parameterization of $g(t)$ (for instance on the selected harmonics), on the initial condition for the minimization routine, on the random seed ...

In brief, the optimization landscape has several local minima corresponding to final values of η close to zero. This leads to the conclusion that, for $T/\tau \gtrsim 1$, the optimization problem is utterly easy and any reasonable parametrization, combined with an efficient minimization algorithm, yields a valid solution.

This fact is related to the assumption of thermodynamic limit, which allows us to minimize only the distance between the centers of localized wave-packets, irrespectively of their (vanishing) spread and shape. In this respect, let us mention that in the proper thermodynamic limit the fidelity in Eq. (3.3) reduces to

$$\mathcal{F}\left(\vec{n}(T), \vec{n}_{\rm tar}\right) = \delta^{(2)}_{\vec{n}(T),\, \vec{n}_{\rm tar}}. \tag{3.24}$$

In the case of large but finite values of N, given that the condition $\eta \ll \frac{1}{Ns}$ is

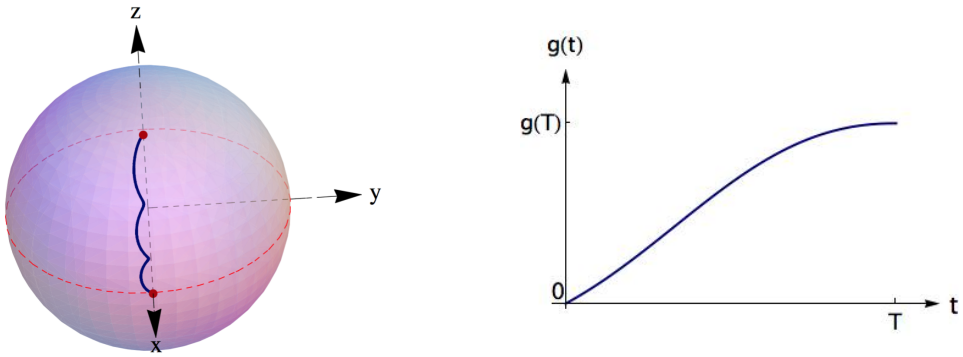

Figure 3.6: Classical trajectory and optimized driving for $s^z_{\mathrm{tar}} = 0.9$ and $T/\tau = 3$, determined numerically by minimizing Eq. (5.6) with respect to the set of free parameters $\{A_k\}_{k=1}^4$. The coordinate $s^z(t)$ increases monotonically in $[0, T]$, and the final error is compatible with zero (of the order of $\eta \approx 1 \times 10^{-8}$).

fulfilled, one has

$$\mathcal{F}\left(\vec{n}_{\mathrm{tar}}, \vec{n}(T)\right) \approx 1 - Ns\,\eta. \tag{3.25}$$

However, this estimate of the fidelity relies on the assumption that decoherence effects as well as wave-packet squeezing can be neglected.

Despite the large number of valid solutions, one could be interested in defining a proper criterion of "simplicity" of the latters, the reason being that a driving such as the one in Fig. 3.7 is clearly inconvenient for any realistic implementation. A first possibility could be solving the optimal control problem together with the condition $\sin(2\phi) < 0$ or $\sin(2\phi) > 0$, which corresponds to $\dot{s}^z > 0$ and $\dot{s}^z < 0$ respectively, depending on s^z_{tar} being positive or negative.

However, solving Eqs. (3.21) as function of the free parameters and together with this constraint is quite intricate.

An easier approach is to think of a generalized ansatz solution, depending on few free parameters, which yields reasonably simple drivings and in particular reduces to the adiabatic protocol in the limit $T \gg 1/\lambda$.

It turns out that a valid trial solution is given by

$$g_{\mathrm{tr}}(a, t_0; t) = \alpha + \beta \tanh\left[a(t - t_0)\right], \tag{3.26}$$

where a and t_0 are free parameters, while the coefficients α and β are fixed in order to satisfy the usual boundary conditions, and are given by

$$\begin{cases} \alpha = \dfrac{2\lambda s^z_{\mathrm{tar}} \tanh(a\,t_0)}{\tanh(a\,t_0) + \tanh[a\,(T - t_0)]} \\ \beta = \dfrac{2\lambda s^z_{\mathrm{tar}}}{\tanh(a\,t_0) + \tanh[a\,(T - t_0)]}. \end{cases} \tag{3.27}$$

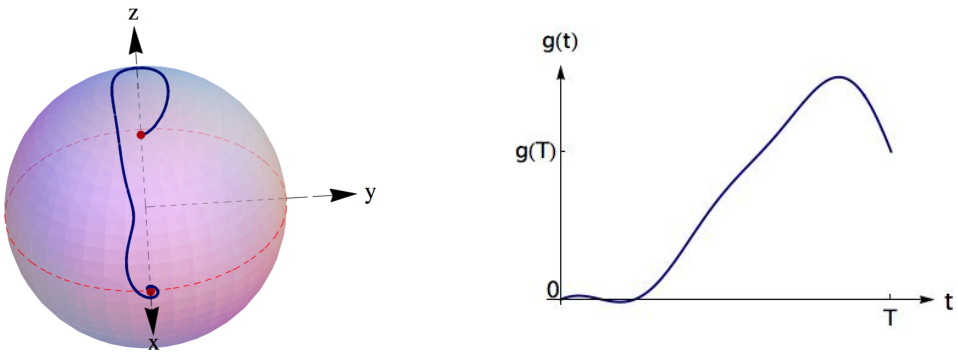

Figure 3.7: The same as in Fig. 3.6, where the only difference is the choice of the random seed required by the minimization algorithm. In this case, the coordinate $s^z(t)$ does not increase monotonically in $[0, T]$. Even though the error is, also in this case, compatible with zero ($\eta \approx 7 \times 10^{-10}$), this is clearly an inconvenient solution for any realistic setting.

Obviously, there is some reasoning behind this trial solution, which we now shortly outline. The underlying idea is that a simple generalization of the linear ramp consists in a ramp of tunable steepness a, with starting time t_0, which is precisely described by Eq. (3.26). We note that $g_{\rm tr}(a, t_0; t)$ is an even function of a, so that we can restrict the search space to $(a, t_0) \in [0, a_{\rm max}] \times [0, T]$, where $a_{\rm max}$ is a cutoff value.

In the limit $a \gg 1$ one finds an instantaneous quench at time t_0, while for $t_0 = 0$ and $a \to 0^+$ one recovers the linear ramp interpolating the boundary conditions, and thus in particular the adiabatic solution for large values of T.

A systematic study for different values of $s^z_{\rm tar}$ and $T/\tau \gtrsim 1$ shows that this ansatz solution (or some straightforward generalizations, for instance including more than one ramp) are sufficient to obtain values of η compatible with zero. In addition, the simplicity of the parameterization guarantees to find trajectories such that $s^z(t)$ increases (or decreases) monotonically in $[0, T]$. An example of this optimized trial solution with the corresponding trajectory is shown in Fig. 3.8.

Let us remark that the ansatz solution in Eq. (3.26) could be easily generalized, for instance by subdividing it in more ramps at different times $t_0, t_1, \ldots$ and with different steepness $a_0, a_1, \ldots$, resulting in more free parameters for the minimization.

As already stated, the minimization problem is trivial for $T/\tau \gtrsim 1$, in the sense that not only an (idealized) analytical solution exists (see section 3.2), but also the optimization problem can easily be solved numerically by choosing a reasonable parameterization for $g(t)$.

The situation changes dramatically for $T/\tau < 0.5$: not only the analytical

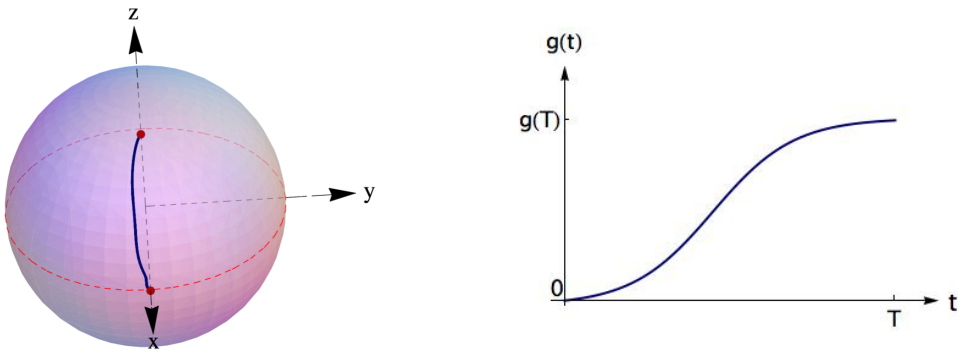

Figure 3.8: An example of the trial solution defined in Eq. (3.26), optimized with respect to a, t_0. We set $s^z_{\text{tar}} = 0.9$ and of $T/\tau = 3$, for comparison with Fig. 3.6 and Fig. 3.7. The error is still compatible with zero ($\eta \approx 2 \times 10^{-9}$), but the corresponding trajectory is simpler, in particular characterized by a monotonic $s^z(t)$ in $[0, T]$.

solution is no longer valid, but also finding a good numerical solution becomes a non-trivial task[5]. A simple parametrization, like the one in Eq. (3.26), does not generally provide a valid solution anymore, so we actually exploit the CRAB technique; we use a correction in the form of Eq. (3.20), with the linear ramp ansatz in Eq. (3.23).

In order to get a qualitative idea of the CRAB algorithm convergence, in Fig. 3.9 we show the optimized $g(t)$ for $s^z_{\text{tar}} = 0.9$ and $T/\tau = 0.4$: from the left to the right panel we consider $n = 0, 2, 4$ harmonics added to the linear ramp. Moreover, in Fig. 3.10 we show the case $n = 6$, with the corresponding optimized driving.

In contrast with the previously considered case of $T/\tau \gtrsim 1$, now the optimized solution with respect to a given set of parameters is unique, in the sense that it does not depend on the choice of the initial condition for the minimization routine, neither on the random seed. Moreover, qualitatively similar solutions are usually found if different parameterizations are chosen.

Interestingly, the classical trajectory shown in Fig. 3.10 may suggest that in order to speed up the evolution, it is convenient to "move away from the $\phi = 0$ meridian and then come back to it". This intuition is correct, and gives some insight in order to determine the exact value of T_{min}, as anticipated in section 3.1. As a preliminary step, let us rewrite the Hamilton equations (3.6) as

$$\begin{cases} \dot{s}^z = -\lambda(1 - (s^z)^2) \sin 2\phi \\ \dot{\phi} = \lambda s^z (1 + \cos 2\phi) - g(t). \end{cases} \tag{3.28}$$

[5]The region $0.5 < T/\tau < 1$ is characterized by a crossover between the two regions.

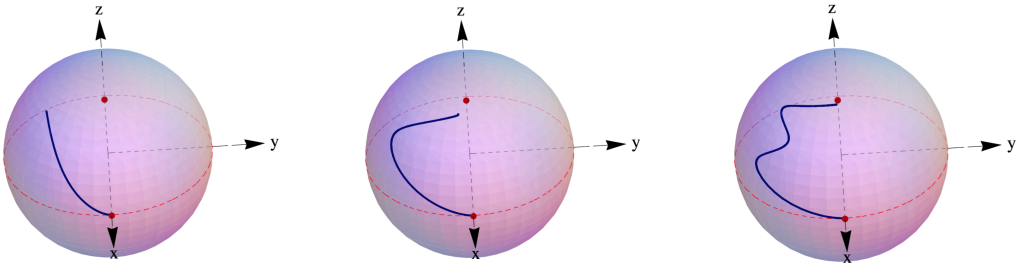

(a) $n = 0$ **(b)** $n = 2$ **(c)** $n = 4$

Figure 3.9: Comparison of classical trajectories, for $s^z_{\text{tar}} = 0.9$ and $T/\tau = 0.4$. In the left panel we show the trajectory corresponding to the linear ansatz, which clearly fails in reaching the target state. In the central and right panel $n = 2, 4$ harmonics are added respectively, but the subspace of protocols spanned by these parameterizations is not sufficiently large, in order to obtain values of η compatible with zero.

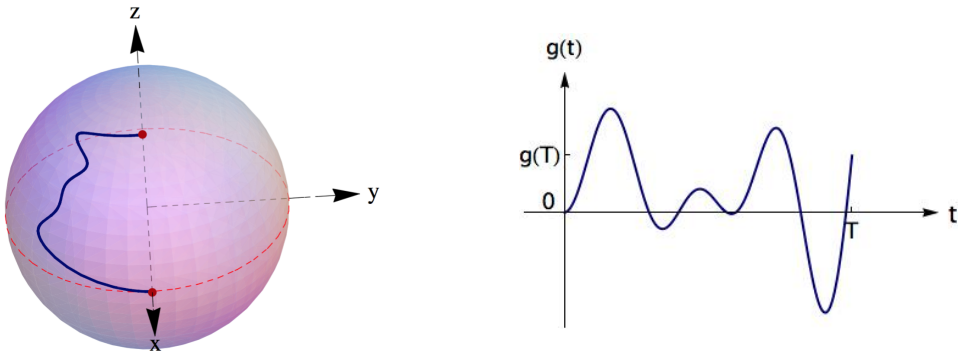

Figure 3.10: Classical trajectory for $n = 6$ harmonics and the corresponding optimized driving. Six harmonics are enough to obtain a final error compatible with zero ($\eta \approx 2 \times 10^{-8}$).

As noted in section 2.3, in the limit $|g| \gg \lambda$, the system precedes around the s^z axis with angular frequency $\omega = |g|$ (thus with vanishing period in the large $|g|$ limit), and the rotation is CW (CCW) for $g > 0$ ($g < 0$).

In addition, the first Hamilton equation above suggests that in order to maximize the value of $\dot{s}^z$, one would like to have $\phi(t) \equiv -\pi/4$ (for positive values of s^z_{tar})[6]. The second equation shows that $\dot{\phi} = 0$ iff $g(t) = \lambda s^z(t)(1 + \cos 2\phi(t))$, which for $\phi(t) \equiv -\pi/4$ reduces to $g(t) = \lambda s^z(t)$.

If one combines these two observations, then realizes that there exists a unique *ideal* protocol, which drives the system to the target state in the fastest way possible. By determining this protocol, we will concurrently find the exact

[6] All the forthcoming treatment holds also for $s^z_{\text{tar}} < 0$, simply by inverting the driving field and by applying reflections on the conjugated coordinates, as stated in section 3.1.

value of $T_{\min}$.

Let us consider the driving

$$\tilde{g}(t) = \begin{cases} g_0, & \text{for } 0 < t \leq t_0 \\ \lambda s^z(t), & \text{for } t_0 < t \leq t_0 + t_1 \\ -g_0, & \text{for } t_0 + t_1 < t \leq 2t_0 + t_1, \end{cases} \tag{3.29}$$

where $g_0 \gg \lambda$ is a strong positive field. This driving protocol first rotates the system (CW) from the initial state to $(s^z = 0, \phi = -\pi/4)$ in a time $t_0 = \pi/4g_0$, which can be made arbitrarily small by choosing a large value of g_0. Then the system is driven along the meridian $\phi = -\pi/4$ up to $(s^z_{\text{tar}}, \phi = -\pi/4)$ in a time t_1, and is finally rotated back (CCW) to the target state in a time t_0.

Clearly, one still has to determine both $s^z(t)$ and the value of t_1, which can be done by solving the first Hamilton equation with $\phi(t) \equiv -\pi/4$:

$$\dot{s}^z = \lambda(1 - (s^z)^2). \tag{3.30}$$

This is readily done by variable separation as

$$\int_0^{s^z} \frac{dz}{\lambda(1 - z^2)} = \int_0^t dt', \tag{3.31}$$

which yields

$$t = \frac{1}{2\lambda} \log \frac{1 + s^z}{1 - s^z}, \tag{3.32}$$

and finally, with a trivial inversion,

$$s^z(t) = \tanh(\lambda t). \tag{3.33}$$

By imposing $s^z = s^z_{\text{tar}}$ in Eq. (3.32), one also determines the value of t_1, which is given by

$$t_1 = \frac{1}{2\lambda} \log \frac{1 + s^z_{\text{tar}}}{1 - s^z_{\text{tar}}}. \tag{3.34}$$

As already noticed, the value of t_0 can be made arbitrarily small, so we conclude that the shortest time possible to reach the target state is

$$T_{\min} = t_1 = \frac{1}{2\lambda} \log \frac{1 + s^z_{\text{tar}}}{1 - s^z_{\text{tar}}}. \tag{3.35}$$

This is accomplished with the driving

$$\tilde{g}(t) = \begin{cases} g_0, & \text{for } 0 < t \leq t_0 \\ \lambda \tanh[\lambda(t - t_0)], & \text{for } t_0 < t \leq t_0 + t_1 \\ -g_0, & \text{for } t_0 + t_1 < t \leq 2t_0 + t_1, \end{cases} \tag{3.36}$$

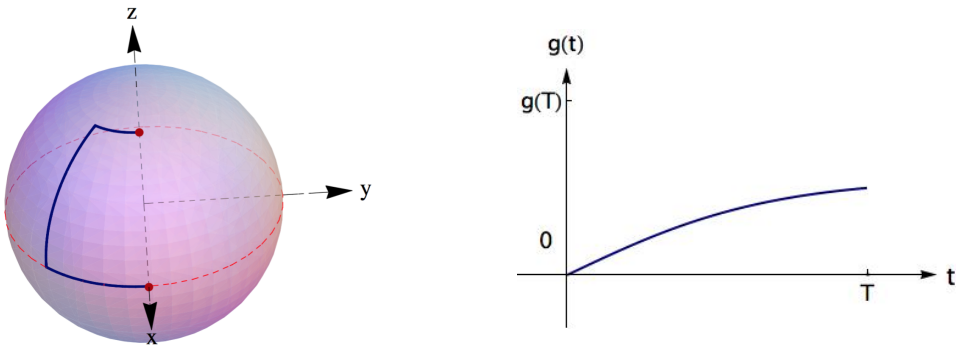

Figure 3.11: Classical trajectory corresponding to the ideal protocol defined in Eq. (3.36) in the limit $g_0 \to \infty$. In this limit, the time t_0 necessary for the initial and final rotations vanishes, while the central part of the driving is shown in the right panel.

with $g_0 \to \infty$ and thus for vanishing t_0 . The classical trajectory corresponding to this protocol is shown in Fig. 3.11, together with the central part of the driving, for $t \in (t_0, t_0 + t_1]$.

Looking back at Fig. 3.10, one clearly recognizes the qualitative features of the ideal trajectory shown in Fig. 3.11.

In conclusion, we plot in Fig. 3.12 the exact value of $T_{\min}$ as a function of s^z_{tar}, together with the estimate given in section 3.1 [see Eq. (3.9)].

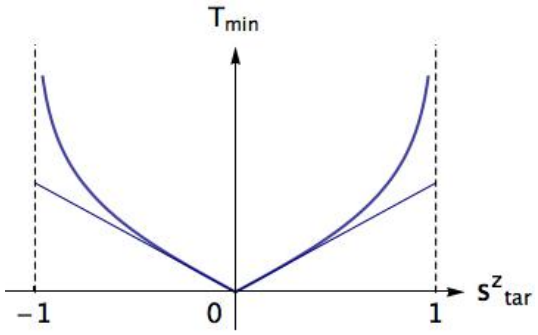

Figure 3.12

Figure 3.13: Minimum time $T_{\min}$ that is necessary to reach the target state, which is given by Eq. (3.35), together with the linear estimate of Eq. (3.9). Clearly, the exact result is a stronger lower bound for T. In the limit of $s^z_{\rm tar} \to 0$ the two values coincide, while the exact $T_{\min}$ diverges logarithmically for $s^z_{\rm tar} \to \pm 1$.

Chapter 4

Perturbation of the LMG model

In this chapter we aim to understand the impact of small perturbations on the LMG model Hamiltonian in Eq. (2.2). This is crucial, considering that the fully-connected Ising model is not usually sufficient to describe realistic features of quantum many-body systems with long-range interactions.

We describe perturbations in the form of additional spatially-decaying longitudinal interactions,

$$H = -\frac{\lambda}{N}\sum_{\mathbf{r},\mathbf{r}'}\sigma^x_{\mathbf{r}}\sigma^x_{\mathbf{r}'} - g\sum_{\mathbf{r}}\sigma^z_{\mathbf{r}} - \sum_{\mathbf{r},\mathbf{r}'}J_{|\mathbf{r}-\mathbf{r}'|}\sigma^x_{\mathbf{r}}\sigma^x_{\mathbf{r}'}, \tag{4.1}$$

where $\mathbf{r}$ runs over a generic d-dimensional lattice sites. The coupling J_r decays to zero, upon increasing the geometrical distance $r = |\mathbf{r} - \mathbf{r}'|$, and can represent short-range as well as long-range perturbations.

In order to study the physics of the perturbed LMG model in Eq. (4.1), we will use a time-dependent spin-wave theory, recently introduced in [2], [3].

In section 4.1 we review the Holstein–Primakoff transformation, which is used to determine the spectrum of lowest excitations for the LMG model in section 4.2. This is relevant in order to fix the notation and to introduce some basic concepts, which are necessary for the description of the spin-wave theory in section 4.3. Some derivations regarding spin-wave theory are discussed in appendix B.

In sections 4.4 and 4.5 we study the impact of perturbations on the equilibrium and dynamical properties of the LMG model.

Finally, in section 4.6, we go back to the unperturbed LMG model and specialize our general results for that case. In this way, we highlight the uniformity of formalism and methods with the most general case of non-zero perturbations.

4.1 Holstein–Primakoff transformation

The Holstein–Primakoff transformation is an exact mapping from boson creation and annihilation operators to angular momentum operators. Beside the intrinsic interest of such mapping, it is useful to generate approximate calculation schemes.

Let us introduce generic angular momentum operators J^α, satisfying the usual commutation relations

$$\left[J^\alpha, J^\beta\right] = i\epsilon^{\alpha\beta\gamma} J^\gamma. \tag{4.2}$$

We fix the quantum number j, which determines the eigenvalue $j(j+1)$ of the total angular momentum operator J^2, and focus our attention on the $(2j+1)$-dimensional Hilbert subspace, spanned by the eigenstates $\{|j, j_z\rangle\}$ for $j_z = -j, \ldots, j$.

The physical intuition behind the Holstein–Primakoff transformation is to map the fully-polarized state $|j, j_z = j\rangle$ to the vacuum bosonic state $|0\rangle$ for a set of boson operators $a, a^\dagger$, with $\left[a, a^\dagger\right] = 1$.

States with lower z-projection of angular momentum are mapped to excited states of the bosonic field in the following way:

$$|j, j_z = j - n\rangle \to |n\rangle \equiv \frac{1}{\sqrt{n!}} (a^\dagger)^n |0\rangle\,, \tag{4.3}$$

so that each boson excitation corresponds to a lowering of the eigenvalue of J^z by one (in units of $\hbar$).

We are now led to rewrite the angular momentum operators J^α as functions $\tilde{J}^\alpha(a, a^\dagger)$ of the boson operators, in such a way that the action of this new operators on $|n\rangle$ be the same as the action of J^α on the state $|j, j_z = j - n\rangle$. This is straightforward for the z-projection of the angular momentum:

$$J^z \to \tilde{J}^z := j - a^\dagger a = j - \hat{n}, \tag{4.4}$$

where $\hat{n}$ is the number operator counting bosonic excitations.

To work out analogous expressions for the operators J^x, J^y it is first convenient to introduce the linear combinations $J^\pm = J^x \pm i J^y$, which act as raising and lowering operators with respect to the spectrum of J^z, without affecting the spectrum of J^2. As known from the angular momentum theory:

$$J^\pm |j, j_z\rangle = \sqrt{j(j+1) - j_z(j_z \pm 1)}\, |j, j_z \pm 1\rangle \tag{4.5}$$

Considering $j_z = j - n$ as in Eq. (4.3), it is rather easy to show that the correct identifications in the above mentioned sense are

$$\begin{cases} J^+ \to \tilde{J}^+ := \sqrt{2j - a^\dagger a}\; a \\ J^- \to \tilde{J}^- := a^\dagger \sqrt{2j - a^\dagger a}, \end{cases} \tag{4.6}$$

which immediately yield the correct expression for $\tilde{J}^x$ and $\tilde{J}^y$.

A doubt might arise, since the dimension of the angular momentum subspace with fixed j is finite and equal to $2j+1$, while the boson operators act on an infinite-dimensional Fock space. In fact, the effectiveness of the Holstein–Primakoff transformation resides precisely in a mathematically consistent truncation of the infinite-dimensional Fock space, to a finite-dimensional subspace of dimension $2j+1$.

This can be checked immediately since for $n = 0$

$$J^+ \left|j, j_z = j\right\rangle = 0 \rightarrow \tilde{J}^+ \left|n = 0\right\rangle = 0 \tag{4.7}$$

and for $n = 2j$

$$J^- \left|j, j_z = -j\right\rangle = 0 \rightarrow \tilde{J}^- \left|n = 2j\right\rangle = 0. \tag{4.8}$$

It is also easily verified a posteriori that the new operators $\tilde{J}^\alpha$ satisfy the correct angular momentum commutation relations. Consequently, the operators $\tilde{J}^\alpha$ identify completely with the operators J^α, and there is no need to maintain a distinct notation anymore.

The Holstein–Primakoff transformation is particularly useful if $j \gg 1$, so that the square roots can be expanded as Taylor series in the parameter $1/\sqrt{j}$. We shall consider only the leading order in this expansion, which amounts to the subsequent approximation:

$$\begin{cases} J^+ = \sqrt{2j}\ a + \mathcal{O}(1/\sqrt{j}) \approx \sqrt{2j}\ a \\ J^- = \sqrt{2j}\ a^\dagger + \mathcal{O}(1/\sqrt{j}) \approx \sqrt{2j}\ a^\dagger. \end{cases} \tag{4.9}$$

To the same degree of approximation one can write

$$\begin{cases} J^x \approx \sqrt{j}(a + a^\dagger)/\sqrt{2} \equiv \sqrt{j}\ q \\ J^y \approx i\sqrt{j}(a^\dagger - a)/\sqrt{2} \equiv \sqrt{j}\ p \end{cases}, \tag{4.10}$$

where the operators q and p, defined in terms of the boson operators, satisfy the canonical commutation relation $[q, p] = i$.

However, this approximation should be handled with care. In fact, now the Hilbert space is not correctly truncated anymore. This is evident by substituting the approximate expressions in Eq. (4.9) in place of $\tilde{J}^\pm$ in Eq. (4.7) and in Eq. (4.8) respectively. The first one is still valid, but the second one does not hold anymore.

This is related to the physical meaning of this approximation, which is actually an harmonic approximation, where the raising and lowering angular momentum operators $J^\pm$ are simply identified with the annihilation and creation operators respectively. While the lowering operator does annihilate the vacuum

state $|0\rangle$, there is no reason why the creation operator should annihilate the excited state $|n = 2j\rangle$. Since j is large by hypothesis, this fact is not a problem if we limit to the description of lowest excitations of the bosonic field.

In conclusion, we remark that Eq. (4.4) still holds exactly, and can be rewritten in terms of the operators q and p as

$$J^z = j - a^\dagger a = j - \frac{q^2 + p^2 - 1}{2}, \tag{4.11}$$

where $\hat{n} := \frac{q^2+p^2-1}{2}$ is the familiar expression for the number operator in terms of canonical operators.

4.2 Lowest excitations of the LMG model

In this section we will use the Holstein–Primakoff transformation in order to describe the spectrum of the lowest excitations above the ground state, for the LMG model in the large N limit. This is an interesting application of the formalism described in the previous section, and we can also introduce some notation that will be adopted for the spin-wave theory.

Let us focus on the rescaled LMG Hamiltonian in Eq. (2.6), which we rewrite here for convenience:

$$\mathcal{H} := \frac{H}{N} = -\lambda\,(\mathcal{S}^x)^2 - g\,\mathcal{S}^z. \tag{4.12}$$

The lowest excitations above the ground state physically account for the quantum fluctuations of the collective degree of freedom $\vec{\mathcal{S}}$ around its average value. These excitations are finite-size corrections to the thermodynamic limit, or equivalently semiclassical corrections to the classical limit[1].

In more detail, the description of the lowest *harmonic* excitations above the ground state corresponds to the leading order $\mathcal{O}(\hbar_{\text{eff}})$ of the semiclassical expansion, as we now show explicitly. Let us consider a large but finite number of spins N, alias a small but finite value of $\hbar_{\text{eff}}$. Since $\left|\vec{J}\right|^2$ is a constant of motion, we refer to a sector with fixed (extensive) value of the total spin magnitude, identified by the quantum number

$$j \equiv Ns\rho, \tag{4.13}$$

see definition (2.9).

[1] We highlighted in section 2.3 that the thermodynamic limit of the LMG model corresponds to its classical limit. In an analogous fashion, first order finite-size corrections correspond to first order quantum correction.

We begin with the paramagnetic phase $g > g_{cr}$, in which the non-degenerate ground state is a fully-polarized state along z. Since the collective degree of freedom is aligned in the z-direction, we can straightforwardly apply the Holstein–Primakoff transformation.

The value of j is extensive in N and we are only interested in the lowest excitations, we can use the harmonic approximation in Eq. (4.10) and in Eq. (4.11). From the definition of the collective degree of freedom $\vec{\mathcal{S}}$ in Eq. (2.5), the harmonic Holstein–Primakoff approximation reads

$$\begin{cases} \mathcal{S}^x \approx (\sqrt{\rho}/\sqrt{Ns})\ \tilde{q}_0 = \sqrt{\rho\ \hbar_{\text{eff}}}\ \tilde{q}_0 \\ \mathcal{S}^y \approx (\sqrt{\rho}/\sqrt{Ns})\ \tilde{p}_0 = \sqrt{\rho\ \hbar_{\text{eff}}}\ \tilde{p}_0 \\ \mathcal{S}^z = \rho - (\tilde{q}_0^2 + \tilde{p}_0^2 - 1)/(2Ns) = \rho - \hbar_{\text{eff}}\,\hat{n}_0, \end{cases} \tag{4.14}$$

where the operators $\tilde{q}_0$, $\tilde{p}_0$ describe fluctuations of the collective $k = 0$ mode away from the z-axis, in directions x and y respectively[2].

By substitution of these approximate expressions in the Hamiltonian in Eq. (4.12), one finds

$$\mathcal{H} = -\lambda\rho\hbar_{\text{eff}}\ \tilde{q}_0^2 - g\rho + g\hbar_{\text{eff}}\ (\tilde{q}_0^2 + \tilde{p}_0^2 - 1)/2 + \mathcal{O}(\hbar_{\text{eff}}^2), \tag{4.15}$$

By exploiting the transformation

$$\begin{cases} \tilde{q}_0 = \left(\dfrac{g}{g - g_{\text{cr}}}\right)^{1/4} \dfrac{b_0^\dagger + b_0}{\sqrt{2}} \\ \tilde{p}_0 = i\left(\dfrac{g}{g - g_{\text{cr}}}\right)^{-1/4} \dfrac{b_0^\dagger - b_0}{\sqrt{2}}, \end{cases} \tag{4.16}$$

the Hamiltonian in Eq. (4.15) is readily rewritten in the standard form

$$\mathcal{H}_> \approx -g\left(\rho + \frac{\hbar_{\text{eff}}}{2}\right) + \hbar_{\text{eff}}\,\omega_>\left(\hat{m}_0 + \frac{1}{2}\right), \tag{4.17}$$

where we defined the number operator $\hat{m}_0 \coloneqq b_0^\dagger b_0$, $\omega_> \coloneqq \sqrt{g(g - g_{cr})}$ and neglected higher order corrections.

The first term represents the classical ground state energy with first order corrections, while the second one is the quadratic Hamiltonian, describing harmonic excitations above the paramagnetic ground state. The latter term includes a zero point energy contribution, which takes into account the energy increase

[2]We adopt here the tilde symbol, for consistency with the more general notation that will be later introduced in chapter 4, where we shall expand in quantum fluctuations also the modes $k \neq 0$.

due to quantum fluctuations of the collective spin around the classical minimum configuration.

We note that in the vacuum state of the oscillator, the first order semiclassical correction lowers the classical energy minimum, since

$$\mathcal{E}^0_> = \frac{E^0_>}{N} = -g\rho + \frac{\hbar_{\rm eff}}{2}\,(\omega_> - g) + \mathcal{O}(\hbar^2_{\rm eff}), \tag{4.18}$$

where the second term is evidently negative.

It is crucial not to confuse the number operator $\hat{n}_0 = (\tilde{q}_0^2 + \tilde{p}_0^2 - 1)/2$, which counts the number of zero-mode excitations of the collective spin, with the number operator $\hat{m}_0 = b_0^\dagger b_0$, which we have just introduced to count the number of lowest harmonic excitations above the paramagnetic ground state. In this respect, let us note that in the ground state of the Hamiltonian in Eq. (4.15), one clearly has $\langle \hat{m}_0 \rangle = 0$, while it is not difficult to show that

$$\langle \hat{n}_0 \rangle = \frac{1}{4}\left(\frac{g}{g - g_{\rm cr}}\right)^{1/2}\left[1 - \left(\frac{g}{g - g_{\rm cr}}\right)^{-1/2}\right]^2. \tag{4.19}$$

The average value of collective spin excitations in the paramagnetic ground state thus depends on the value of the external field $g > g_{\rm cr}$. In particular, for strong fields $g \gg g_{\rm cr}$ one has $\langle \hat{n}_0 \rangle \approx 0$, while in the limit $g \to g^+_{\rm cr}$, the average number of excitations diverges with exponent 1/2:

$$\langle \hat{n}_0 \rangle \sim \frac{1}{4}\left(\frac{g}{g - g_{\rm cr}}\right)^{1/2}. \tag{4.20}$$

Remarkably, this invalidates the Holstein–Primakoff harmonic approximation at the quantum critical point $g_{\rm cr}$.

We now examine the ferromagnetic phase $g < g_{cr}$, in which the ground state is two-fold degenerate, corresponding to the minima of the classical Hamiltonian for $(\theta^*, 0)$ and (θ^*, π), with θ^* defined in Eq. (2.23). The spectra of lowest excitations above the ferromagnetic ground states are identical by symmetry, so we can restrict to the minimum occurring in $(\theta^*, 0)$.

The Holstein–Primakoff transformation and the subsequent harmonic approximation can be generalized for a collective degree of freedom pointing in arbitrary direction in space. While conceptually this is just an obvious generalization, technically it requires some manipulations, which we now explain.

As a first step, we introduce a rotated reference frame $\mathcal{R}$ with Z-direction aligned with the average collective degree of freedom $\langle \vec{\mathcal{S}} \rangle$. The new frame components $(\hat{X}, \hat{Y}, \hat{Z})$ are parametrized as follows in the original reference frame

$(\hat{x}, \hat{y}, \hat{z})$:

$$\hat{X} \equiv \begin{pmatrix} \cos\theta\cos\phi \\ \cos\theta\sin\phi \\ -\sin\theta \end{pmatrix}, \hat{Y} \equiv \begin{pmatrix} -\sin\phi \\ \cos\phi \\ 0 \end{pmatrix}, \hat{Z} \equiv \begin{pmatrix} \sin\theta\cos\phi \\ \sin\theta\sin\phi \\ \cos\theta \end{pmatrix}, \tag{4.21}$$

where θ and ϕ are the familiar polar angles in the original frame. We decompose the operator $\vec{\mathcal{S}}$ on the basis corresponding to $\mathcal{R}$ as

$$\vec{\mathcal{S}} = \hat{X}\,\mathcal{S}^X + \hat{Y}\,\mathcal{S}^Y + \hat{Z}\,\mathcal{S}^Z, \tag{4.22}$$

and accordingly we rewrite the rescaled Hamiltonian (4.12) as

$$\begin{aligned} \mathcal{H} = &-\lambda[(\hat{X}\cdot\hat{x})\mathcal{S}^X + (\hat{Y}\cdot\hat{x})\mathcal{S}^Y + (\hat{Z}\cdot\hat{x})\mathcal{S}^Z]^2 \\ &-g[(\hat{X}\cdot\hat{z})\mathcal{S}^X + (\hat{Y}\cdot\hat{z})\mathcal{S}^Y + (\hat{Z}\cdot\hat{z})\mathcal{S}^Z]. \end{aligned} \tag{4.23}$$

In the rotated frame $\mathcal{R}$, we can now resort to the standard Holstein–Primakoff transformation used before, which we immediately write in the harmonic approximation:

$$\begin{cases} \mathcal{S}^X \approx (\sqrt{\rho}/\sqrt{Ns})\ \tilde{q}_0 = \sqrt{\rho\ \hbar_{\text{eff}}}\ \tilde{q}_0 \\ \mathcal{S}^Y \approx (\sqrt{\rho}/\sqrt{Ns})\ \tilde{p}_0 = \sqrt{\rho\ \hbar_{\text{eff}}}\ \tilde{p}_0 \\ \mathcal{S}^Z = \rho - (\tilde{q}_0^2 + \tilde{p}_0^2 - 1)/(2Ns) = \rho - \hbar_{\text{eff}}\,\hat{n}_0. \end{cases} \tag{4.24}$$

If we now substitute the polar coordinates $(\theta^*, 0)$ of the classical minimum in Eq. (4.21), we find

$$\hat{X} \equiv \begin{pmatrix} \cos\theta^* \\ 0 \\ -\sin\theta^* \end{pmatrix}, \hat{Y} \equiv \begin{pmatrix} 0 \\ 1 \\ 0 \end{pmatrix}, \hat{Z} \equiv \begin{pmatrix} \sin\theta^* \\ 0 \\ \cos\theta^* \end{pmatrix}, \tag{4.25}$$

which finally implies

$$\begin{aligned} \mathcal{H} = &-\lambda\big[\cos(\theta^*)\sqrt{\rho\ \hbar_{\text{eff}}}\,\tilde{q}_0 + \rho\sin(\theta^*) - \sin(\theta^*)\hbar_{\text{eff}}(\tilde{q}_0^2 + \tilde{p}_0^2 - 1)/2\big]^2 \\ &-g\big[-\sin(\theta^*)\sqrt{\rho\ \hbar_{\text{eff}}}\,\tilde{q}_0 + \rho\cos(\theta^*) - \cos(\theta^*)\hbar_{\text{eff}}(\tilde{q}_0^2 + \tilde{p}_0^2 - 1)/2\big]. \end{aligned} \tag{4.26}$$

In order to obtain an harmonic approximation, it is sufficient to retain terms of $\mathcal{O}(\hbar_{\text{eff}})$ in the previous expression; with the transformation

$$\begin{cases} \tilde{q}_0 = \left(\dfrac{g_{\text{cr}}^2}{g_{\text{cr}}^2 - g^2}\right)^{1/4} \dfrac{b_0^\dagger + b_0}{\sqrt{2}} \\ \tilde{p}_0 = i\left(\dfrac{g_{\text{cr}}^2}{g_{\text{cr}}^2 - g^2}\right)^{-1/4} \dfrac{b_0^\dagger - b_0}{\sqrt{2}}, \end{cases} \tag{4.27}$$

one finds

$$\mathcal{H}_< \approx -\left(\frac{g^2}{4\lambda} + \lambda\rho^2 + \lambda\rho\hbar_{\text{eff}}\right) + \hbar_{\text{eff}}\,\omega_<\left(\hat{m}_0 + \frac{1}{2}\right), \tag{4.28}$$

where $\hat{m}_0 \coloneqq b_0^\dagger b_0$, $\omega_< \coloneqq \sqrt{(g_{cr}^2 - g^2)}$ and we neglected higher order corrections. In analogy with the previous case, the first term is the classical ground state energy with first order correction, while the second one is the quantum harmonic oscillator Hamiltonian, including a zero point energy contribution. Similarly to the paramagnetic phase, also in the ferromagnetic case the first order semiclassical correction lowers the classical energy minimum, since

$$\mathcal{E}_<^0 = \frac{E_<^0}{N} = -g\rho + \frac{\hbar_{\text{eff}}}{2}\left(\omega_< - g_{cr}\right) + \mathcal{O}(\hbar_{\text{eff}}^2), \tag{4.29}$$

where the second term is evidently negative.

The same warning about the different meaning of the number operators $\hat{n}_0 = (\tilde{q}_0^2 + \tilde{p}_0^2 - 1)/2$ and $\hat{m}_0 = b_0^\dagger b_0$ is still valid. Also in the ferromagnetic ground state one obviously has $\langle \hat{m}_0 \rangle = 0$, while it can be shown that

$$\langle \hat{n}_0 \rangle = \frac{1}{4}\frac{g_{\text{cr}}}{\sqrt{g_{\text{cr}}^2 - g^2}}\left[1 - \frac{\sqrt{g_{\text{cr}}^2 - g^2}}{g_{\text{cr}}}\right]^2. \tag{4.30}$$

The average value of collective spin excitations depends on the external field $g < g_{\text{cr}}$. In particular, for weak fields $g \ll g_{\text{cr}}$ one has $\langle \hat{n}_0 \rangle \approx 0$, while in the limit $g \to g_{\text{cr}}^-$, the average number of excitations diverges with exponent 1/2:

$$\langle \hat{n}_0 \rangle \sim \frac{1}{4}\left[\frac{g_{\text{cr}}}{2(g_{\text{cr}} - g)}\right]^{1/2}. \tag{4.31}$$

Again, the Holstein–Primakoff harmonic approximation is not valid at the quantum critical point g_{cr}.

This is related to the fact that the energy gap (above the ground state) of the zero mode excitations closes at the critical point, with a critical exponent 1/2 as $g \to g_{cr}^{\pm}$ (see Fig. 4.1).

As a final remark, we mention that it is actually possible to include in this description also modes with $k \neq 0$, or spin waves. A thorough discussion of spin waves is given in the next section: we now anticipate that spin waves can be treated as free bosonic excitations, in the limit of small perturbations from a fully-polarized state.

However, in the unperturbed LMG model, spin waves do not alter the dynamics, as previously shown in Eq. (2.4). It thus suffices for now to anticipate one reasonable result, proved in the next section: If we define the total occupation number of spin waves as $N_{\text{sw}} \coloneqq \sum_{k\neq 0} \hat{n}_k$ (where $\hat{n}_k$ is the occupation

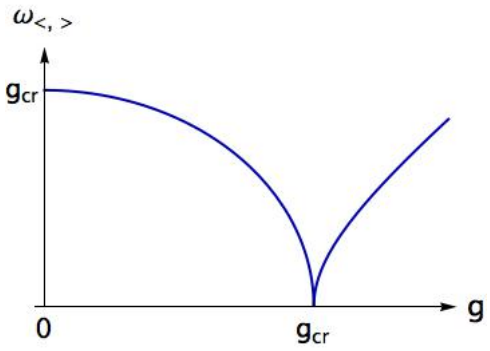

Figure 4.1: Frequency $\omega_{<,>}$ (or energy, since we fixed $\hbar = 1$) of lowest harmonic excitations above the ground state, for $g < g_{cr}$ and $g > g_{cr}$ respectively. In both cases, approaching the critical point the gap closes with a square root singularity.

number operator of mode k), then the maximal value of total spin magnitude equals $\left|\vec{J}\right|^2 = j(j+1)$, with $j = Ns - N_{\rm sw}$[3].

Accordingly, the maximal value of ρ is now reduced to

$$\rho = 1 - N_{\rm sw}/(Ns), \tag{4.32}$$

which can be substituted in Eqs. (4.17) and (4.28), yielding the complete spectrum of lowest excitations of the LMG model in the large N limit:

$$\begin{aligned} \mathcal{H}_> &\approx -g + \hbar_{\rm eff}\,\frac{\omega_> - g}{2} + \hbar_{\rm eff}\,(\omega_> \hat{m}_0 + g N_{\rm sw}) \\ \mathcal{H}_< &\approx -\left(\frac{g^2}{4\lambda} + \lambda\right) + \hbar_{\rm eff}\,\frac{\omega_< - 2\lambda}{2} + \hbar_{\rm eff}\,(\omega_< \hat{m}_0 + 2\lambda N_{\rm sw})\,, \end{aligned} \tag{4.33}$$

valid for $g > g_{\rm cr}$ and $g < g_{\rm cr}$ respectively with $g_{\rm cr} = 2\lambda(1 - N_{\rm sw}/(Ns))$.[4]. The previous result in Eq. (4.33) is accurate at first order in the spin-wave density $N_{\rm sw}/(Ns)$.

Let us make two noteworthy observations on the above result. In the first place, all the spin-wave excitations have a finite gap g/s or $2\lambda/s$[5], therefore they are not excited at zero temperature. In the second place, spin waves exhibit a flat dispersion relation, independent of the wavevector: this is a characterizing feature of fully-connected models, which in no way can carry information on spatial scales, or equivalently on finite wavelengths. In other words, you may not observe wave-like phenomena in a model without spatial dimensions.

[3] In brief, spin waves lower the total spin magnitude, while zero mode excitations do not.
[4] In these expressions $\omega_>$ and $\omega_<$ are intended to be evaluated for $\rho = 1$ (i.e. for $g_{\rm cr} = 2\lambda$).
[5] We remark that $H = N\mathcal{H}$ and $\hbar_{\rm eff} = 1/(Ns)$.

Relying on the spin waves description in terms of free bosonic excitations, one can straightforwardly take into account small temperature effects. In the ferromagnetic phase, the average number of k-mode excitations at a given temperature T is

$$\langle n_k \rangle = \frac{1}{e^{\frac{2\lambda/s}{T}} - 1} \tag{4.34}$$

with zero chemical potential and $k_B \equiv 1$. This is accurate only for temperatures $T \ll 2\lambda/s$, since a temperature of the order of the gap would result in a severe disturbance and break the validity of the spin-wave approximation. Thanks to Eq. (4.32), one finds the statistical thermal correction to the total spin magnitude

$$\rho(T) = 1 - \frac{1}{s} \frac{1}{e^{\frac{2\lambda/s}{T}} - 1}. \tag{4.35}$$

The same results hold true for the paramagnetic phase, by replacing the ferromagnetic gap $2\lambda/s$ with the paramagnetic gap g/s.

4.3 Spin-wave theory

As sketched at the beginning of this chapter, we aim to account for the effect of perturbations on the infinite-range LMG model, which are described as additional spatially-decaying interactions in Eq. (4.1).

We remark that the LMG model is defined on a fully-connected graph, without any spatial dimension; on the contrary we are now introducing a lattice dimensionality by choosing the specific form of J_r. For simplicity, we shall focus on the one-dimensional case and choose periodic boundary conditions. Accordingly, we obtain the Hamiltonian

$$H = -\frac{\lambda}{N} \sum_{i,j=1}^{N} \sigma_i^x \sigma_j^x - g \sum_{i=1}^{N} \sigma_i^z - \frac{1}{2} \sum_{i,j} J_{(i-j)} \sigma_i^x \sigma_j^x, \tag{4.36}$$

where we denoted by $i, j = 1, \ldots, N$ the lattice sites and multiplied the second sum for one half, in order to count only once each pair interaction[6]. However, we remark that the spin-wave formalism introduced in the following can be extended for any lattice dimensionality.

In analogy to the previous section, it is convenient to rewrite the Hamiltonian (4.36) in terms of the Fourier components operators defined in Eq. (2.3). This is

[6] If one wants to exclude unphysical self-interaction terms in the last sum, then can simply set $J_0 = 0$. However, as already noticed for the plain LMG model, self-interactions become negligible in the large N limit.

accomplished by substitution in Eq. (4.36) of the inverse Fourier transforms

$$\sigma_j^\alpha = \frac{1}{N}\sum_k e^{ikj}\tilde{\sigma}_k^\alpha, \tag{4.37}$$

where the sum is over the values $k = 2\pi n/N$ for $n = -N/2+1, \ldots, N/2$.

The result is given by

$$H = -\frac{\bar{\lambda}}{N}\left(\tilde{\sigma}_{k=0}^x\right)^2 - g\,\tilde{\sigma}_{k=0}^z - \frac{1}{N}\sum_{k\neq 0}\tilde{J}_k\;\tilde{\sigma}_k^x\tilde{\sigma}_{-k}^x, \tag{4.38}$$

where $\tilde{J}_k \coloneqq \sum_{r=0}^N e^{-ikr}J_r$, $\bar{\lambda} \coloneqq \lambda + \tilde{J}_0$ and $\tilde{J}_k = \tilde{J}_{-k}$ are real coefficients[7].

It is crucial to observe that the perturbation couples all the Fourier components with $k \neq 0$ to the collective degree of freedom $\vec{\mathcal{S}} \coloneqq \vec{\tilde{\sigma}}_0/N$ defined in (2.5), implying that the dynamics of the system now depends on the whole set of Fourier operators.

Heuristically, when the coefficients $\tilde{J}_{k\neq 0}$ are sufficiently small, the perturbation on both equilibrium and dynamical properties of the LMG model is expected to be small. In the following, we will treat the integrability-breaking terms perturbatively, in a quadratic approximation, which is the backbone of the spin-wave theory. Despite its perturbative nature, a noteworthy feature of the latter is that, within its framework, one can always check *a posteriori* the validity of the approximation by measuring the spin wave-density ϵ, as will be rigorously explained in the following.

Technically, this quadratic approximation is a non-trivial task, which relies on the Holstein–Primakoff harmonic approximation, depicted in section 4.1, performed with respect to the direction of the average collective spin $\langle\vec{\mathcal{S}}\rangle$.

Let us start by describing this approach for *equilibrium*. It is convenient to adopt the rotated reference frame $\mathcal{R}$, previously defined in Eq. (4.21), where the Z-direction is aligned with the equilibrium average of the collective spin $\langle\vec{\mathcal{S}}\rangle$. We decompose the single spins on the basis of $\mathcal{R}$ as

$$\vec{\sigma}_j = \hat{X}\,\sigma_j^X + \hat{Y}\,\sigma_j^Y + \hat{Z}\,\sigma_j^Z. \tag{4.39}$$

[7]The Fourier transform of a real even function $J_{(i-j)} \equiv J_r$ is a real even function $\tilde{J}_k$.

Accordingly, the Hamiltonian (4.38) can be rewritten as

$$\begin{aligned}\mathcal{H} =& \frac{H}{N} = -\bar{\lambda}\left[\left(\hat{X}\cdot\hat{x}\right)\frac{\tilde{\sigma}_0^X}{N} + \left(\hat{Y}\cdot\hat{x}\right)\frac{\tilde{\sigma}_0^Y}{N} + \left(\hat{Z}\cdot\hat{x}\right)\frac{\tilde{\sigma}_0^Z}{N}\right]^2 - g\left[\left(\hat{X}\cdot\hat{z}\right)\frac{\tilde{\sigma}_0^X}{N} + \right.\\ &\left.\left(\hat{Y}\cdot\hat{z}\right)\frac{\tilde{\sigma}_0^Y}{N} + \left(\hat{Z}\cdot\hat{z}\right)\frac{\tilde{\sigma}_0^Z}{N}\right] - \sum_{k\neq 0}\tilde{J}_k\left[\left(\hat{X}\cdot\hat{x}\right)\frac{\tilde{\sigma}_k^X}{N} + \left(\hat{Y}\cdot\hat{x}\right)\frac{\tilde{\sigma}_k^Y}{N} + \left(\hat{Z}\cdot\hat{x}\right)\frac{\tilde{\sigma}_k^Z}{N}\right]\cdot\\ &\left[\left(\hat{X}\cdot\hat{x}\right)\frac{\tilde{\sigma}_{-k}^X}{N} + \left(\hat{Y}\cdot\hat{x}\right)\frac{\tilde{\sigma}_{-k}^Y}{N} + \left(\hat{Z}\cdot\hat{x}\right)\frac{\tilde{\sigma}_{-k}^Z}{N}\right],\end{aligned} \tag{4.40}$$

in terms of the Fourier transforms $\tilde{\sigma}_k^{X,Y,Z}$ of $\sigma_j^{X,Y,Z}$, defined as in Eq. (2.3). The first two terms correspond to the usual LMG Hamiltonian in the new rotated frame.

In order to carry out the approximation, we introduce the spin-wave canonical variables via the Holstein–Primakoff transformation, which is now applied to each spin s and expanded to lowest order in $1/\sqrt{s}$:

$$\begin{cases}\sigma_j^X = \dfrac{q_j}{\sqrt{s}} + \dots,\\ \sigma_j^Y = \dfrac{p_j}{\sqrt{s}} + \dots,\\ \sigma_j^Z = 1 - \dfrac{n_j}{s} \equiv 1 - \dfrac{q_j^2 + p_j^2 - 1}{2s},\end{cases} \tag{4.41}$$

with q_j and p_j conjugate canonical variables that represent small deviations of the spin away from the $\hat{Z}$-axis, along the directions $\hat{X}$ and $\hat{Y}$ respectively.

Accordingly, after introducing the coordinates $\tilde{q}_k = N^{-1/2}\sum_j e^{-ikj}q_j$ and $\tilde{p}_k = N^{-1/2}\sum_j e^{-ikj}p_j$ in Fourier space, we get

$$\begin{cases}\dfrac{\tilde{\sigma}_k^X}{N} = \dfrac{\tilde{q}_k}{\sqrt{Ns}} + \dots,\\ \dfrac{\tilde{\sigma}_k^Y}{N} = \dfrac{\tilde{p}_k}{\sqrt{Ns}} + \dots,\\ \dfrac{\tilde{\sigma}_k^Z}{N} = \delta_{k,0} - \displaystyle\sum_{k'}\frac{\tilde{q}_{k'}\tilde{q}_{k-k'} + \tilde{p}_{k'}\tilde{p}_{k-k'} - \delta_{k,0}}{2Ns}.\end{cases} \tag{4.42}$$

Even though Eqs. (4.41) are formally identical to the harmonic approximation introduced in Eqs. (4.10) and (4.11), it does not appear to be a valid expansion, since the condition $1/\sqrt{s} \ll 1$ is *not* fulfilled[8].

This objection is indeed correct and sets the limit of validity for the spin-wave theory, which holds only in the subspace of the total Hilbert space with

[8] In fact, one often has $s = 1/2$, implying that $1/\sqrt{s} = \sqrt{2}$, which is not any smaller than one. Even for bigger values of s, the condition $1/\sqrt{s} \ll 1$ is not satisfied.

small number of spin excitations, with respect to the fully-polarized state in Z-direction. However, this space is not easily described in the basis of single spin operators, but is clearly visualized in Fourier space.

In Appendix B, we describe in detail the spin-wave theory in Fourier space, and we rederive Eq. (4.42) on somewhat more solid bases. In particular, we prove that the operators $[\tilde{q}_k, \tilde{p}_{k'}] = i\,\delta_{k,-k'}$ are a set of canonical operators (including the peculiar case of $k = 0$); moreover, the number operators associated to spin-wave excitations ($k \neq 0$) or zero-mode collective excitations are shown to be given by

$$n_k = \frac{1}{2}\left(\tilde{q}_k \tilde{q}_{-k} + \tilde{p}_k \tilde{p}_{-k} - 1\right), \tag{4.43}$$

for the case of a $1d$-lattice.

We can now proceed to rewrite our model Hamiltonian (4.40) by substitution of the approximation in Eq. (4.42). The result is given by

$$\mathcal{H} = \mathcal{H}_0 + \mathcal{U}_2 + \mathcal{U}_3 + \mathcal{U}_4, \tag{4.44}$$

where the $k = 0$ contribution is

$$\begin{aligned}
\mathcal{H}_0 = &- \bar{\lambda}\left(\hat{Z}\cdot\hat{x}\right)^2 \left[1 - \hbar_{\text{eff}}(n_0 + N_{\text{sw}})\right]^2 - g\left(\hat{Z}\cdot\hat{z}\right)\left(1 - \hbar_{\text{eff}}(n_0 + N_{\text{sw}})\right) \\
&- 2\bar{\lambda}\,\hbar_{\text{eff}}^{1/2}\left(\hat{Z}\cdot\hat{x}\right)\left(1 - \hbar_{\text{eff}} N_{\text{sw}}\right)\left[\left(\hat{X}\cdot\hat{x}\right)\tilde{q}_0 + \left(\hat{Y}\cdot\hat{x}\right)\tilde{p}_0\right] \\
&+ \hbar_{\text{eff}}^{3/2}\,\bar{\lambda}\left(\hat{Z}\cdot\hat{x}\right)\left[\left(\hat{X}\cdot\hat{x}\right)(n_0\tilde{q}_0 + \tilde{q}_0 n_0) + \left(\hat{Y}\cdot\hat{x}\right)(n_0\tilde{p}_0 + \tilde{p}_0 n_0)\right] \\
&- g\,\hbar_{\text{eff}}^{1/2}\left[\left(\hat{X}\cdot\hat{z}\right)\tilde{q}_0 + \left(\hat{Y}\cdot\hat{z}\right)\tilde{p}_0\right] \\
&- \bar{\lambda}\,\hbar_{\text{eff}}\left[\left(\hat{X}\cdot\hat{x}\right)^2\tilde{q}_0^2 + \left(\hat{Y}\cdot\hat{x}\right)^2\tilde{p}_0^2 + 2\left(\hat{X}\cdot\hat{x}\right)\left(\hat{Y}\cdot\hat{x}\right)\frac{\tilde{q}_0\tilde{p}_0 + \tilde{p}_0\tilde{q}_0}{2}\right],
\end{aligned} \tag{4.45}$$

while the $k \neq 0$ contribution from the perturbation is split into three terms, with $\mathcal{U}_j$ including all the terms of j-th order in the spin-wave canonical operators. We note that the term in the third line of $\mathcal{H}_0$ takes care of the non-zero commutation relations between n_0 and $\tilde{q}_0, \tilde{p}_0$.

The explicit form of the operators $\mathcal{U}_j$ is given by

$$\begin{aligned}
\mathcal{U}_2 &= -\hbar_{\text{eff}} \sum_{k\neq 0} \tilde{J}_k \left[\left(\hat{X}\cdot\hat{x}\right)^2 \tilde{q}_k\tilde{q}_{-k} + \left(\hat{Y}\cdot\hat{x}\right)^2 \tilde{p}_k\tilde{p}_{-k} + 2\left(\hat{X}\cdot\hat{x}\right)\left(\hat{Y}\cdot\hat{x}\right)\frac{\tilde{q}_k\tilde{p}_{-k}+\tilde{p}_k\tilde{q}_{-k}}{2}\right] \\
\mathcal{U}_3 &= \hbar_{\text{eff}}^{3/2} \sum_{k\neq 0} \tilde{J}_k \left(\hat{Z}\cdot\hat{x}\right) \times \\
&\quad \times \left\{ \left(\hat{X}\cdot\hat{x}\right)\left[\tilde{q}_k \sum_{k'} \frac{\tilde{q}_{k'}\tilde{q}_{-k-k'}+\tilde{p}_{k'}\tilde{p}_{-k-k'}}{2} + \sum_{k'} \frac{\tilde{q}_{k'}\tilde{q}_{k-k'}+\tilde{p}_{k'}\tilde{p}_{k-k'}}{2}\tilde{q}_{-k}\right] + \right. \\
&\quad \left. + \left(\hat{Y}\cdot\hat{x}\right)\left[\tilde{p}_k \sum_{k'} \frac{\tilde{q}_{k'}\tilde{q}_{-k-k'}+\tilde{p}_{k'}\tilde{p}_{-k-k'}}{2} + \sum_{k'} \frac{\tilde{q}_{k'}\tilde{q}_{k-k'}+\tilde{p}_{k'}\tilde{p}_{k-k'}}{2}\tilde{p}_{-k}\right]\right\} \\
\mathcal{U}_4 &= -\hbar_{\text{eff}}^2 \sum_{k\neq 0} \tilde{J}_k \left(\hat{Z}\cdot\hat{x}\right)^2 \sum_{k'} \frac{\tilde{q}_{k'}\tilde{q}_{k-k'}+\tilde{p}_{k'}\tilde{p}_{k-k'}}{2} \sum_{k''} \frac{\tilde{q}_{k''}\tilde{q}_{-k-k''}+\tilde{p}_{k''}\tilde{p}_{-k-k''}}{2}.
\end{aligned} \tag{4.46}$$

We remark that the Hamiltonian in Eq. (4.44) is a good approximation of the exact Hamiltonian in Eq. (4.38), only in the Hilbert space sector with the majority of spins aligned along the Z-direction, or equivalently in the limit of small excitations density $n_0 + N_{\text{sw}} \approx N_{\text{sw}} \ll Ns$, as stated in Eq. (B.28). This treatment is clearly valid for all possible orientations of the Z-direction[9].

The next step consists in the actual quadratic expansion, which amounts to the lowest non-trivial order of approximation. The physical idea is that we will consider spin waves as free bosonic excitations, which interact only with the collective $k = 0$ mode. We shall therefore neglect interactions among the spin waves, and study in this limit the impact of quantum fluctuations on the LMG equilibrium and dynamical properties.

Accordingly, the Hamiltonian in Eq. (4.44) is simplified as described in the following lines. Let us preliminarily notice that each term of j-th order in the canonical operators multiplies a factor $(\hbar_{\text{eff}}^{j/2})$.

We will keep all terms up to quadratic order in the canonical operators, or equivalently up to $(\propto \hbar_{\text{eff}})$, which are some contributions from $\mathcal{H}_0$ and the whole $\mathcal{U}_2$. On the contrary, we shall neglect all quartic terms $(\propto \hbar_{\text{eff}}^2)$, which come from the first line of $\mathcal{H}_0$ and the whole $\mathcal{U}_4$. Regarding the cubic part $(\propto \hbar_{\text{eff}}^{3/2})$, the only relevant terms involve one zero-momentum operator and two operators with opposite momenta $(k, -k)$, which may be interpreted as describing the interaction between a zero mode excitation and a pair of spin waves with opposite momenta.

Let us first apply this approximation to $\mathcal{H}_0$: we neglect the quartic terms in the first line and the third line altogether, which is of cubic order in the zero-mode

[9] The Z-direction is defined in terms of the rotation angles θ and ϕ, as in Eq. (4.21). For now, these are free parameters that will be fixed in the next sections.

operators. Rearranging the terms one finds

$$\begin{aligned}\mathcal{H}_0 = &- \bar{\lambda}\left(\hat{Z}\cdot\hat{x}\right)^2 - g\left(\hat{Z}\cdot\hat{z}\right) - 2\,\hbar_{\text{eff}}^{1/2}\bar{\lambda}\left(\hat{Z}\cdot\hat{x}\right)\left[\left(\hat{X}\cdot\hat{x}\right)\tilde{q}_0 + \left(\hat{Y}\cdot\hat{x}\right)\tilde{p}_0\right] \\ &- \hbar_{\text{eff}}^{1/2}\,g\left[\left(\hat{X}\cdot\hat{z}\right)\tilde{q}_0 + \left(\hat{Y}\cdot\hat{z}\right)\tilde{p}_0\right] + \hbar_{\text{eff}}(n_0+N_{\text{sw}})\left[2\bar{\lambda}\left(\hat{Z}\cdot\hat{x}\right)^2 + g\left(\hat{Z}\cdot\hat{z}\right)\right] \\ &- \hbar_{\text{eff}}\,\bar{\lambda}\left[\left(\hat{X}\cdot\hat{x}\right)^2\tilde{q}_0^2 + \left(\hat{Y}\cdot\hat{x}\right)^2\tilde{p}_0^2 + 2\left(\hat{X}\cdot\hat{x}\right)\left(\hat{Y}\cdot\hat{x}\right)\frac{\tilde{q}_0\tilde{p}_0+\tilde{p}_0\tilde{q}_0}{2}\right] \\ &+ 2\hbar_{\text{eff}}^{3/2}\,\bar{\lambda}\left(\hat{Z}\cdot\hat{x}\right)N_{\text{sw}}\left[\left(\hat{X}\cdot\hat{x}\right)\tilde{q}_0 + \left(\hat{Y}\cdot\hat{x}\right)\tilde{p}_0\right].\end{aligned} \tag{4.47}$$

One might notice that the term in the third line above is in the same form as those in $\mathcal{U}_2$, and therefore can be included in that sum by redefining $\tilde{J}_k$ as

$$\tilde{J}_k' = \begin{cases}\tilde{J}_k, & \text{for } k\neq 0\\ \bar{\lambda} = \lambda + \tilde{J}_0, & \text{for } k = 0\end{cases} \tag{4.48}$$

and letting the sum run over all k, included $k=0$. In order to simplify the notation, we shall drop the prime symbol from now on.

Moreover, by applying the same approximation to $\mathcal{U}_3$, one is left with only the subsequent terms

$$\begin{aligned}&+ 2\hbar_{\text{eff}}^{3/2}\left(\hat{Z}\cdot\hat{x}\right)\tilde{q}_0\sum_{k\neq 0}\tilde{J}_k\left[\left(\hat{X}\cdot\hat{x}\right)\tilde{q}_k\tilde{q}_{-k} + \left(\hat{Y}\cdot\hat{x}\right)\frac{\tilde{q}_k\tilde{p}_{-k}+\tilde{p}_k\tilde{q}_{-k}}{2}\right] \\ &+ 2\hbar_{\text{eff}}^{3/2}\left(\hat{Z}\cdot\hat{x}\right)\tilde{p}_0\sum_{k\neq 0}\tilde{J}_k\left[\left(\hat{Y}\cdot\hat{x}\right)\tilde{p}_k\tilde{p}_{-k} + \left(\hat{X}\cdot\hat{x}\right)\frac{\tilde{q}_k\tilde{p}_{-k}+\tilde{p}_k\tilde{q}_{-k}}{2}\right]\end{aligned} \tag{4.49}$$

We can finally sum up all terms and obtain

$$\begin{aligned}\mathcal{H} = &- \bar{\lambda}\left(\hat{Z}\cdot\hat{x}\right)^2 - g\left(\hat{Z}\cdot\hat{z}\right) + \hbar_{\text{eff}}(n_0+N_{\text{sw}})\left[2\bar{\lambda}\left(\hat{Z}\cdot\hat{x}\right)^2 + g\left(\hat{Z}\cdot\hat{z}\right)\right] \\ &- \hbar_{\text{eff}}\sum_k\tilde{J}_k\left[\left(\hat{X}\cdot\hat{x}\right)^2\tilde{q}_k\tilde{q}_{-k} + \left(\hat{Y}\cdot\hat{x}\right)^2\tilde{p}_k\tilde{p}_{-k} + 2\left(\hat{X}\cdot\hat{x}\right)\left(\hat{Y}\cdot\hat{x}\right)\frac{\tilde{q}_k\tilde{p}_{-k}+\tilde{p}_k\tilde{q}_{-k}}{2}\right] \\ &- 2\,\hbar_{\text{eff}}^{1/2}\bar{\lambda}\left(\hat{Z}\cdot\hat{x}\right)\left[\left(\hat{X}\cdot\hat{x}\right)\tilde{q}_0 + \left(\hat{Y}\cdot\hat{x}\right)\tilde{p}_0\right] - \hbar_{\text{eff}}^{1/2}\,g\left[\left(\hat{X}\cdot\hat{z}\right)\tilde{q}_0 + \left(\hat{Y}\cdot\hat{z}\right)\tilde{p}_0\right] \\ &+ 2\hbar_{\text{eff}}^{3/2}\,\bar{\lambda}\left(\hat{Z}\cdot\hat{x}\right)N_{\text{sw}}\left[\left(\hat{X}\cdot\hat{x}\right)\tilde{q}_0 + \left(\hat{Y}\cdot\hat{x}\right)\tilde{p}_0\right] \\ &+ 2\hbar_{\text{eff}}^{3/2}\left(\hat{Z}\cdot\hat{x}\right)\tilde{q}_0\sum_{k\neq 0}\tilde{J}_k\left[\left(\hat{X}\cdot\hat{x}\right)\tilde{q}_k\tilde{q}_{-k} + \left(\hat{Y}\cdot\hat{x}\right)\frac{\tilde{q}_k\tilde{p}_{-k}+\tilde{p}_k\tilde{q}_{-k}}{2}\right] \\ &+ 2\hbar_{\text{eff}}^{3/2}\left(\hat{Z}\cdot\hat{x}\right)\tilde{p}_0\sum_{k\neq 0}\tilde{J}_k\left[\left(\hat{Y}\cdot\hat{x}\right)\tilde{p}_k\tilde{p}_{-k} + \left(\hat{X}\cdot\hat{x}\right)\frac{\tilde{q}_k\tilde{p}_{-k}+\tilde{p}_k\tilde{q}_{-k}}{2}\right].\end{aligned} \tag{4.50}$$

It is convenient for our further analysis to rearrange the terms as follows

$$\begin{aligned}\mathcal{H} = &- \bar{\lambda}\left(\hat{Z}\cdot\hat{x}\right)^2 - g\left(\hat{Z}\cdot\hat{z}\right) + \hbar_{\rm eff}(n_0+N_{\rm sw})\left[2\bar{\lambda}\left(\hat{Z}\cdot\hat{x}\right)^2 + g\left(\hat{Z}\cdot\hat{z}\right)\right] \\ &- \hbar_{\rm eff}\sum_k \tilde{J}_k\left[\left(\hat{X}\cdot\hat{x}\right)^2\tilde{q}_k\tilde{q}_{-k} + \left(\hat{Y}\cdot\hat{x}\right)^2\tilde{p}_k\tilde{p}_{-k} + 2\left(\hat{X}\cdot\hat{x}\right)\left(\hat{Y}\cdot\hat{x}\right)\frac{\tilde{q}_k\tilde{p}_{-k}+\tilde{p}_k\tilde{q}_{-k}}{2}\right] \\ &+ \hbar_{\rm eff}^{1/2}\tilde{q}_0\Bigg\{-2\bar{\lambda}\left(1-\hbar_{\rm eff}N_{\rm sw}\right)(\hat{Z}\cdot\hat{x})(\hat{X}\cdot\hat{x}) - g(\hat{X}\cdot\hat{z}) \\ &\qquad + 2(\hat{Z}\cdot\hat{x})\hbar_{\rm eff}\sum_{k\neq 0}\tilde{J}_k\left[(\hat{X}\cdot\hat{x})\,\tilde{q}_k\tilde{q}_{-k} + (\hat{Y}\cdot\hat{x})\,\frac{\tilde{q}_k\tilde{p}_{-k}+\tilde{p}_k\tilde{q}_{-k}}{2}\right]\Bigg\} \\ &+ \hbar_{\rm eff}^{1/2}\tilde{p}_0\Bigg\{-2\bar{\lambda}\left(1-\hbar_{\rm eff}N_{\rm sw}\right)(\hat{Z}\cdot\hat{x})(\hat{Y}\cdot\hat{x}) - g(\hat{Y}\cdot\hat{z}) \\ &\qquad + 2(\hat{Z}\cdot\hat{x})\hbar_{\rm eff}\sum_{k\neq 0}\tilde{J}_k\left[(\hat{Y}\cdot\hat{x})\,\tilde{p}_k\tilde{p}_{-k} + (\hat{X}\cdot\hat{x})\,\frac{\tilde{q}_k\tilde{p}_{-k}+\tilde{p}_k\tilde{q}_{-k}}{2}\right]\Bigg\},\end{aligned} \tag{4.51}$$

where one easily recognizes the classical energy (first and second terms), the quadratic contributions (third and fourth terms) and the remaining cubic part, describing the interaction between the collective degree of freedom and the spin-wave excitations. The various scalar products between versors can be expressed in terms of the rotation angles θ and ϕ, by exploiting the definition in Eq. (4.21). Therefore, the Hamiltonian depends parametrically on these angles, which define the Z-direction of the frame $\mathcal{R}$.

The Hamiltonian in Eq. (4.51) is our starting point for describing the impact of small perturbations on the equilibrium and out of equilibrium physics of the LMG model.

4.4 Equilibrium of perturbed LMG model

In this section we address the description of the impact of perturbations on the LMG ground state, expecting only small corrections for small values of $\tilde{J}_{k\neq 0}$.

The Hamiltonian in Eq. (4.51) describes quantum fluctuations at the quadratic order, and its validity is restricted to the Hilbert space sector with small density of excitations, see Eq. (B.28).

One could in principle calculate its ground state, evaluate the ground state averages of the collective degree of freedom $\langle\vec{\tilde{\sigma}}_0\rangle$ as a function of θ and ϕ, and then determine a posteriori the angles θ and ϕ such that $\langle\vec{\tilde{\sigma}}_0\rangle$ aligns with Z. The

Eq. (4.42) for $k = 0$ shows that it is equivalent to requiring

$$\langle \tilde{q}_0 \rangle = \langle \tilde{p}_0 \rangle = 0. \tag{4.52}$$

Exact eigenstates of a quantum Hamiltonian are stationary states, so these averages would not evolve in time, yielding the correct equilibrium description of quantum fluctuations at the quadratic order.

However, the Hamiltonian of Eq. (4.51) is cubic and this prevents us from an exact solution. It is therefore convenient to describe its ground state in the Gaussian approximation.

A generic Gaussian state is uniquely determined by the averages of the canonical operators and two points equal-time correlation functions. In contrast with the exact framework, averages in an approximate ground state do generally evolve in time. In order for this Gaussian state to be a meaningful description of the perturbed ground state, we thus have to require this set of averages and correlation functions to be constant in time. This can be done by fixing the value of the angles θ and ϕ, as we now show explicitly.

The evolution of an observable in the Heisenberg representation is given by the well-known Heisenberg equation, which for the operators $\tilde{q}_k$ and $\tilde{p}_k$ is[10]

$$\begin{cases} i\dfrac{d}{dt}\tilde{q}_k = [\tilde{q}_k, N\mathcal{H}] \\ i\dfrac{d}{dt}\tilde{p}_k = [\tilde{p}_k, N\mathcal{H}]\,, \end{cases} \tag{4.53}$$

valid for both $k \neq 0$ and $k = 0$. Given the canonical commutation relations in Eq. (B.14), one finds

$$\begin{cases} s\dfrac{d}{dt}\tilde{q}_k = (2\bar{\lambda}\sin^2\theta\cos^2\phi + g\cos\theta - 2\tilde{J}_k\sin^2\phi)\tilde{p}_k \\ \qquad\qquad + 2\tilde{J}_k\cos\theta\sin\phi\cos\phi\,\tilde{q}_k + \delta_{k,0}\,\hat{b} \\ s\dfrac{d}{dt}\tilde{p}_k = -(2\bar{\lambda}\sin^2\theta\cos^2\phi + g\cos\theta - 2\tilde{J}_k\cos^2\theta\cos^2\phi)\tilde{q}_k \\ \qquad\qquad - 2\tilde{J}_k\cos\theta\sin\phi\cos\phi\,\tilde{p}_k - \delta_{k,0}\,\hat{a}, \end{cases} \tag{4.54}$$

where the operators $\hat{a}$ and $\hat{b}$ are nothing but the first and second curly braces of Eq. (4.51) respectively[11]. Consistently with the approximation of non-interacting spin waves, the equations for the canonical spin-wave operators ($k \neq 0$) are derived neglecting non-linear contributions. On the contrary, the equations for

[10] We recall that $\mathcal{H} = H/N$ is the energy per spin.

[11] We remark with the notation that $\hat{a}$ and $\hat{b}$ are operators, depending on the spin-wave canonical operators (with $k \neq 0$).

the collective mode canonical operators ($k = 0$) also include terms describing the interaction with spin-wave modes.

We can now derive the evolution laws for the parameters characterizing the Gaussian state, which are the mean values $\langle \tilde{q}_k(t) \rangle$ and $\langle \tilde{p}_k(t) \rangle$ and the equal-time correlation functions

$$\begin{cases} \Delta_k^{qq}(t) \coloneqq \big\langle \tilde{q}_k(t)\tilde{q}_{-k}(t) \big\rangle, \\ \Delta_k^{pp}(t) \coloneqq \big\langle \tilde{p}_k(t)\tilde{p}_{-k}(t) \big\rangle, \\ \Delta_k^{qp}(t) \coloneqq \dfrac{1}{2}\big\langle \tilde{q}_k(t)\tilde{p}_{-k}(t) + \tilde{p}_k(t)\tilde{q}_{-k}(t) \big\rangle. \end{cases} \tag{4.55}$$

The correlation functions involving different pairs of canonical operators are assumed to be identically zero at all times.

The equations for the averages are simply given by

$$\begin{cases} s\dfrac{d}{dt}\langle \tilde{q}_k \rangle = (2\bar{\lambda}\sin^2\theta\cos^2\phi + g\cos\theta - 2\tilde{J}_k\sin^2\phi)\langle \tilde{p}_k \rangle \\ \qquad\qquad + 2\tilde{J}_k\cos\theta\sin\phi\cos\phi\ \langle \tilde{q}_k \rangle + \delta_{k,0}\ \langle \hat{b} \rangle \\ s\dfrac{d}{dt}\langle \tilde{p}_k \rangle = -(2\bar{\lambda}\sin^2\theta\cos^2\phi + g\cos\theta - 2\tilde{J}_k\cos^2\theta\cos^2\phi)\langle \tilde{q}_k \rangle \\ \qquad\qquad - 2\tilde{J}_k\cos\theta\sin\phi\cos\phi\ \langle \tilde{p}_k \rangle - \delta_{k,0}\ \langle \hat{a} \rangle . \end{cases} \tag{4.56}$$

We note that the quantum mean values for $k \neq 0$ follow the classical equations of motion[12], while the zero mode averages have a more complex evolution, since $\langle \hat{a} \rangle$ and $\langle \hat{b} \rangle$ depend on the equal-time correlation functions defined above. An explicit calculation in fact yields

$$\begin{aligned} \langle \hat{a} \rangle =& -2\bar{\lambda}\left(1 - \hbar_{\text{eff}}\sum_{k\neq 0}\frac{\Delta_k^{qq} + \Delta_k^{pp} - 1}{2}\right)\sin\theta\cos\theta\cos^2\phi \\ &+ g\sin\theta + 2\sin\theta\cos\phi\,\hbar_{\text{eff}}\sum_{k\neq 0}\tilde{J}_k\left(\cos\theta\cos\phi\Delta_k^{qq} - \sin\phi\Delta_k^{qp}\right) \\ \langle \hat{b} \rangle =& 2\bar{\lambda}\left(1 - \hbar_{\text{eff}}\sum_{k\neq 0}\frac{\Delta_k^{qq} + \Delta_k^{pp} - 1}{2}\right)\sin\theta\sin\phi\cos\phi \\ &+ 2\sin\theta\cos\phi\,\hbar_{\text{eff}}\sum_{k\neq 0}\tilde{J}_k\left(-\sin\phi\Delta_k^{pp} + \cos\theta\cos\phi\Delta_k^{qp}\right). \end{aligned} \tag{4.57}$$

[12] This is an immediate consequence of the Ehrenfest theorem and the linearity of Heisenberg equations.

The equations for the equal-time correlation functions are

$$\begin{cases} s\dfrac{d}{dt}\Delta_k^{qq} = & 4\tilde{J}_k \cos\theta \sin\phi \cos\phi \Delta_k^{qq} \\ & + 2(2\bar{\lambda}\sin^2\theta\cos^2\phi + g\cos\theta - 2\tilde{J}_k\sin^2\phi)\Delta_k^{qp} + 2\delta_{k,0}\langle\tilde{q}_0\hat{b}\rangle \\ s\dfrac{d}{dt}\Delta_k^{pp} = & -4\tilde{J}_k \cos\theta \sin\phi \cos\phi \Delta_k^{pp} \\ & - 2(2\bar{\lambda}\sin^2\theta\cos^2\phi + g\cos\theta - 2\tilde{J}_k\cos^2\theta\cos^2\phi)\Delta_k^{qp} - 2\delta_{k,0}\langle\tilde{p}_0\hat{a}\rangle \\ s\dfrac{d}{dt}\Delta_k^{qp} = & -(2\bar{\lambda}\sin^2\theta\cos^2\phi + g\cos\theta - 2\tilde{J}_k\cos^2\theta\cos^2\phi)\Delta_k^{qq} \\ & + (2\bar{\lambda}\sin^2\theta\cos^2\phi + g\cos\theta - 2\tilde{J}_k\sin^2\phi)\Delta_k^{pp} + \delta_{k,0}(\langle\tilde{p}_0\hat{b}\rangle - \langle\tilde{q}_0\hat{a}\rangle). \end{cases} \tag{4.58}$$

Let us start by examining the equations above for the spin-wave canonical operators ($k \neq 0$), looking for a stationary solution. The equations for the mean values (4.56) with initial condition $\langle\tilde{q}_k(0)\rangle = \langle\tilde{p}_k(0)\rangle = 0$ yield as (unique) solution that these initial conditions do not evolve in time

$$\langle\tilde{q}_k(t)\rangle = \langle\tilde{p}_k(t)\rangle \equiv 0. \tag{4.59}$$

The equations for the correlation functions (4.58) are actually not independent, since the subsequent exact property of Gaussian states holds at all times

$$4\left(\Delta^{qp}\right)^2 = 4\Delta^{qq}\Delta^{pp} - 1, \tag{4.60}$$

implying that we can focus on the equations for Δ_k^{qq} and Δ_k^{pp} only.

At this point it is convenient to observe that the collective spin $\langle\vec{\tilde{\sigma}}_0\rangle$ at equilibrium lies in the xz-plane, since the Hamiltonian does not contain interactions along the y-direction. This symmetry argument immediately implies that $\phi^* = 0$ or π. We thus have to look for a stationary solution of the simplified equations for $k \neq 0$

$$\begin{cases} s\dfrac{d}{dt}\Delta_k^{qq} = +2(2\bar{\lambda}\sin^2\theta + g\cos\theta)\Delta_k^{qp} \\ s\dfrac{d}{dt}\Delta_k^{pp} = -2(2\bar{\lambda}\sin^2\theta + g\cos\theta - 2\tilde{J}_k\cos^2\theta)\Delta_k^{qp}, \end{cases} \tag{4.61}$$

with the constraint in Eq. (4.60). It is apparent that if we choose any initial condition such that $\Delta_k^{qp}(0) = 0$, the (unique) solution is stationary

$$\begin{cases} \Delta_k^{qq}(t) \equiv \Delta_k^{qq}(0) \\ \Delta_k^{pp}(t) \equiv \Delta_k^{pp}(0), \end{cases} \tag{4.62}$$

and consequently also $\langle\hat{a}\rangle$ and $\langle\hat{b}\rangle$ are time independent real constants.

We now move to the equations for collective mode ($k = 0$) averages. Taking into account the above symmetry argument they reduce to

$$\begin{cases} s\dfrac{d}{dt}\langle\tilde{q}_0\rangle = (2\bar{\lambda}\sin^2\theta + g\cos\theta)\langle\tilde{p}_0\rangle + \langle\hat{b}\rangle \\ s\dfrac{d}{dt}\langle\tilde{p}_0\rangle = -(2\bar{\lambda}\sin^2\theta + g\cos\theta - 2\tilde{J}'_0\cos^2\theta)\langle\tilde{q}_0\rangle - \langle\hat{a}\rangle\,. \end{cases} \tag{4.63}$$

In light of Eq. (4.52), the initial conditions $\langle\tilde{q}_0(0)\rangle = \langle\tilde{p}_0(0)\rangle = 0$ guarantee that the spin-wave approximation is valid, and must hold at any time. This is verified if and only if the Eqs. (4.63) are homogeneous, so that the constants $\langle\hat{a}\rangle$ and $\langle\hat{b}\rangle$ must be zero. These constants are now given by

$$\begin{aligned} \langle\hat{a}\rangle &= -2\bar{\lambda}\left(1 - \hbar_{\text{eff}}\sum_{k\neq 0}\frac{\Delta_k^{qq} + \Delta_k^{pp} - 1}{2}\right)\sin\theta\cos\theta + g\sin\theta + 2\sin\theta\hbar_{\text{eff}}\sum_{k\neq 0}\tilde{J}_k\cos\theta\Delta_k^{qq} \overset{!}{=} 0 \\ \langle\hat{b}\rangle &= 2\sin\theta\hbar_{\text{eff}}\sum_{k\neq 0}\tilde{J}_k\cos\theta\Delta_k^{qp} \overset{!}{=} 0. \end{aligned} \tag{4.64}$$

The second condition is already satisfied, while the first one yields an equation of state for the angle θ.

We are only left to requiring the stationarity of the collective mode correlation functions. This is immediate, since thanks to Wick theorem the following correlation functions are zero:

$$\langle\tilde{q}_0\hat{a}\rangle = \langle\tilde{q}_0\hat{b}\rangle = \langle\tilde{p}_0\hat{a}\rangle = \langle\tilde{p}_0\hat{b}\rangle = 0. \tag{4.65}$$

This means that the Eq. (4.61) holds for $k = 0$ as well, so that it is enough to choose $\Delta_0^{qp}(0) = 0$ in order to have a stationary solution

$$\begin{cases} \Delta_0^{qq}(t) \equiv \Delta_0^{qq}(0) \\ \Delta_0^{pp}(t) \equiv \Delta_0^{pp}(0). \end{cases} \tag{4.66}$$

We finally arrived to the conclusion that any Gaussian state with zero averages $\langle\tilde{q}_k\rangle = \langle\tilde{p}_k\rangle = 0$ and zero equal-time correlation functions $\Delta_k^{qp} = 0$ is stationary if one fixes $\phi = \phi^* = 0$ or π and $\theta = \theta^*$ given by the solution of the equation of state in Eq. (4.64).

This statement clarifies that one still has the freedom of choosing the N values of Δ_k^{qq}, while the remaining Δ_k^{pp} are fixed by the constraints in Eq. (4.60). It is natural to fix these parameters with a variational approach, by minimizing the energy average $\langle\mathcal{H}\rangle$, with the Hamiltonian $\mathcal{H}$ given in Eq. (4.51). In light of

Eq. (4.65), this is equivalent to finding the ground state of the quadratic part of this Hamiltonian, which can be written as

$$\mathcal{H}_{\text{quad}} = -\bar{\lambda}\sin^2\theta - g\cos\theta + \hbar_{\text{eff}}\sum_k h_k, \tag{4.67}$$

where h_k has the form

$$h_k = \alpha_k \frac{\tilde{q}_k\tilde{q}_{-k}}{2} + \beta\,\frac{\tilde{p}_k\tilde{p}_{-k}-1}{2}, \tag{4.68}$$

with coefficients given by

$$\begin{cases} \alpha_k = 2\bar{\lambda}\sin^2\theta + g\cos\theta - 2\tilde{J}_k\cos^2\theta \\ \beta = 2\bar{\lambda}\sin^2\theta + g\cos\theta. \end{cases} \tag{4.69}$$

We notice that $h_k = h_{-k}$ (since the coefficient $\tilde{J}_k$ are even in k) and clearly $[h_k, h_{k'}] = 0$.

It can be checked that the transformation[13]

$$\begin{cases} \tilde{q}_k = \left(\dfrac{\beta}{\alpha_k}\right)^{1/4} \dfrac{b^\dagger_{-k} + b_k}{\sqrt{2}} \\ \tilde{p}_k = i\left(\dfrac{\alpha_k}{\beta}\right)^{1/4} \dfrac{b^\dagger_{-k} - b_k}{\sqrt{2}}. \end{cases} \tag{4.70}$$

diagonalizes the Hamiltonian h_k yielding

$$h_k = \sqrt{\alpha_k\beta}\left(m_k + \frac{1}{2}\right), \tag{4.71}$$

with[14]

$$m_k \coloneqq \frac{1}{2}\left({b^\dagger}_k b_k + {b^\dagger}_{-k} b_{-k}\right). \tag{4.72}$$

The quadratic Hamiltonian in Eq. (4.67) can thus be rewritten as

$$\mathcal{H}_{\text{quad}} = -\bar{\lambda}\sin^2\theta - g\cos\theta + \hbar_{\text{eff}}\sum_k \frac{\omega_k - \omega_k^{(0)}}{2} + \hbar_{\text{eff}}\sum_k \omega_k\, m_k, \tag{4.73}$$

with the definitions

$$\omega_k \coloneqq \sqrt{\alpha_k\beta} = \sqrt{(2\bar{\lambda}\sin^2\theta + g\cos\theta - 2\tilde{J}_k\cos^2\theta)(2\bar{\lambda}\sin^2\theta + g\cos\theta)} \tag{4.74}$$

[13] This is a simple generalization of the transformation in Eq. (B.13), which regards both the spin-wave and zero-mode excitations.

[14] The operators m_k give the number of excitations of the Hamiltonian h_k in Eq. (4.68), and should not be confused with the number operators n_k [see Eq (4.43)], which count the number of spin-wave or collective excitations of the mode k. This is the same warning as in section 4.2, in a more general setting where also spin-wave modes ($k \neq 0$) are included.

and

$$\omega_k^{(0)} \equiv \omega^{(0)} := 2\bar{\lambda}\sin^2\theta + g\cos\theta. \tag{4.75}$$

The equation (4.74) gives the spin-wave dispersion relation, which depends parametrically on the angle θ and is an even function of k.

In the limit where $\tilde{J}_{k\neq 0} = 0$, one recovers the LMG model, with $\tilde{J}_0 = \lambda$. The spin-wave modes ($k \neq 0$) dispersion relation flattens and coincides with the frequency in Eq. (4.75), while for the collective mode one has

$$\omega_0 = \sqrt{(2\lambda\sin^2\theta + g\cos\theta - 2\lambda\cos^2\theta)(2\lambda\sin^2\theta + g\cos\theta)} = \sqrt{(\omega^{(0)} - 2\lambda\cos^2\theta)\,\omega^{(0)}}. \tag{4.76}$$

As a useful check, we verify that in this limit one recovers the quantum harmonic oscillator Hamiltonian describing lowest excitations above the LMG ground state, see Eq (4.33).[15].

The ground state of the quadratic Hamiltonian is labeled by eigenvalues $m_k = 0$ for all k. This correctly implies the ground state expectation values

$$\begin{cases} \langle\tilde{q}_k\rangle = 0 \\ \langle\tilde{p}_k\rangle = 0 \end{cases} \tag{4.77}$$

and the correlation functions

$$\begin{cases} \langle\tilde{q}_k\tilde{q}_{-k}\rangle = \dfrac{1}{2}\dfrac{\omega^{(0)}}{\omega_k} \\ \langle\tilde{p}_k\tilde{p}_{-k}\rangle = \dfrac{1}{2}\dfrac{\omega_k}{\omega^{(0)}} \\ \langle\dfrac{\tilde{q}_k\tilde{p}_{-k} + \tilde{p}_k\tilde{q}_{-k}}{2}\rangle = 0, \end{cases} \tag{4.78}$$

which satisfy the necessary conditions for stationarity $\Delta_k^{qp} = 0$ and further determine uniquely our Gaussian state.

The last remaining task that completes our discussion is to find the solution θ^* of the equation of state, which now reads

$$\sin\theta^*\left[-2\bar{\lambda}(1-\epsilon)\cos\theta^* + g + \cos\theta^*\,\hbar_{\text{eff}}\sum_{k\neq 0}\tilde{J}_k\sqrt{\frac{2\bar{\lambda}\sin^2\theta^* + g\cos\theta^*}{2\bar{\lambda}\sin^2\theta^* + g\cos\theta^* - 2\tilde{J}_k\cos^2\theta^*}}\right] = 0, \tag{4.79}$$

where we defined the total spin depletion

$$\epsilon = \frac{\langle N_{\text{sw}}\rangle}{Ns}\Big|_{\theta=\theta^*}. \tag{4.80}$$

[15]This is easily done by imposing $\theta = 0$ for the paramagnetic phase and $\cos\theta^* = g/g_{\text{cr}}$ for the ferromagnetic phase. Moreover, in this case the operators $m_{k\neq 0}$ do coincide with the number operators that count the spin wave excitations, since $\alpha_{k\neq 0} = \beta$.

This quantity is easily evaluated exploiting the correlation functions in Eq. (4.78):

$$\epsilon = \frac{\langle N_{\rm sw}\rangle}{Ns} = \frac{\hbar_{\rm eff}}{2}\sum_{k\neq 0}\left(\frac{1}{2}\frac{\omega^{(0)}}{\omega_k} + \frac{1}{2}\frac{\omega_k}{\omega^{(0)}} - 1\right)_{\theta=\theta^*} \tag{4.81}$$

and from Eq. (B.27) follows an explicit expression for the total spin value

$$\frac{\left|\left\langle \vec{\tilde{\sigma}}_{k=0}\right\rangle\right|}{N} = 1 - \frac{\langle N_{\rm sw}\rangle}{Ns} \equiv 1 - \epsilon. \tag{4.82}$$

We correctly obtained $\epsilon \geq 0$ and we also note that $\epsilon = \mathcal{O}(\tilde{J}^2_{k\neq 0})$, precisely

$$\epsilon = \hbar_{\rm eff}\left(\frac{\cos^2\theta}{2\,\omega^{(0)}(\theta)}\right)^2_{\theta=\theta^*}\sum_{k\neq 0}\left[\tilde{J}^2_k + \mathcal{O}(\tilde{J}^3_k)\right]. \tag{4.83}$$

Let us now address the last task of solving the equation of state (4.79) and thus determine θ^*. One immediately notices that $\theta^* = 0$ is always a solution, and in general another solution can be evaluated by imposing the vanishing of the term in square brackets. Since all of our treatment is valid for small perturbations of the LMG model, these two solutions are readily recognized as the paramagnetic and ferromagnetic ground states in the presence of quantum fluctuations.

As expected due to the symmetry of the problem, the paramagnetic equilibrium state is still characterized by a collective degree of freedom pointing in the $\theta^* = 0$ direction and the ferromagnetic equilibrium state is still characterized by two degenerate solutions for $\phi = \phi^* = 0$ or π and $\theta = \theta^*$. However, the equilibrium value of θ^* in the ferromagnetic phase is modified by the perturbation.

Also the equilibrium quantum critical point $g_{\rm cr}$ is shifted due to quantum fluctuations and we can estimate this correction as follows. Firstly we compute the variational energy of our Gaussian state as a function of θ (with fixed $\phi^* = 0$ or π), let us call it $\mathcal{E}(\theta) \coloneqq \langle\mathcal{H}\rangle_\theta$. One can check that it reads

$$\mathcal{E}(\theta) \coloneqq \langle\mathcal{H}\rangle_\theta = \langle\mathcal{H}_{\rm quad}\rangle_\theta = -\bar{\lambda}\sin^2\theta - g\cos\theta + \hbar_{\rm eff}\sum_{k\neq 0}\frac{\omega_k - \omega^{(0)}}{2}. \tag{4.84}$$

The critical point can be characterized as the value $g_{\rm cr}$ such that for $g > g_{\rm cr}$ the paramagnetic solution $\theta^* = 0$ is a minimum of $\mathcal{E}(\theta)$, while for $g < g_{\rm cr}$ it is an unstable stationary point. An expansion of $\mathcal{E}(\theta)$ to the quadratic order in a neighborhood of $\theta^* = 0$ yields

$$\begin{aligned}\mathcal{E}(\theta) \underset{\theta\to 0}{=} -g + \frac{1}{Ns}\sum_{k\neq 0}\frac{1}{2}\left(\sqrt{g(g-2\tilde{J}_k)} - g\right) + \Bigg\{g - 2\bar{\lambda} + \frac{1}{Ns}\sum_{k\neq 0}\Bigg[\\ \sqrt{g(g-2\tilde{J}_k)}\frac{1}{2}\left(\frac{2\bar{\lambda} - g/2 + 2\tilde{J}_k}{g-2\tilde{J}_k} + \frac{2\bar{\lambda} - g/2}{g}\right) - \left(2\bar{\lambda} - g/2\right)\Bigg]\Bigg\}\frac{\theta^2}{2} + \mathcal{O}(\theta^4).\end{aligned} \tag{4.85}$$

The vanishing linear term indicates that $\theta^* = 0$ is indeed a stationary point for the variational energy, but it is a minimum if and only if $g > g_{\rm cr}$, where

$$g_{\rm cr} \coloneqq 2\bar{\lambda} - \frac{1}{Ns}\sum_{k\neq 0}\left[\sqrt{g(g-2\tilde{J}_k)}\frac{1}{2}\left(\frac{2\bar{\lambda}-g/2+2\tilde{J}_k}{g-2\tilde{J}_k}+\frac{2\bar{\lambda}-g/2}{g}\right)-\left(2\bar{\lambda}-g/2\right)\right] \tag{4.86}$$

is itself a function of g. An exact solution of this implicit equation is clearly unfeasible, but it can be addressed perturbatively. This is done by expanding the r.h.s. at order n in the small parameters $\tilde{J}_{k\neq 0}$, and by substituting in its expression the old value of g determined at the step $n-1$. The first two iterations of this perturbative expansion yield the mean-field result

$$g_{\rm cr}^{(0)} = 2\bar{\lambda} \tag{4.87}$$

and the quadratic correction

$$g_{\rm cr}^{(2)} = 2\bar{\lambda}\left\{1 - \frac{5}{16}\frac{1}{Ns}\sum_{k\neq 0}\left(\frac{\tilde{J}_k}{\bar{\lambda}}\right)^2\right\} + \mathcal{O}(\tilde{J}_{k\neq 0}^3). \tag{4.88}$$

The effect of the perturbation is to lower the value of $g_{\rm cr}^{(0)}$ and therefore to destabilize the ordered ferromagnetic phase. This could be predicted relying on physical intuition.

In order to check the validity of the results above and to gain some physical insight, let us consider a few simple limit cases. In the mean-field limit $\tilde{J}_{k\neq 0} = 0$, our results must coincide with the unperturbed LMG model. Consistently, the critical point is $g_{\rm cr} = 2\lambda$ and the spin-wave band $\omega_k = \omega^{(0)}$ is flat, implying $\epsilon = 0$. The equation of state gives back $\cos\theta^* = g/g_{\rm cr}$ in the ferromagnetic phase, and obviously $\theta^* = 0$ in the paramagnetic phase, retrieving the LMG equilibrium properties.

As soon as a spatially-decaying interaction $\tilde{J}_{k\neq 0} \neq 0$ is turned on, quantum fluctuations affect the equilibrium state both in the paramagnetic and ferromagnetic phases. The value of $g_{\rm cr}$ is lowered by quantum fluctuations as depicted above. In the paramagnetic phase ($g > g_{\rm cr}$) the ground state is still in $\theta^* = 0$ as in the mean-field case, but the total spin magnitude is lowered by $\epsilon > 0$. The spin-wave dispersion relation is

$$\omega_{k,>} = \sqrt{g(g-2\tilde{J}_k)} \tag{4.89}$$

and in the limit of $g \to \infty$ we get $\omega_{k,>} \to \omega^{(0)} = g$ and therefore $\epsilon \to 0$, implying that no spin-wave excitations are present for large values of the external field g.

In the ferromagnetic phase ($g < g_{\rm cr}$) the value of θ^* is fixed by the equation of state. In the limit of $g \to 0$ the Hamiltonian Eq. (4.36) is diagonalizable in the

basis of $\{\sigma_j^x\}$ and no significant quantum features are present (all operators in it commute). The system is expected to exhibit full ferromagnetic ordering with $\theta^* = \pi/2$ and also in this limit the band flattens, as both $\omega_{k,<}$ and $\omega^{(0)}$ tend to $2\bar{\lambda}$. This implies that no spin-wave excitations are present for vanishing external field g.

In contrast, spin waves are excited for finite values of g, in correspondence of a competition between ferromagnetic ordering and the transverse field, in other words in non-trivial cases where interesting quantum effects are present. The spin-wave excitations are expected to be maximal at the equilibrium critical point $g_{\rm cr} = 2\bar{\lambda} - \mathcal{O}(\tilde{J}^2_{k\neq 0})$, where this competition is most intense. However, while the zero-mode excitations are gapless at the quantum critical point, as shown in section 4.2, finite k spin-wave excitations have a finite gap.

4.5 Dynamics of perturbed LMG model

The impact of small perturbations on the dynamical properties of the LMG model can be assessed along the same lines of the previous section, with a suitable generalization of the same concepts to an evolving system. The spin-wave expansion will be performed with respect to a time-dependent rotated frame $\mathcal{R}$, with the angles $\theta(t), \phi(t)$ describing the evolution of the average collective spin $\langle\vec{\sigma}_0\rangle$.

This generalization relies on the assumption of validity of the spin-wave expansion for the initial condition at $t = 0$, and in the time interval relevant for the dynamics. In other words, we assume that a small density of excitations is produced during the dynamics, in the sense that the condition

$$\frac{n_0 + N_{\rm sw}}{Ns} \ll 1 \tag{4.90}$$

holds true not only for the initial state at $t = 0$, but also at subsequent times[16].

The rotation of the fixed frame into the time dependent frame $\mathcal{R}$ is realized by the unitary operator

$$V(\theta(t), \phi(t)) = e^{i\phi\, s \sum_j \sigma_j^z}\, e^{i\theta\, s \sum_j \sigma_j^y}, \tag{4.91}$$

[16] This is expected to be correct for a limited interval of time, which in general may depend on the specific driving protocol $g(t)$.

which acts as a global rotation on the spins[17]:

$$\begin{cases} V\sigma_j^x V^\dagger = \hat{X}(t)\cdot\vec{\sigma}_j \equiv \sigma_j^X \\ V\sigma_j^y V^\dagger = \hat{Y}(t)\cdot\vec{\sigma}_j \equiv \sigma_j^Y \\ V\sigma_j^z V^\dagger = \hat{Z}(t)\cdot\vec{\sigma}_j \equiv \sigma_j^Z, \end{cases} \tag{4.92}$$

where we made explicit the parametric dependence on time of the $\mathcal{R}$ versors, defined in Eq. (4.21).

The Heisenberg equations of motion for the operators σ_j^α ($\alpha \in \{X, Y, Z\}$) include an additional term, due to their parametric dependence on time[18]

$$\frac{d}{dt}\sigma_j^\alpha = \frac{1}{i}\left[\sigma_j^\alpha, H\right] + \frac{\partial\sigma_j^\alpha}{\partial t}, \tag{4.93}$$

where the last term is the parametric time derivative. The latter term can be readily rewritten as

$$\left[\sigma_j^\alpha, V\dot{V}^\dagger\right], \tag{4.94}$$

by noting that the unitarity of V implies $\dot{V}V^\dagger + V\dot{V}^\dagger = 0$. In conclusion, the equations of motion read

$$\frac{d}{dt}\sigma_j^\alpha = \frac{1}{i}\left[\sigma_j^\alpha, \widetilde{H}\right], \quad \text{with } \widetilde{H} \coloneqq H + iV\dot{V}^\dagger, \tag{4.95}$$

where H is the model Hamiltonian[19]. From a physical perspective, the last term can be interpreted as the inertial force contribution in the mobile frame $\mathcal{R}$, equal to

$$iV\dot{V}^\dagger = -s\,\vec{\omega}(t)\cdot\sum_{j=1}^{N}\vec{\sigma}_j = -s\,\vec{\omega}(t)\cdot\tilde{\vec{\sigma}}_0, \tag{4.96}$$

where we introduced the vector $\vec{\omega} = (\omega^X, \omega^Y, \omega^Z)$, with components $\omega^X = -\sin\theta\,\dot{\phi}$, $\omega^Y = \dot{\theta}$, and $\omega^Z = \cos\theta\,\dot{\phi}$. Interestingly, if one describes the dynamics in the frame $\mathcal{R}$, then observes an inertial force formally equivalent to an additional time-dependent external field coupled to each spin.

We now introduce the same approximation detailed in the last section, thus expanding to the quadratic order in spin-wave operators and retaining only the

[17] The operator $s\,\sigma_j^\alpha$ is the generator of rotations around the α-axis for the spin $\vec{s_j} \equiv s\,\vec{\sigma_j}$, for $\alpha = x, y, z$. The operator above is then the composition of two CCW rotations: the first of an angle θ around the y-axis and the second of an angle ϕ around the z-axis. These two rotations in general do not commute.

[18] All the operators are understood to be in the Heisenberg representation of the time evolution.

[19] These equations hold for any self-adjoint operator in the form $VAV^\dagger$, in particular for the spin-wave canonical operators in the frame $\mathcal{R}$ (see below).

interaction between spin waves and the collective total spin. In this framework, the reduced Hamiltonian $\mathcal{H} = H/N$ is still given by Eq. (4.51); with the additional inertial contribution it reads

$$\begin{aligned}
\widetilde{\mathcal{H}} \coloneqq \frac{\widetilde{H}}{N} =& -\bar{\lambda}\left(\hat{Z}\cdot\hat{x}\right)^2 - g\left(\hat{Z}\cdot\hat{z}\right) - s\cos\theta\,\dot{\phi} \\
&+ \hbar_{\text{eff}}(n_0+N_{\text{sw}})\left[2\bar{\lambda}\left(\hat{Z}\cdot\hat{x}\right)^2 + g\left(\hat{Z}\cdot\hat{z}\right) + s\cos\theta\,\dot{\phi}\right] \\
&- \hbar_{\text{eff}}\sum_k \tilde{J}_k\left[\left(\hat{X}\cdot\hat{x}\right)^2\tilde{q}_k\tilde{q}_{-k} + \left(\hat{Y}\cdot\hat{x}\right)^2\tilde{p}_k\tilde{p}_{-k} + 2\left(\hat{X}\cdot\hat{x}\right)\left(\hat{Y}\cdot\hat{x}\right)\frac{\tilde{q}_k\tilde{p}_{-k}+\tilde{p}_k\tilde{q}_{-k}}{2}\right] \\
&+ \hbar_{\text{eff}}^{1/2}\tilde{q}_0\Bigg\{ s\sin\theta\,\dot{\phi} - 2\bar{\lambda}\left(1-\hbar_{\text{eff}}N_{\text{sw}}\right)(\hat{Z}\cdot\hat{x})(\hat{X}\cdot\hat{x}) - g(\hat{X}\cdot\hat{z}) \\
&\qquad + 2(\hat{Z}\cdot\hat{x})\hbar_{\text{eff}}\sum_{k\neq 0}\tilde{J}_k\left[(\hat{X}\cdot\hat{x})\,\tilde{q}_k\tilde{q}_{-k} + (\hat{Y}\cdot\hat{x})\,\frac{\tilde{q}_k\tilde{p}_{-k}+\tilde{p}_k\tilde{q}_{-k}}{2}\right]\Bigg\} \\
&+ \hbar_{\text{eff}}^{1/2}\tilde{p}_0\Bigg\{ -s\dot{\theta} - 2\bar{\lambda}\left(1-\hbar_{\text{eff}}N_{\text{sw}}\right)(\hat{Z}\cdot\hat{x})(\hat{Y}\cdot\hat{x}) - g(\hat{Y}\cdot\hat{z}) \\
&\qquad + 2(\hat{Z}\cdot\hat{x})\hbar_{\text{eff}}\sum_{k\neq 0}\tilde{J}_k\left[(\hat{Y}\cdot\hat{x})\,\tilde{p}_k\tilde{p}_{-k} + (\hat{X}\cdot\hat{x})\,\frac{\tilde{q}_k\tilde{p}_{-k}+\tilde{p}_k\tilde{q}_{-k}}{2}\right]\Bigg\},
\end{aligned} \tag{4.97}$$

with time-dependent $\hat{X}(t)$, $\hat{Y}(t)$, $\hat{Z}(t)$, defined in terms of the angles $\theta(t)$ and $\phi(t)$ as in Eq. (4.21).

Let us remark that all the steps that brought us to this Hamiltonian are still valid, in particular the spin-wave approximation in Eq. (4.42), with the important difference that the canonical operators $\tilde{q}_k$, $\tilde{p}_k$ are now referred to the moving frame $\mathcal{R}$ and depend parametrically on time. The correct Heisenberg equations for these operators are then

$$\begin{cases} \dfrac{d}{dt}\tilde{q}_k = \dfrac{1}{i}\left[\tilde{q}_k, \widetilde{H}\right] \\ \dfrac{d}{dt}\tilde{p}_k = \dfrac{1}{i}\left[\tilde{p}_k, \widetilde{H}\right], \end{cases} \tag{4.98}$$

valid for both $k \neq 0$ and $k = 0$. In close analogy with the previous section, one finds

$$\begin{cases} s\dfrac{d}{dt}\tilde{q}_k = (2\bar{\lambda}\sin^2\theta\cos^2\phi + g\cos\theta - 2\tilde{J}_k\sin^2\phi + s\cos\theta\,\dot{\phi})\tilde{p}_k \\ \qquad\qquad + 2\tilde{J}_k\cos\theta\sin\phi\cos\phi\,\tilde{q}_k + \delta_{k,0}\,\hat{b} \\ s\dfrac{d}{dt}\tilde{p}_k = -(2\bar{\lambda}\sin^2\theta\cos^2\phi + g\cos\theta - 2\tilde{J}_k\cos^2\theta\cos^2\phi + s\cos\theta\,\dot{\phi})\tilde{q}_k \\ \qquad\qquad - 2\tilde{J}_k\cos\theta\sin\phi\cos\phi\,\tilde{p}_k - \delta_{k,0}\,\hat{a}, \end{cases} \tag{4.99}$$

where the operators $\hat{a}$ and $\hat{b}$ indicate the first and second curly braces of Eq. (4.51) respectively, and we neglected non-linear contributions to the evolution of canonical spin-wave operators ($k \neq 0$). It is easy to check that Eq. (4.99) correctly reduce to Eq. (4.54) in the specific case $\dot{\theta} = \dot{\phi} = 0$.

For the spin-wave expansion to be valid, the condition

$$\langle \tilde{q}_0(t) \rangle = \langle \tilde{p}_0(t) \rangle = 0 \tag{4.100}$$

must hold not only at the initial time $t = 0$, but also for the evolving system at $t > 0$. Namely, one must choose an initial condition such that $\langle \tilde{q}_0(0) \rangle = \langle \tilde{p}_0(0) \rangle = 0$, and the equations for the mean values must admit as (unique) solution $\langle \tilde{q}_0(t) \rangle \equiv 0$ and $\langle \tilde{p}_0(t) \rangle \equiv 0$. These equations are clearly obtained by Eq. (4.99) by replacing each operator with its mean value.

In complete analogy with the equilibrium treatment of the previous chapter, this requires the averages of the curly braces to be zero. These conditions yield a pair of classical evolution equations for $\theta(t)$ and $\phi(t)$

$$\begin{cases} s\dfrac{d}{dt}\theta = +2\bar{\lambda}[1-\epsilon(t)]\sin\theta\cos\phi\sin\phi - 2\Big(\hbar_{\text{eff}}\displaystyle\sum_{k\neq 0}\tilde{J}_k\Delta_k^{pp}(t)\Big)\sin\theta\cos\phi\sin\phi \\ \qquad\qquad + 2\Big(\hbar_{\text{eff}}\displaystyle\sum_{k\neq 0}\tilde{J}_k\Delta_k^{qp}(t)\Big)\cos\theta\sin\theta\cos^2\phi, \\ s\dfrac{d}{dt}\phi = -g + 2\bar{\lambda}[1-\epsilon(t)]\cos\theta\cos^2\phi - 2\Big(\hbar_{\text{eff}}\displaystyle\sum_{k\neq 0}\tilde{J}_k\Delta_k^{qq}(t)\Big)\cos\theta\cos^2\phi \\ \qquad\qquad + 2\Big(\hbar_{\text{eff}}\displaystyle\sum_{k\neq 0}\tilde{J}_k\Delta_k^{qp}(t)\Big)\sin\phi\cos\phi, \end{cases} \tag{4.101}$$

which depend also on the spin-wave correlation functions defined in Eq. (4.55), and on the non-equilibrium spin-wave density

$$\epsilon(t) \coloneqq \frac{1}{Ns}\sum_{k\neq 0}\big\langle n_k(t)\big\rangle = \frac{1}{Ns}\sum_{k\neq 0}\frac{\Delta_k^{qq}(t)+\Delta_k^{pp}(t)-1}{2}. \tag{4.102}$$

Also the Eqs. (4.101) correctly reduce to the equilibrium counterpart in Eqs. (4.57), as long as $\dot{\theta} = \dot{\phi} = 0$.

We can now substitute the above expressions for $\dot{\theta}$ and $\dot{\phi}$ in Eq. (4.99) and retain only linear terms in the spin-wave operators, finding

$$\begin{cases} s\dfrac{d}{dt}\tilde{q}_k = +2\bar{\lambda}\cos^2\phi\;\tilde{p}_k - 2\tilde{J}_k\sin^2\phi\;\tilde{p}_k + 2\tilde{J}_k\cos\theta\cos\phi\sin\phi\;\tilde{q}_k + \delta_{k,0}\,\hat{b}, \\ s\dfrac{d}{dt}\tilde{p}_k = -2\bar{\lambda}\cos^2\phi\;\tilde{q}_k + 2\tilde{J}_k\cos^2\theta\cos^2\phi\;\tilde{q}_k - 2\tilde{J}_k\cos\theta\cos\phi\sin\phi\;\tilde{p}_k - \delta_{k,0}\,\hat{a}, \end{cases} \tag{4.103}$$

which in turn yield the evolution equations for the mean values

$$\begin{cases} s\dfrac{d}{dt}\langle\tilde{q}_k\rangle = +2\bar{\lambda}\cos^2\phi\ \langle\tilde{p}_k\rangle - 2\tilde{J}_k\sin^2\phi\ \langle\tilde{p}_k\rangle + 2\tilde{J}_k\cos\theta\cos\phi\sin\phi\ \langle\tilde{q}_k\rangle\,, \\ s\dfrac{d}{dt}\langle\tilde{p}_k\rangle = -2\bar{\lambda}\cos^2\phi\ \langle\tilde{q}_k\rangle + 2\tilde{J}_k\cos^2\theta\cos^2\phi\ \langle\tilde{q}_k\rangle - 2\tilde{J}_k\cos\theta\cos\phi\sin\phi\ \langle\tilde{p}_k\rangle \end{cases} \tag{4.104}$$

and for the equal-time correlation functions

$$\begin{cases} s\dfrac{d}{dt}\Delta_k^{qq} = 4\tilde{J}_k\cos\theta\cos\phi\sin\phi\,\Delta_k^{qq} + 4\left(\bar{\lambda}\cos^2\phi - \tilde{J}_k\sin^2\phi\right)\Delta_k^{qp} + 2\delta_{k,0}\langle\tilde{q}_0\hat{b}\rangle\ , \\ s\dfrac{d}{dt}\Delta_k^{pp} = -4\tilde{J}_k\cos\theta\cos\phi\sin\phi\,\Delta_k^{pp} - 4\left(\bar{\lambda}\cos^2\phi - \tilde{J}_k\cos^2\theta\cos^2\phi\right)\Delta_k^{qp} - 2\delta_{k,0}\langle\tilde{p}_0\hat{a}\rangle\,, \\ s\dfrac{d}{dt}\Delta_k^{qp} = -2\left(\bar{\lambda}\cos^2\phi - \tilde{J}_k\cos^2\theta\cos^2\phi\right)\Delta_k^{qq} + 2\left(\bar{\lambda}\cos^2\phi - \tilde{J}_k\sin^2\phi\right)\Delta_k^{pp} \\ \qquad\qquad + \delta_{k,0}(\langle\tilde{p}_0\hat{b}\rangle - \langle\tilde{q}_0\hat{a}\rangle). \end{cases} \tag{4.105}$$

The dynamical evolution of an initial Gaussian state is completely determined by Eq. (4.104) and Eq. (4.105), since the equations of motion are linear. In addition, by choosing the initial state such that $\langle\tilde{q}_k(0)\rangle = \langle\tilde{p}_k(0)\rangle = 0$, the averages remain zero at all times, so one can focus on the correlation functions only. Again, the terms multiplying the Kronecker delta equal zero thanks to the Wick theorem:

$$\langle\tilde{q}_0\hat{a}\rangle = \langle\tilde{q}_0\hat{b}\rangle = \langle\tilde{p}_0\hat{a}\rangle = \langle\tilde{p}_0\hat{b}\rangle = 0. \tag{4.106}$$

Finally, one has to take into account the constraints

$$4\left(\Delta_k^{qp}\right)^2 = 4\Delta_k^{qq}\Delta_k^{pp} - 1, \tag{4.107}$$

which are an exact property of the evolving Gaussian state, and are thus satisfied at all times and for all values of k.

In conclusion, the dynamics of the system at the Gaussian level is completely specified by a set of $2N+2$ coupled equations of motion, with the first two in Eq. (4.101) for the dynamics of the collective spin, and the other $2N$ equations for the evolution of the correlation functions

$$\begin{cases} s\dfrac{d}{dt}\Delta_k^{qq} = 4\tilde{J}_k\cos\theta\cos\phi\sin\phi\,\Delta_k^{qq} + 4\left(\bar{\lambda}\cos^2\phi - \tilde{J}_k\sin^2\phi\right)\Delta_k^{qp} \\ s\dfrac{d}{dt}\Delta_k^{qp} = -2\left(\bar{\lambda}\cos^2\phi - \tilde{J}_k\cos^2\theta\cos^2\phi\right)\Delta_k^{qq} + 2\left(\bar{\lambda}\cos^2\phi - \tilde{J}_k\sin^2\phi\right)\Delta_k^{pp}, \end{cases} \tag{4.108}$$

where Δ_k^{pp} are expressed in terms of Δ_k^{qq} and Δ_k^{qp} thanks to Eq. (4.107).

In addition, one has to specify suitable initial conditions, which can correspond to the Gaussian approximate ground state of the initial time Hamiltonian,

thus relying on the results of the previous section. As soon as the external field $g(t)$ varies in time, the non-equilibrium dynamical evolution (at the Gaussian level) of this initial state is described by the equations derived above.

The physical picture emerging from these equations is clear: the LMG dynamics for the collective degree of freedom $\langle\vec{\tilde{\sigma}}_0\rangle$ is modified by the spin-wave excitations, with corrections at linear order in the small parameters $\tilde{J}_{k\neq 0}$ [see Eq. (4.101)]. Concurrently, the motion of the collective degree of freedom described by $\theta(t)$ and $\phi(t)$ drives the evolution of the spin-wave Gaussian state [see Eq. (4.108)].

The energy of the system is easily evaluated by averaging the Hamiltonian (written in the fixed frame as in Eq. (4.51)) over the equilibrium or non-equilibrium Gaussian state. In light of the previous arguments, only the quadratic part gives a non-zero contribution, which reads[20]

$$\begin{aligned}\frac{E}{N} =& -\bar{\lambda}\rho^2\sin^2\theta\cos^2\phi - g\rho\cos\theta + \hbar_{\text{eff}}\, n_0\left(2\bar{\lambda}\sin^2\theta\cos^2\phi + g\cos\theta\right)\\ &- \hbar_{\text{eff}}\sum_k \tilde{J}_k\left(\cos^2\theta\cos^2\phi\,\Delta_k^{qq} + \sin^2\phi\,\Delta_k^{pp} - 2\cos\theta\sin\phi\cos\phi\,\Delta_k^{qp}\right),\end{aligned} \tag{4.109}$$

where the first two terms are the (reduced) classical energy of the collective degree of freedom, and $\rho = 1-\epsilon$. In the absence of an external driving, i.e. for constant g, the energy is conserved up to order $\mathcal{O}(\epsilon^2)$: the inexact conservation of energy is an expected consequence of the approximations introduced, in particular of the approximate description for the ground state. In the case of a time dependent driving field $g(t)$, the angles θ and ϕ, as well as ρ, n_0 and the two-points correlation functions are all time dependent functions, and the energy is obviously not conserved anymore.

As a final remark, we note that the evolution does not conserve the average occupation number of each spin-wave mode $\langle n_{k\neq 0}\rangle$, except for the limit case $\tilde{J}_{k\neq 0} = 0$, where we retrieve the unperturbed LMG model.

In the next section, we concisely specialize our general results for the unperturbed LMG model. While this section could have been placed before the generic discussion on spin waves, we decided to postpone it, in order to remark that it relies on the same formal expansion adopted for the general case, applied only to the collective mode $k = 0$.

[20] This expression is correct up to order $\mathcal{O}(\epsilon^2)$.

4.6 "Spin-wave" expansion for the unperturbed LMG model

In the case of vanishing perturbations, i.e. for $\tilde{J}_{k\neq 0} = 0$, one retrieves the plain LMG model, and the Hamiltonian in Eq. (4.97) reduces to a systematic expansion of the exact LMG Hamiltonian, which is performed in the rotating frame $\mathcal{R}$.

This expansion is carried out in the operators $\tilde{q}_0$ and $\tilde{p}_0$, describing collective spin fluctuations along $\hat{X}(t)$ and $\hat{Y}(t)$ respectively; the latters are the transverse directions with respect to $\hat{Z}(t)$, which is self-consistently aligned with the average total spin $\langle\vec{\tilde{\sigma}}_0\rangle$.

The reduced Hamiltonian now reads

$$\mathcal{H} = \mathcal{H}_{\rm cl} + \hbar_{\rm eff}^{1/2}\mathcal{H}_{\rm lin} + \hbar_{\rm eff}\mathcal{H}_{\rm quad} + \mathcal{O}(\hbar_{\rm eff}^{3/2}), \tag{4.110}$$

where[21]

$$\begin{cases} \mathcal{H}_{\rm cl} = -\lambda\sin^2\theta\cos^2\phi - g\cos\theta - \cos\theta\,\dot{\phi} \\ \\ \mathcal{H}_{\rm lin} = \tilde{q}_0\big[\sin\theta\,\dot{\phi} - 2\lambda(1-\epsilon)\sin\theta\cos^2\phi\cos\theta + g\sin\theta\big] + \\ \qquad\quad \tilde{p}_0\big[-\dot{\theta} + 2\lambda(1-\epsilon)\sin\theta\sin\phi\cos\phi\big] \\ \\ \mathcal{H}_{\rm quad} = \big[2\lambda\sin^2\theta\cos^2\phi + g\cos\theta + \cos\theta\,\dot{\phi}\big]\big(n_0 + N_{\rm sw}\big) \\ \qquad\quad -\lambda\left[\cos^2\theta\cos^2\phi\,\tilde{q}_0^2 + \sin^2\phi\,\tilde{p}_0^2 \;-2\cos\theta\sin\phi\cos\phi\frac{\tilde{q}_0\tilde{p}_0 + \tilde{p}_0\tilde{q}_0}{2}\right]. \end{cases} \tag{4.111}$$

For the LMG model, one clearly has $\dot{\epsilon}(t) \equiv \hbar_{\rm eff}\dot{N}_{\rm sw}(t) = 0$, and thus the equations of motion for the collective spin [see Eq. (4.101)] reduce to the usual Hamilton equations in Eq. (2.35), which describe the LMG dynamics in the thermodynamic limit. On the same footing as the general discussion in the previous section, these equations are easily found by imposing the linear term $\mathcal{H}_{\rm lin}$ to vanish. By writing $\rho = 1 - \epsilon = \text{const}$, one finds

$$\begin{cases} \dot{\theta} = \lambda\rho\sin\theta\sin 2\phi \\ \dot{\phi} = -g + \lambda\rho\cos\theta(1+\cos 2\phi), \end{cases} \tag{4.112}$$

which are easily checked to be equivalent to Eq. (2.35).

[21] We rescale time as $t' = t/s$, for consistency with the treatise of the classical model, see section 2.1 onwards.

Moreover, if one substitutes the classical equations back in Eq. (4.111), then finds

$$\begin{cases} \mathcal{H}_{\rm cl} = -\,\lambda\cos^2\phi(1+\cos^2\theta) \\ \\ \mathcal{H}_{\rm quad} = \left(\lambda\sin^2\theta\,\dfrac{1+\cos 2\phi}{2}\right)\tilde{q}_0^2 + \lambda\cos 2\phi\,\tilde{p}_0^2 + \lambda\cos\theta\sin 2\phi\dfrac{\tilde{q}_0\tilde{p}_0+\tilde{p}_0\tilde{q}_0}{2} \\ \qquad\qquad + \lambda(1+\cos 2\phi)(1+\cos^2\theta)N_{\rm sw}. \end{cases} \tag{4.113}$$

In light of the discussion in section 2.2, we know that, for large but finite values of N, Eqs. (4.112) approximately describe the evolution of spin coherent states, at the level of total spin averages [see Eq. (2.15)]. As noted above, this description completely neglects decoherence effects taking place at the Ehrenfest time $t_{\rm Ehr}$.

However, while at the Ehrenfest time scale the wave-packet semiclassical picture completely breaks down[22], one could think of giving a better description of the short-time coherent evolution of the initial state.

The first non-trivial order of approximation consists in describing the quantum state as a Gaussian wave packet, i.e. to treat quantum fluctuations of the collective mode $k = 0$ at the quadratic order[23]. As depicted above for the general case of non-zero perturbations, this approximate description of both equilibrium and dynamics is yielded by the Hamiltonian in Eq. (4.110), truncated at the quadratic order.

We discussed thoroughly in the last sections that, as soon as non-zero perturbations are included, also quantum fluctuations for $k \neq 0$ spin-wave modes enter in the dynamical evolution of the system. In this respect, let us mention that it is somewhat improper to refer to collective mode excitations as "spin-waves", since they correspond to infinite wave-length and do not carry any information on spatial scales[24].

The Gaussian wave-packet evolution in the rotating frame $\mathcal{R}$, is determined

[22] In fact, by definition of the Ehrenfest time, wave-packet spreading becomes $\mathcal{O}(1)$.

[23] As mentioned in appendix A, it can be proven formally that a spin-coherent state reduces to an harmonic oscillator coherent state, for large values of N.

[24] In fact, zero-mode excitations enter in the dynamical evolution of the fully-connected LMG model, where no spatial scales exist.

univocally by the dynamical equations[25] for two-points correlation functions

$$\begin{cases} \dfrac{d}{dt}\Delta_0^{qq} = 4\lambda\cos\theta\cos\phi\sin\phi\,\Delta_0^{qq} + 4\left(\lambda\cos^2\phi - \lambda\sin^2\phi\right)\,\Delta_0^{qp} \\ \dfrac{d}{dt}\Delta_0^{qp} = -\,2\left(\lambda\cos^2\phi - \lambda\cos^2\theta\cos^2\phi\right)\Delta_0^{qq} + 2\left(\lambda\cos^2\phi - \lambda\sin^2\phi\right)\Delta_0^{pp}, \end{cases} \tag{4.114}$$

which may be rewritten as

$$\begin{cases} \dfrac{d}{dt}\Delta_0^{qq} = 2\lambda\cos\theta\sin 2\phi\,\Delta_0^{qq} + 4\lambda\cos 2\phi\,\Delta_0^{qp} \\ \dfrac{d}{dt}\Delta_0^{qp} = -\,\lambda\sin^2\theta(1+\cos 2\phi)\,\Delta_0^{qq} + 2\lambda\cos 2\phi\,\Delta_0^{pp}, \end{cases} \tag{4.115}$$

with Δ_0^{pp} expressed in terms of Δ_0^{qq} and Δ_0^{qp} as

$$\Delta_0^{pp} = \frac{1}{\Delta_0^{qq}}\left(\frac{1}{4} + (\Delta_0^{qp})^2\right). \tag{4.116}$$

Note that the dynamical evolution for the zero-mode correlation functions depends on the classical trajectory $(\theta(t), \phi(t))$, which is in turn determined by the initial condition and by the value of g, or more generally by the time-dependent driving $g(t)$. However, there is no feedback effect from the zero-mode fluctuations on the collective classical dynamics, at this level of approximation.

As a substantial improvement, in comparison with the fully-classical treatise (which is exact only in the thermodynamic limit), Eqs. (4.115) describe not only the displacement of the initial localized wave-packet, but also squeezing effects.

One can define the collective spin squeezing as the minimal transverse variance of collective spin fluctuations [22]

$$\xi^2 \coloneqq \frac{\min_{|\hat{u}|=1,\ \hat{u}\perp\hat{Z}(t)}\left\langle\left(\hat{u}\cdot\vec{J}\right)^2\right\rangle}{j/2}. \tag{4.117}$$

The latter expression can be rewritten in the maximal spin sector ($j = Ns$) in terms of the collective degree of freedom $\vec{\mathcal{S}}$, defined in Eq. (2.5), as

$$\xi^2 \coloneqq 2Ns\,\min_{|\hat{u}|=1,\ \hat{u}\perp\hat{Z}(t)}\left\langle\left(\hat{u}\cdot\vec{\mathcal{S}}\right)^2\right\rangle. \tag{4.118}$$

This quantity formalizes the intuitive idea of a deformation of the inital spin coherent state, which generally occurs during the dynamics. It follows from the definition in Eq. (4.117) that $\xi = 1$ only for the spin coherent state[26] given by $|\hat{Z}(t)\rangle \equiv |\theta(t), \phi(t)\rangle$.

[25] These equations are a specific case of Eqs. (4.108), with $\tilde{J}_{k\neq 0} = 0$ and $\tilde{J}_0 \equiv \bar{\lambda} = \lambda$.

[26] Compare with Eq. (A.8).

Remarkably, one can prove that the collective spin squeezing ξ^2 can be written as [23]

$$\xi^2(t) = 1 + 2\,\langle n_0(t)\rangle - 2\sqrt{\langle n_0(t)\rangle\,\big(1 + \langle n_0(t)\rangle\,\big)}, \tag{4.119}$$

where $\langle n_0(t)\rangle$ is the average number of zero-mode collective excitations

$$\langle n_0(t)\rangle = \frac{\Delta_0^{qq}(t) + \Delta_0^{pp}(t) - 1}{2}. \tag{4.120}$$

This result holds in the large-N limit, so that we are actually dealing with standard squeezed states of the harmonic oscillator, with canonical operators $\tilde{q}_0$, $\tilde{p}_0$.

It is not difficult to check that, in the limit $\langle n_0\rangle \ll 1$, one has

$$\xi^2 = 1 - 2\sqrt{\langle n_0\rangle} + \mathcal{O}\big(\,\langle n_0\rangle\,\big), \tag{4.121}$$

retrieving the spin coherent state in direction $\hat{Z}(t)$ for $\langle n_0\rangle = 0$. In the opposite limit $\langle n_0\rangle \gg 1$, one finds

$$\xi^2 = \frac{1}{4\,\langle n_0\rangle} + \mathcal{O}\left[\left(\frac{1}{\langle n_0\rangle}\right)^2\right]. \tag{4.122}$$

More precisely, this is the limit where $\langle n_0\rangle \lesssim N$,[27] therefore massively squeezed states have

$$\xi \approx \frac{1}{\sqrt{N}}. \tag{4.123}$$

As a conclusive remark, we mention that, thanks to the integrability of the LMG model, one can also resort to exact diagonalization techniques, in order to find an exact numerical description of the dynamics. In contrast, as soon as integrability-breaking finite-range interactions are introduced (alias as soon as $\tilde{J}_{k\neq 0} \neq 0$), exact diagonalization techniques can be adopted only for small chains, typically up to $N = 16$ spins, since the Hilbert space dimension increases exponentially as $(2s+1)^N$.

[27] Note that $N \gg 1$, as usual.

Chapter 5

Robustness of optimal protocols to quantum fluctuations

In this chapter we aim to understand the effects of quantum fluctuations on the optimal (or sub-optimal) dynamics. More precisely, let us consider the optimized protocols determined in chapter 3, for the LMG model in the thermodynamic limit. Upon the introduction of weak integrability-breaking perturbations [as in the Hamiltonian in Eq. (4.36)], which are treated at the quadratic order in quantum fluctuations [as in Eq. (4.97)], it is quite natural to address the following questions:

- How is it possible to quantify the effects of the perturbation on the optimal dynamics?
- Are these effects less or more significant, depending on the specific choice for the target state?

In order to answer to these questions, we first reformulate them more precisely, in section 5.1. Finally, in section 5.2, we introduce a specific expression for the perturbation and discuss the results.

5.1 Optimal control in the presence of quantum fluctuations

In this section, for the sake of clarity, we will explain in more detail our purpose. The equations of motion for the average total spin $\langle \vec{\mathcal{S}} \rangle$ (parametrized by the angles $\theta(t)$, $\phi(t)$) are given by Eq. (4.101), and include the quantum feedback from the spin-wave two-points correlation functions $\{\Delta_k^{qq}, \Delta_k^{qp}, \Delta_k^{pp}\}_{k\neq 0}$.

The time evolution of the latters, as explained in the previous section, is self-consistently determined by the evolution of the collective degree of freedom, through Eq. (4.108), where use has been made of the Gaussian constraint in Eq. (4.107). We remark here that the equations for the two independent correlation functions of each mode k are not directly coupled to the corresponding equations for other modes ($k' \neq k$). However, these equations are all coupled to the ones for $\theta(t)$ and $\phi(t)$.

In addition, the fluctuations for the collective mode ($k = 0$) are described by the two-points correlation functions $\{\Delta_0^{qq}, \Delta_0^{qp}, \Delta_0^{pp}\}$, which yield no feedback on the collective average dynamics; their evolution is governed by Eq. (4.115), with the usual Gaussian constraint. These equations are in fact decoupled from all the others, at the present level of approximation.

In close analogy with the previous chapters, we will consider as initial condition the fully-polarized state along the x-direction, which is the spin coherent state $|\theta_0 = \pi/2, \phi_0 = 0\rangle$. In the Gaussian approximation, this state is mapped to a coherent Gaussian wave-packet, with

$$\begin{cases} \Delta_k^{qq}(0) = 1/2 \\ \Delta_k^{qp}(0) = 0 \end{cases} \tag{5.1}$$

for all k (included $k = 0$).

This localized wave-packet is the (approximate) ground state of the Hamiltonian in Eq. (4.51) for $g = 0$, as detailed in section 4.4. Note that Eqs. (5.1) immediately imply that no spin waves are excited in the initial state, i.e. $\epsilon(0) = 0$, and similarly that $\langle n_0(0)\rangle = 0$. In addition, we choose a target state of the same form as in chapter 3, which is a spin coherent state in direction $|\theta_{\rm tar}, \phi_{\rm tar} = 0\rangle$.

We then select an optimal (or sub-optimal) protocol $g_{\rm opt}(t)$, determined for the LMG model in the thermodynamic limit [see sections 3.2 and 3.3] which, if substituted in place of g in Eq. (4.101), drives the perturbed system's dynamics in the time interval $t \in [0, T]$.

As mentioned above, we are interested in quantifying the effects of the perturbation on the optimal dynamics.

We consider the integrability-breaking terms such as "quantum noise", which in principle can prevent our system from reaching the target state at time T. In this framework, even though we have a specific model for the noise (which corresponds to a specific form of $\tilde{J}_{k\neq 0}$), we are not interested in controlling the perturbed dynamics. As anticipated, we are rather interested in assessing the impact of perturbations on the optimized dynamics, which has been previously determined for the unperturbed LMG model.

A reasonable quantity that describes the effects of pertubations on the op-

timal dynamics is the time-averaged spin-wave density, which reads

$$\bar{\epsilon} = \frac{1}{T}\int_0^T dt\, \epsilon(t). \tag{5.2}$$

In the unperturbed LMG model, by choosing as initial condition the spin coherent state $|\theta_0 = \pi/2, \phi_0 = 0\rangle$ (or any other state in the maximal total spin sector), one has $\epsilon(t) \equiv 0$, due to the total spin conservation. As soon as weak integrability-breaking terms are introduced, not only spin-wave excitations decrease the total spin value, but they also give a quantum feedback on the evolution of the average total spin $\langle\vec{\mathcal{S}}\rangle$ [see Eqs. (4.101)].

Remarkably, in the presence of non-zero perturbation, it is easy to check that $\bar{\epsilon} = 0$ iff $\Delta_k^{qq}(t) = \Delta_k^{pp}(t) \equiv 1/2$ and thus $\Delta_k^{qp}(t) \equiv 0$. In this limit case[1], Eqs. (4.101) reduce to the classical Hamilton equations (4.112) with $\rho = 1$.

In conclusion, let us highlight that quantum noise is here described as an additional term in the Hamiltonian, whose effects on the unperturbed optimal dynamics are studied in a fully-quantum (although approximate) description. This is a radically different description of noise from stochastic classical noise, which is used for instance in Langevin equations.

5.2 Nearest-neighbor perturbation

In order to study numerically the impact of quantum fluctuations on the optimized dynamics, we first need to choose a specific form for the integrability-breaking perturbation $J_{|i-j|}$, leading to a specific expression for the exact Hamiltonian in Fourier space

$$H = -\frac{\bar{\lambda}}{N}\left(\tilde{\sigma}^x_{k=0}\right)^2 - g\,\tilde{\sigma}^z_{k=0} - \frac{1}{N}\sum_{k\neq 0}\tilde{J}_k\;\tilde{\sigma}^x_k\tilde{\sigma}^x_{-k}, \tag{5.3}$$

and its quadratic expansion in Eq. (4.51).

We will consider a system where nearest-neighbor interaction is added to the infinite-range interaction of the LMG model, described by the Hamiltonian

$$H = -\frac{\lambda}{N}\sum_{i,j=1}^{N}\sigma^x_i\sigma^x_j - g\sum_{i=1}^{N}\sigma^z_i - J\sum_i\sigma^x_i\sigma^x_{i+1}, \tag{5.4}$$

on a 1d lattice with periodic boundary conditions. The parameter J controls the strength of the perturbation. By exploiting the parity of the perturbation

[1]This condition is not verified for any non-trivial dynamics, but it serves as a plausible argument, in order to justify the choice of $\bar{\epsilon}$ for quantifying noise effects on the optimal dynamics.

coefficients $J_{|i-j|}$, one easily evaluates $\tilde{J}_k = J\cos k$, which is correctly checked to be an even and real function, defined for the reciprocal lattice sites $k = 2\pi n/N$ for $n = -N/2+1, \ldots, N/2$. Consistently with the notation introduced in Eq. (4.48), we redefine

$$\tilde{J}'_k = \begin{cases} \tilde{J}_k, & \text{for } k \neq 0 \\ \bar{\lambda} = \lambda + \tilde{J}_0 = \lambda + J, & \text{for } k = 0, \end{cases} \tag{5.5}$$

and immediately drop the prime to simplify the notation. Accordingly, we shall measure energy in units of $\tilde{J}_0 \equiv \bar{\lambda}$, while the rescaled time $t' = t/s$ is measured in inverse units of energy.

Let us now present some relevant results, which may also hint possible directions for further investigation.

In numerical simulations we fix $N = 100$, and we choose the initial and target states as discussed in section 5.1.

As a preliminary comment, we remark that our analysis is restricted to perturbation intensity values $J/\bar{\lambda}$ such that the spin-wave expansion is a valid approximation (i.e. the condition in Eq. (4.90) is fulfilled at all times). This corresponds to total spin values $\rho(t) = 1 - \epsilon(t)$ close to maximal, and to the physical intuition that the large majority of spins is aligned to the direction $\hat{Z}(t) \coloneqq \big(\theta(t), \phi(t)\big)$ during the dynamical evolution, with small excitations density production for the collective ($k = 0$) and spin-wave ($k \neq 0$) modes.

In this regime, it is meaningful to compare the unperturbed optimal trajectory for the LMG model, driven by the optimized protocol $g_{\text{opt}}(t)$, with the corresponding one for the perturbed system[2]. Moreover, a reasonable choice for the figure of merit $\mathcal{M}$ is still provided by the non-negative quantity

$$\eta \coloneqq 1 - \vec{n}_{\text{tar}} \cdot \vec{n}(T). \tag{5.6}$$

where $|\vec{n}_{\text{tar}}\rangle = |\theta_{\text{tar}}, 0\rangle$ is the usual target coherent state, while the final versor $\vec{n}(T) = \big(\theta(T), \phi(T)\big)$ yields information only on the final direction of the average total spin $\langle\vec{\mathcal{S}}\rangle$, but it does not provide any description of the two-points correlation functions characterizing the final Gaussian state. Consequently, another complementary figure of merit is represented by the final spin depletion $\epsilon(T)$.

As anticipated above, for assigned values of s^z_{tar} and T/τ,[3] let us select an optimized protocol $g_{\text{opt}}(t)$, with the corresponding optimal dynamics for the

[2]Note that, if one represents the evolution of the perturbed model in the classical phase space, the dynamics is not constrained anymore on a sphere of fixed radius, since $\rho(t)$ is not constant in time.

[3]We apply here the same conventions as in chapter 3: in particular, the target fully-polarized state is characterized by the point $s^z_{\text{tar}} = \cos\theta_{\text{tar}}$, and the period τ refers to the ferromagnetic orbit connecting the initial and the target state.

unperturbed LMG model.

We now provide an answer to the first question that was raised at the beginning of this chapter: Thanks to the formalism introduced in chapter 4, we can actually determine numerically the dynamics of the perturbed system, under the driving $g_{\rm opt}(t)$.

In particular, it is interesting to quantify the impact of the perturbation on the optimal trajectory, as a function of perturbation intensity $J/\bar{\lambda}$. In fact, this is a relevant problem for realistic implementations of controlled quantum systems, where typically some additional perturbation cannot be ruled out. The only hypothesis here, is that one is able to provide a reasonable description of this additional perturbing term in the Hamiltonian, or "quantum noise".

In this respect, let us mention that, while a nearest-neighbor perturbation might be a reasonable guess under some experimental conditions, the spin-wave formalism can equally well describe any short- or long-range perturbation, for instance power law decaying interactions. The only difference is the explicit expression for the coefficients $\tilde{J}_k$, which enter in our description.

Clearly, for small enough values of $J/\bar{\lambda}$, one expects the trajectory of the perturbed system to be qualitatively similar to the unperturbed trajectory; on the contrary, for larger values of $J/\bar{\lambda}$, there should be a more significant modification of the optimal dynamics.

As an illustrative example, in Figs. 5.1 and 5.2, we show the impact of quantum fluctuations on the double-quench protocol and on a numerically optimized protocol, respectively. We set $s^z_{\rm tar} = 0.95$ and $T/\tau = 0.5$, drawing the optimal trajectory (for the unperturbed LMG model) with a red line, and the perturbed dynamics with a thick blue line. As usual, the initial and target states are marked with red points.

In this fashion, one could carry out a systematic quantitative study, and determine the maximum value of $J/\bar{\lambda}$ that can be tolerated, in order to reach some target state with a certain accuracy.

Firstly, one would need a more refined definition for the figure of merit $\mathcal{M}$, for instance by evaluating the fidelity between the displaced squeezed final state $|\psi(T)\rangle$ and the target coherent state. This would require some non-trivial manipulations, since these Gaussian states are defined in the rotating frame $\mathcal{R}$, therefore it is not immediately obvious how to evaluate their overlap. We leave this problem open for future investigation.

In addition, with this proper redefinition for the figure of merit, one could study whether some specific form for the optimal (or sub-optimal) protocol $g_{\rm opt}(t)$ is systematically more robust with respect to the introduction of quantum noise,

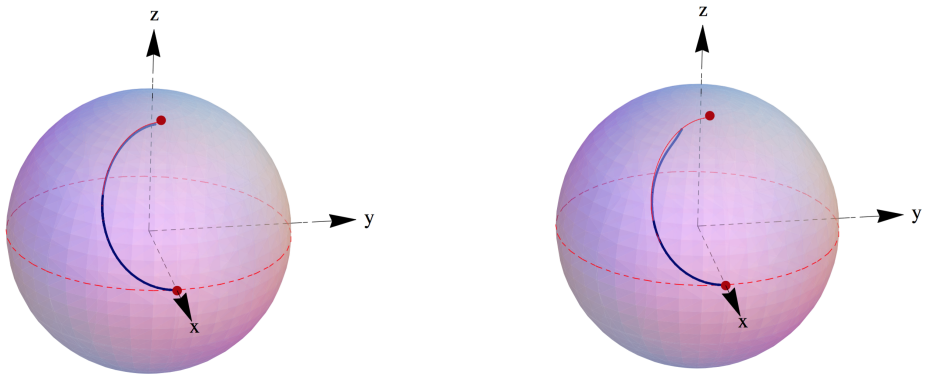

(a) $J/\bar{\lambda} = 0.2$ **(b)** $J/\bar{\lambda} = 0.5$

Figure 5.1: Impact of quantum fluctuations on the double-quench protocol, with target point $s^z_{\text{tar}} = 0.95$ and $T/\tau = 0.5$. The optimal trajectory is drawn in red, while the perturbed one is in blue. In the left panel we set $J/\bar{\lambda} = 0.2$, finding $\bar{\epsilon} \approx 6.8 \times 10^{-3}$. The perturbed orbit is qualitatively unaltered and covers the optimal trajectory, which is hardly visible. The corresponding values for the figures of merit are $\eta \approx 7.8 \times 10^{-4}$ and $\epsilon(T) \approx 1.8 \times 10^{-2}$.
In the right panel we set $J/\bar{\lambda} = 0.5$, finding $\bar{\epsilon} \approx 3.9 \times 10^{-2}$: the perturbed orbit is qualitatively different from the original one. In this case, spin-wave excitations yield a significantly larger disturbance on the optimal dynamics, with $\eta \approx 2.1 \times 10^{-2}$ and $\epsilon(T) \approx 1.1 \times 10^{-1}$.

and how this possibly depends on the choice for the target state and the final time T.

We can finally address the second question that was posed at the beginning of this chapter. Physical intuition may suggest that, for target states progressively closer to the paramagnetic ground state[4], the perturbing effects on the optimal dynamics might become more relevant. This is indeed the case, as shown in Fig. 5.3, where we plot the averaged spin-wave density production $\bar{\epsilon}$ as a function of s^z_{tar}, for $T/\tau = 0.5$[5]. Note the linear scale on the x axis and the logarithmic scale on the y axis.

[4]The paramagnetic ground state, as explained in chapter 2, is obviously given by the fully-polarized state along z.

[5]We checked that this result does not depend on the specific choice for T/τ.

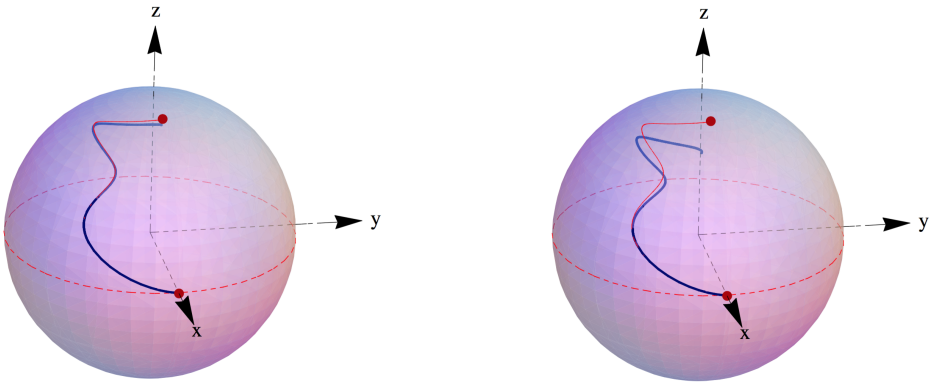

(a) $J/\bar{\lambda} = 0.2$ **(b)** $J/\bar{\lambda} = 0.5$

Figure 5.2: The same as in Fig. 5.1, for a numerically optimized protocol. We used the CRAB algorithm, with the first $n = 4$ harmonics of Eq. (3.20), and the linear ramp ansatz in Eq. (3.23). In the left panel we set $J/\bar{\lambda} = 0.2$, finding $\bar{\epsilon} \approx 7.3 \times 10^{-3}$. In close analogy with the left panel of Fig. 5.1, the perturbed dynamics covers almost exactly the optimal trajectory, and we get $\eta \approx 1.3 \times 10^{-4}$, $\epsilon(T) \approx 3.2 \times 10^{-2}$. In contrast, in the right panel, we set $J/\bar{\lambda} = 0.5$ and obtain $\bar{\epsilon} \approx 4.4 \times 10^{-2}$. In the latter case, spin-wave excitations alter more significantly the dynamics and we obtain $\eta \approx 7.2 \times 10^{-3}$, $\epsilon(T) \approx 1.9 \times 10^{-1}$.

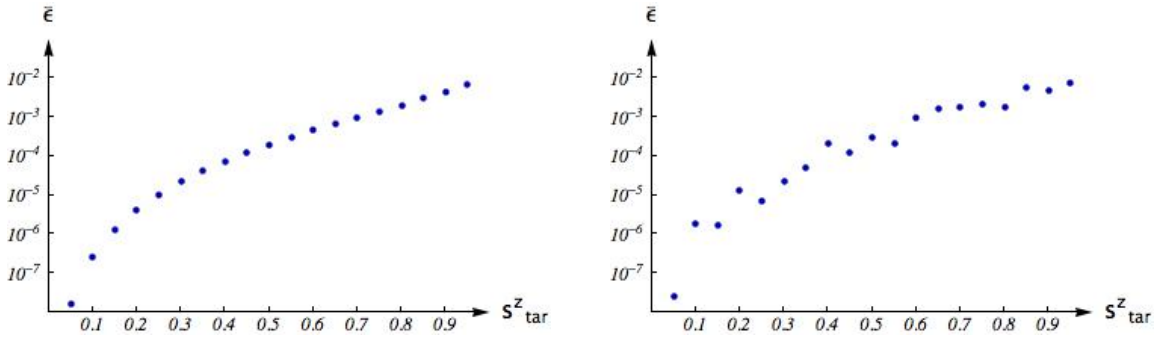

Figure 5.3: Lin-log plot of the averaged spin-wave density production $\bar{\epsilon}$ as a function of $s^z_{\rm tar}$, for $T/\tau = 0.5$, both for the double-quench protocol (left panel) and for a numerically optimized protocol (right panel). The latter is obtained with CRAB, in the same way as in Fig. 5.2. In both cases, we clearly observe an overall increase of $\bar{\epsilon}$ with $s^z_{\rm tar}$, although it is not perfectly monotonic in the right panel.

Chapter 6

Conclusions

In this thesis we firstly considered the quantum optimal control problem for the LMG model in the thermodynamic limit. Moreover, we described the effects of a finite-range integrability-breaking perturbation, by using a time-dependent spin-wave expansion with respect to the direction of the average total spin $\langle \vec{\mathcal{S}} \rangle$.

The main results of this thesis are derived in chapters 3 and 5.

In chapter 3, we characterized different optimal (or sub-optimal) protocols, in order to drive the LMG model to a target state, in a fixed time T. We exploited both analytical methods (based on the knowledge of the classical phase portrait) and numerical methods, in particular the CRAB technique. We showed that the number of solutions critically depend on the value of T, and, remarkably, we determined a lower bound $T_{\min}$ below which the target state cannot be reached exactly.

In chapter 5, we described the effects of "quantum noise", i.e. weak additional short-range perturbations, on the optimal dynamics. We provided some qualitative results, and a possible framework for more systematic studies of the impact of quantum fluctuations on the optimal dynamics.

This thesis could lead to a number of further investigations. For example, for the unperturbed LMG model, one could think of controlling explicitly not only the coherent quantum evolution of the average total spin, but also the collective spin squeezing [see Eq. (4.119)]. In fact, one could be interested in minimizing the final squeezing of the Gaussian wave-packet, in order to maximize the overlap with the target coherent state. This approach could yield refined versions of the optimal protocols, if compared with those determined by controlling only the classical collective dynamics, as in chapter 3.

In addition, it could be interesting to substitute these optimized drivings in the fullly-quantum Schrödinger equation, so as to compare the final fidelity with the one obtained with different quantum control methods. In fact, we remark

that exact numerical diagonalization is an easy task for the LMG model, since it can be performed in the maximal total spin sector, with dimension $\mathcal{O}(N)$.

I think that these optimized protocols, determined at the level of the Gaussian approximation, could yield good values for the final fidelity, or at least represent a convenient starting point for more refined optimizations.

Finally, at the end of chapter 5, we suggested some possible directions for a more quantitative analysis on the impact of quantum fluctuations on optimal dynamics.

More in general, I suspect that phase space methods could be an ideal, although rarely explored, playground in order to study quantum optimal control. In particular, it could be interesting to recast the quantum optimal control problem at the level of Wigner functions, where some insightful approximations can then be introduced, such as the TWA.

As a final comment, it is quite certain that quantum optimal control will take full advantage of the machine learning "revolution". In particular, reinforcement learning methods [24] will probably represent unmatched techniques for determining optimal protocols, as well as for providing heuristic insight on the physics of quantum many-body systems.

Appendix A

A short review on spin coherent states

The scope of this short appendix is to give a concise operative review on spin coherent states. The subject of generalized coherent states is an extremely interesting field, with far-reaching applications in diverse domains of physics and mathematics.

In the following, we will just outline some results that are of interest for the present thesis, avoiding technical details and demonstrations. The interested reader is referred to excellent books, such as [25] and [26].

As a first step, we give the definition of spin coherent states. Let us consider the spin operator $\vec{J}$ and refer to a subspace of fixed total spin, labeled by the quantum number j.

A spin coherent state system is generated by a family of unitary transformations from an appropriate reference state

$$|\vec{n}\rangle \equiv |\theta, \phi\rangle \coloneqq U(\theta, \phi)\, |\psi_0\rangle\,, \tag{A.1}$$

where the versor $\vec{n} = (\sin\theta\cos\phi, \sin\theta\sin\phi, \cos\theta)$ selects a direction in space by usual spherical coordinates, and $U(\theta, \phi) = \exp\left(i\theta\, \vec{m}\cdot\vec{J}\right)$, with the versor $\vec{m} = (\sin\phi, -\cos\phi, 0)$ being orthogonal to both $\vec{n}$ and the reference north pole versor $\vec{n}_0 = (0, 0, 1)$.

The usual choice for the reference state is one of the two states $|\psi_0\rangle = |j, j_z = \pm j\rangle$, since it yields a spin coherent system of states with smallest possible dispersion for the total spin operator $|\vec{J}|^2$,

$$(\Delta|\vec{J}|)^2 \equiv \sum_{\alpha=x,y,z} (\Delta J^\alpha)^2 = j. \tag{A.2}$$

Heuristically, this is the preferable choice for the reference state, since the generated spin coherent states resemble classical states, as closely as possible.

For the sake of definiteness, we choose $|\psi_0\rangle = |j, j_z = j\rangle$. Note that also the highest and lowest weight states $|\pm\vec{n}_0\rangle = |j, j_z = \pm j\rangle$ belong to the coherent states system, even though the above definition for the versor $\vec{m}$ is not valid for $\theta = 0, \pi$.

The above definition for coherent states in Eq (A.1) can be expressed in words as: One starts from the highest weight state $|\psi_0\rangle = |j, j_z = j\rangle$ and applies a rotation of angle θ around a properly defined axis $\vec{m}$, which rotates the initial coherent state to the generic coherent state $|\theta, \phi\rangle$. We remark that this rotation in spin space can be visualized as a common rotation of $3d$ vectors in Euclidean space.

We now summarize some relevant properties of spin coherent states, referring to the literature for explicit proofs and for a more in depth analysis of the topic.

1. A spin coherent states system is a over-complete set of states, and the resolution of identity can be written as an integral over the unit sphere S^2

$$\frac{2j+1}{4}\int_{S^2} d^2n\, |\vec{n}\rangle\, \langle\vec{n}| = \mathbb{1}. \tag{A.3}$$

2. It follows that two generic spin coherent states are not orthogonal, as can be checked by evaluating their fidelity[1]

$$\mathcal{F}\,(\vec{n}, \vec{m}) = |\langle\vec{n}|\vec{m}\rangle|^2 = \left(\frac{1+\vec{n}\cdot\vec{m}}{2}\right)^{2j}. \tag{A.4}$$

3. The spin projections averages have an evident geometrical meaning

$$\langle\vec{n}\,|\vec{J}\,|\vec{n}\,\rangle = j\,\vec{n}, \tag{A.5}$$

and in particular one has

$$\vec{n}\cdot\vec{J}\,|\vec{n}\rangle = j\,|\vec{n}\rangle\,. \tag{A.6}$$

4. The highest weight state $|\vec{n}\rangle = |j, j_z = j\rangle$ minimizes the product of spin fluctuations in orthogonal directions, in the sense that the Heisenberg uncertainty relation

$$(\Delta J^x)^2(\Delta J^y)^2 \leq \frac{1}{4}\,\langle J^z\rangle^2 \tag{A.7}$$

is satisfied as an equality. This is easily proven since $\langle J^x\rangle = \langle J^y\rangle = 0$ from the previous property, while obviously $\langle J^z\rangle = j$, and one can easily check

[1] The exact phase of the overlap between two coherent states can be evaluated explicitly, and it is found to be related to a semiclassical quantization of the sphere. For details, see reference [25].

that $(\Delta J^x)^2 = (\Delta J^y)^2 = j/2$. The same property applies to a generic spin coherent state $|\vec{n}\rangle$, upon suitable rotations of the spin operators, i.e. by substitution of J^α with $\tilde{J}^\alpha := U(\theta,\phi)J^\alpha U^\dagger(\theta,\phi)$, and reads

$$(\Delta \tilde{J}^x)^2(\Delta \tilde{J}^y)^2 = \frac{1}{4}\left\langle \tilde{J}^z \right\rangle^2 = \frac{j^2}{4}. \tag{A.8}$$

5. A remarkable expression for correlation functions of two operators in a (spin) coherent state is given in reference [27]. It is written as a systematic expansion in powers of the quantum parameter $1/j$ (or equivalently $\hbar$ for standard coherent states), involving only single-operator averages in the coherent state. For our purposes it is enough to retain that

$$\left\langle J^\alpha J^\beta \right\rangle = \left\langle J^\alpha \right\rangle \left\langle J^\beta \right\rangle + \mathcal{O}\left(\frac{1}{j}\right). \tag{A.9}$$

Spin coherent states, in close analogy with coherent states of the harmonic oscillator[2], have an important role in semiclassical physics. It is a well-known fact that oscillator coherent states closely mimick the classical evolution for an harmonic oscillator Hamiltonian.

An analogous result holds for spin coherent states [27], if we consider the Zeeman Hamiltonian, which describes the coupling of the spin to an external magnetic field

$$H_Z = -\vec{J}\cdot\vec{h}. \tag{A.10}$$

Skipping technical details, this result is quite natural, since the time evolution generated by the Zeeman Hamiltonian is a rotation around the axis defined by the magnetic field $\vec{h}$. Consequently, the initial coherent state is rotated, without the occurrence of decoherence effects. Let us point out the analogy between this Hamiltonian and the harmonic oscillator Hamiltonian, having both of them an equidistant energy spectrum.

In conclusion, we mention that in the large N limit, spin coherent states reduce to harmonic oscillator coherent states [25], as can be formally proved by using the Holstain–Primakoff mapping in the harmonic approximation, see Eq. (4.9).

[2]These states were studied by Schrödinger in the first years after the advent of quantum mechanics, so they are often referred to as standard coherent states.

Appendix B

Spin-wave theory in Fourier space

In the present appendix we would like to analyze in more detail the spin-wave theory and remark its generality. In order to do so, we consider a generic d-dimensional lattice model with spin operators $s^{\alpha}_{\mathbf{r}}$, where $\alpha = x, y, z$ refers to a fixed reference frame.

The main physical insight to develop the spin-wave theory is that we aim to describe only small perturbations above a fully-polarized (ground) state, say in the z-direction.

It is convenient to focus on the single-spin raising and lowering operators $s^{\pm}_{\mathbf{r}} := s^{x}_{\mathbf{r}} \pm i s^{y}_{\mathbf{r}}$. The following manipulations hold true for any lattice site, so we drop the label $\mathbf{r}$ and lower the component index, in order to simplify the notation.

It is immediate to verify the operator identity[1]

$$\hat{s}_{-}\hat{s}_{+} = \hat{s}^2 - \hat{s}_z^2 - \hat{s}_z, \tag{B.1}$$

which leads to the following identity for the eigenvalues in their common basis of eigenstates

$$\lambda_{s_z} = (s - s_z)(s + s_z + 1), \tag{B.2}$$

where we denote with λ_{s_z} the eigenvalues of the operator $\hat{s}_{-}\hat{s}_{+}$.

First of all, we remind that the operators s_x, s_y can be trivially rewritten in terms of $s_{\pm}$, just exploiting the definition of the latters. One could wish to rewrite also the operator s_z as a simple function of $s_{\pm}$. Heuristically, this could simplify the description of the problem, but the *actual reason* why one would like to achieve this will become clear in the following. For the sake of clarity, we first prepone the solution of this problem.

In fact, if we try to rewrite s_z as a simple function of $s_{\pm}$, we soon encounter some difficulties: if one solves the Eq. (B.1) for s_z, then finds two solutions

[1] Here we highlight that these are operators, by adopting the "hat" notation, in order to avoid confusion with the corresponding eigenvalues.

involving a square root. The exact representation of the operator s_z in terms of $s_\pm$ is consequently far from simple and inconvenient.

However, if we want to describe small perturbations away from the fully-polarized state, it might be tempting to write in some sense that $s_z \approx s \gg 1$. If this were so, the previous equation for the eigenvalues would simplify to

$$\lambda_{s_z} \approx 2s(s - s_z). \tag{B.3}$$

It would now be trivial to solve it for s_z, and to obtain via spectral decomposition a simple approximated expression for the operator s_z in terms of $s_\pm$, which reads

$$\hat{s}_z \approx s\mathbb{1} - \frac{\hat{s}_-\hat{s}_+}{2s}. \tag{B.4}$$

The problem is that the argument leading to this approximation sounds like a poor excuse, as vividly stated in [28]. In fact, the single spin value in each site is always $\mathcal{O}(1)$, often equal to $1/2$, meaning that the statement $s \gg 1$ is unacceptable.

The real justification behind the success of formula (B.3) is that it is actually exact for $s_z = s$ and $s_z = s - 1$. This is easily checked, and further implies that Eq. (B.4) is an operator *identity* for $s = 1/2$.

More in general, this sets a natural limit for the validity of the spin-wave theory: we are neglecting the possibility of multiple individual spin excitations at the same site, which is in manifest agreement with our initial physical idea. The previous statement can be rephrased more formally, by saying that Eq. (B.4) is exact if we truncate the Hilbert space of each spin to $s_z = s, s - 1$.

The next step of spin-wave theory is more conveniently carried out in Fourier space. Focusing again on raising and lowering operators, we define their Fourier transforms as

$$\tilde{S}^\pm_{\mathbf{k}} = \frac{1}{\sqrt{N}} \sum_{\mathbf{r}} e^{-i\mathbf{k}\cdot\mathbf{r}} s^\pm_{\mathbf{r}}, \tag{B.5}$$

where $\mathbf{k}$ varies over the sites of the reciprocal lattice, defined symmetrically with respect to the origin $\mathbf{k} = \mathbf{0}$[2]. This is convenient, since we remark that the adjoint of $\tilde{S}^+_{\mathbf{k}}$ is the operator $\tilde{S}^-_{-\mathbf{k}}$.

It is trivial to verify that for every choice of $\mathbf{k}$ and $\mathbf{k}'$

$$\left[\tilde{S}^+_{\mathbf{k}}, \tilde{S}^+_{\mathbf{k}'}\right] = \left[\tilde{S}^-_{\mathbf{k}}, \tilde{S}^-_{\mathbf{k}'}\right] = 0. \tag{B.6}$$

The other relevant commutation relations are also easily calculated, but give a rather cumbersome result

$$\left[\tilde{S}^+_{\mathbf{k}}, \tilde{S}^-_{\mathbf{k}'}\right] = \frac{2}{N} \sum_{\mathbf{r}} e^{-i(\mathbf{k}+\mathbf{k}')\cdot\mathbf{r}} s^z_{\mathbf{r}}. \tag{B.7}$$

[2] This assures that for every site $\mathbf{k}$ of the reciprocal lattice, also $-\mathbf{k}$ belongs to it.

Therefore, using Fourier transforms as such does not simplify the original lattice model by any mean; however, it is now easier to make physically meaningful approximations. If all the values of $s^z_{\mathbf{r}}$ were equal, then the r.h.s. of Eq. (B.7) would always be zero but for $\mathbf{k} = -\mathbf{k}'$. As already stated, we are considering small deviations from a fully-polarized state in z-direction, i.e. one has $s^z_{\mathbf{r}} = s$ for the overwhelming majority of lattice sites $\mathbf{r}$. If $\mathbf{k} \neq -\mathbf{k}'$ the commutator is therefore of $\mathcal{O}(1/N)$ and can be neglected for large N. In conclusion, we can write to a good approximation

$$\left[\tilde{S}^+_{\mathbf{k}}, \tilde{S}^-_{\mathbf{k}'}\right] = 2s\,\delta_{\mathbf{k},-\mathbf{k}'}. \tag{B.8}$$

The commutation relations of Eq. (B.6) and Eq. (B.8) resemble those of a set of bosons. We rename these operators to use the familiar notation for annihilation and creation operators

$$\begin{cases} a_{\mathbf{k}} \coloneqq \dfrac{\tilde{S}^+_{\mathbf{k}}}{\sqrt{2s}} \\ a^\dagger_{\mathbf{k}} \coloneqq \dfrac{\tilde{S}^-_{-\mathbf{k}}}{\sqrt{2s}}. \end{cases} \tag{B.9}$$

With the previous definition we conclude that the pairs of operators $\{\, a_{\mathbf{k}}, a^\dagger{}_{\mathbf{k}} \,\}_{\mathbf{k}}$ define a set of boson operators, including the particular case where $\mathbf{k} = \mathbf{0}$.

We now want to rewrite the Fourier transform components

$$\tilde{S}^\alpha_{\mathbf{k}} = \frac{1}{\sqrt{N}} \sum_{\mathbf{r}} e^{-i\mathbf{k}\cdot\mathbf{r}} s^\alpha_{\mathbf{r}} \tag{B.10}$$

in the framework of the spin-wave approximation. This can be done immediately for $\tilde{S}^x_{\mathbf{k}}$ and $\tilde{S}^y_{\mathbf{k}}$, given the usual expressions for the operators $s^x_{\mathbf{r}}, s^y_{\mathbf{r}}$ in terms of the raising and lowering operators $s^\pm_{\mathbf{r}}$:

$$\tilde{S}^x_{\mathbf{k}} = \frac{1}{2}(\tilde{S}^+_{\mathbf{k}} + \tilde{S}^-_{\mathbf{k}}) = \sqrt{s}\tilde{q}_{\mathbf{k}} \tag{B.11}$$

$$\tilde{S}^y_{\mathbf{k}} = \frac{1}{2i}(\tilde{S}^+_{\mathbf{k}} - \tilde{S}^-_{\mathbf{k}}) = \sqrt{s}\tilde{p}_{\mathbf{k}}, \tag{B.12}$$

where we defined the operators

$$\begin{cases} \tilde{q}_{\mathbf{k}} = \dfrac{a^\dagger_{-\mathbf{k}} + a_{\mathbf{k}}}{\sqrt{2}} \\ \tilde{p}_{\mathbf{k}} = i\dfrac{a^\dagger_{-\mathbf{k}} - a_{\mathbf{k}}}{\sqrt{2}}. \end{cases} \tag{B.13}$$

Thanks to the boson commutation relations, it immediately follows that the operators $\{\, \tilde{q}_{\mathbf{k}}, \tilde{p}_{-\mathbf{k}} \,\}_{\mathbf{k}}$ are pairs of canonical operators for every choice of $\mathbf{k}$ (included $\mathbf{k} = \mathbf{0}$):

$$[\tilde{q}_{\mathbf{k}}, \tilde{p}_{\mathbf{k}'}] = i\,\delta_{\mathbf{k},-\mathbf{k}'}. \tag{B.14}$$

However, it is important to observe that these operators are not hermitian, since $\tilde{q}^{\dagger}_{\mathbf{k}} = \tilde{q}_{-\mathbf{k}}$ and $\tilde{p}^{\dagger}_{\mathbf{k}} = \tilde{p}_{-\mathbf{k}}$.

We wish we could rewrite also the operators $\tilde{S}^{z}_{\mathbf{k}}$ in terms of these canonical operators in a straightforward way. This reduces to rewriting s_z as a simple function of $s_{\pm}$, the problem that we tackled in the beginning of the section. As promised, it is now apparent the advantage of this procedure, since it allows us to rewrite all the operators in terms of the conjugated variables $\{\, \tilde{q}_{\mathbf{k}}, \tilde{p}_{-\mathbf{k}} \,\}_{\mathbf{k}}$. We now make use of the Eq. (B.4), which implies the following (approximated) expression

$$\tilde{S}^{z}_{\mathbf{k}} = s\sqrt{N}\delta_{\mathbf{k},\mathbf{0}} - \frac{1}{\sqrt{N}} \sum_{\mathbf{r}} e^{-i\mathbf{k}\cdot\mathbf{r}} \frac{s^{-}_{\mathbf{r}} s^{+}_{\mathbf{r}}}{2s}. \tag{B.15}$$

By using the inverse of Eq. (B.5) and introducing the canonical operators in the expression above, one can check that

$$\tilde{S}^{z}_{\mathbf{k}} = s\sqrt{N}\delta_{\mathbf{k},\mathbf{0}} - \sum_{\mathbf{k}'} \frac{\tilde{q}_{\mathbf{k}'}\tilde{q}_{\mathbf{k}-\mathbf{k}'} + \tilde{p}_{\mathbf{k}'}\tilde{p}_{\mathbf{k}-\mathbf{k}'} - \delta_{\mathbf{k},\mathbf{0}}}{2\sqrt{N}}. \tag{B.16}$$

It might seem natural to define the number operators in the usual way

$$n_{\mathbf{k}} \coloneqq {a^{\dagger}}_{\mathbf{k}} a_{\mathbf{k}} \equiv \frac{\tilde{S}^{-}_{-\mathbf{k}}\tilde{S}^{+}_{\mathbf{k}}}{2s}, \tag{B.17}$$

but their expression in canonical coordinates

$$n_{\mathbf{k}} = \frac{1}{2}\left[\tilde{q}_{\mathbf{k}}\tilde{q}_{-\mathbf{k}} + \tilde{p}_{\mathbf{k}}\tilde{p}_{-\mathbf{k}} + i\left(\tilde{q}_{-\mathbf{k}}\tilde{p}_{\mathbf{k}} - \tilde{p}_{-\mathbf{k}}\tilde{q}_{\mathbf{k}}\right)\right] \tag{B.18}$$

would not be the usual simple expression for boson number operators.

Since the modes $\mathbf{k}$ and $-\mathbf{k}$ are coupled[3], it is appropriate to define the number operators as

$$n_{\mathbf{k}} \coloneqq \frac{1}{2}\left({a^{\dagger}}_{\mathbf{k}} a_{\mathbf{k}} + {a^{\dagger}}_{-\mathbf{k}} a_{-\mathbf{k}}\right) \equiv \frac{\tilde{S}^{-}_{-\mathbf{k}}\tilde{S}^{+}_{\mathbf{k}} + \tilde{S}^{-}_{\mathbf{k}}\tilde{S}^{+}_{-\mathbf{k}}}{4s}. \tag{B.19}$$

With this definition the usual expression holds

$$n_{\mathbf{k}} = \frac{1}{2}\left(\tilde{q}_{\mathbf{k}}\tilde{q}_{-\mathbf{k}} + \tilde{p}_{\mathbf{k}}\tilde{p}_{-\mathbf{k}} - 1\right), \tag{B.20}$$

moreover it is evident that $n_{\mathbf{k}} = n_{-\mathbf{k}}$. The physical meaning of this definition is that the operator $n_{\mathbf{k}} + n_{-\mathbf{k}} = 2n_{\mathbf{k}}$ correctly counts the excitations of the coupled modes $\mathbf{k}$ and $-\mathbf{k}$. From now on we shall always refer to the definition of $n_{\mathbf{k}}$ given in Eq. (B.19).

[3] Meaning that the operators with labels $\mathbf{k}$ and $-\mathbf{k}$ have non zero commutation relations.

We also define the total number of spin-wave excitations as

$$N_{\text{sw}} \coloneqq \sum_{\mathbf{k}\neq\mathbf{0}} n_{\mathbf{k}}, \tag{B.21}$$

while we remark that $n_{\mathbf{0}}$ is the number of excitations of the collective degree of freedom.

In conclusion, we managed to rewrite the Fourier operators $\tilde{S}^{\alpha}_{\mathbf{k}}$ in terms of the set of conjugated operators $\{\, \tilde{q}_{\mathbf{k}}, \tilde{p}_{-\mathbf{k}} \,\}_{\mathbf{k}}$, building on the physical assumption of describing a state close to the fully-polarized state along the z-direction. The result is given by

$$\begin{cases} \tilde{S}^{x}_{\mathbf{k}} = \sqrt{s}\tilde{q}_{\mathbf{k}} \\ \tilde{S}^{y}_{\mathbf{k}} = \sqrt{s}\tilde{p}_{\mathbf{k}} \\ \tilde{S}^{z}_{\mathbf{k}} = s\sqrt{N}\delta_{\mathbf{k},\mathbf{0}} - \displaystyle\sum_{\mathbf{k}'} \frac{\tilde{q}_{\mathbf{k}'}\tilde{q}_{\mathbf{k}-\mathbf{k}'} + \tilde{p}_{\mathbf{k}'}\tilde{p}_{\mathbf{k}-\mathbf{k}'} - \delta_{\mathbf{k},\mathbf{0}}}{2\sqrt{N}}. \end{cases} \tag{B.22}$$

We remark that this result relies on two approximations, precisely on the expression of s_z in terms of $s_{\pm}$ in Eq. (B.4) and on the approximate commutators in Eq. (B.8). The spin-wave theory is thus valid only if $s^{z}_{\mathbf{r}} = s$ for the majority of the sites and for big sizes N of the lattice.

Before concluding this section, it is extremely interesting to rewrite the total spin operator $\left|\vec{J}\right|^2$ and its projection along the z-direction J^z in terms of the spin-wave operators[4]. The equations Eq. (B.22) for $\mathbf{k} = \mathbf{0}$ immediately imply

$$\begin{cases} J^{x}_{\mathbf{0}} = \sqrt{Ns}\tilde{q}_{\mathbf{0}} \\ J^{y}_{\mathbf{0}} = \sqrt{Ns}\tilde{p}_{\mathbf{0}} \\ J^{z}_{\mathbf{0}} = Ns - \displaystyle\sum_{\mathbf{k}} n_{\mathbf{k}} = Ns - n_{\mathbf{0}} - N_{\text{sw}} \end{cases} \tag{B.23}$$

If $N_{\text{sw}} = 0$, these equations for the collective spin reduce to the Holstein–Primakoff approximation in Eq. (4.14)[5].

The result for $J^{z}_{\mathbf{0}}$ shows that both the spin waves and the excitations of the collective degree of freedom can lower the z-projection of the total spin. The total spin operator $\left|\vec{J}\right|^2$ can be written as:

$$\begin{aligned} \left|\vec{J}\right|^2 &= Ns(2n_{\mathbf{0}} + 1) + \left[Ns - \sum_{\mathbf{k}} n_{\mathbf{k}}\right]^2 = \\ &= (Ns)^2 + n^2_{\mathbf{0}} - 2(Ns - n_{\mathbf{0}})\sum_{\mathbf{k}\neq\mathbf{0}} n_{\mathbf{k}} + \left(\sum_{\mathbf{k}\neq\mathbf{0}} n_{\mathbf{k}}\right)^2 + Ns \end{aligned} \tag{B.24}$$

[4] Consistently with the definition adopted in previous chapters, we define the total spin operators as $J^{\alpha} = \sum_{\mathbf{r}} s^{\alpha}_{\mathbf{r}}$.

[5] The only difference being that here we consider only the maximum total spin sector $\rho = 1$.

Since $Ns \gg n_{\mathbf{0}}$ and $Ns \gg 1$, to a very good approximation one can ignore all the terms containing $n_{\mathbf{0}}$ in the last equation and also add 1 to Ns in the third term, obtaining:

$$\left|\vec{J}\right|^2 \approx (Ns)^2 - 2(Ns+1)\sum_{\mathbf{k}\neq\mathbf{0}} n_{\mathbf{k}} + \left(\sum_{\mathbf{k}\neq\mathbf{0}} n_{\mathbf{k}}\right)^2 + Ns. \tag{B.25}$$

The last line can eventually be rewritten as[6]

$$\left|\vec{J}\right|^2 = j(j+1), \tag{B.26}$$

where

$$j = Ns - \sum_{\mathbf{k}\neq\mathbf{0}} n_{\mathbf{k}} = Ns - N_{\mathrm{sw}}. \tag{B.27}$$

It is crucial to observe that the spin-wave excitations lower the value of the total spin $\left|\vec{J}\right|^2$, which is not a constant of motion anymore if $N_{\mathrm{sw}} \neq 0$. This is a major difference from the unperturbed LMG model (which is recovered for $N_{\mathrm{sw}} = 0$). On the other hand, the zero mode excitations do not lower the total spin magnitude.

In light of Eq. (B.23), the physical idea of describing small deviations from a fully-polarized state in z-direction can be reformulated as follows: the spin-wave approximation is valid only in the sector of the total Hilbert space in which $J^z_{\mathbf{0}} \approx Ns$, or equivalently for states with small excitations density[7]

$$\frac{\langle n_{\mathbf{0}}\rangle + \langle N_{\mathrm{sw}}\rangle}{Ns} \approx \frac{\langle N_{\mathrm{sw}}\rangle}{Ns} \ll 1. \tag{B.28}$$

This condition clearly implies through Eq. (B.27) that $j \approx Ns$.

Final remarks and possible improvements

It was already pointed out above that the whole spin-wave theory, and in particular the results in Eq. (B.22), rely on two approximations only: the expression of s_z in terms of $s_\pm$ in Eq. (B.4) and the approximate commutators in Eq. (B.8). The first approximation is indeed exact for $s = 1/2$, which is often the case of interest. Therefore, if one wanted to go beyond the spin-wave theory, then would probably have to think of a better approximation for the commutators in Eq. (B.7), with respect to the one of bosons in Eq. (B.8).

[6] We now write it as an equality, forgetting about the subextensive term that we dropped.

[7] The approximation holds only if the zero mode excitations $\langle n_{\mathbf{0}}\rangle$ are small compared to the total spin-wave excitations $\langle N_{\mathrm{sw}}\rangle$.

Another possible direction for working out a better approximation could be to systematically expand Eq. (4.42) to higher orders, so as to rewrite the model Hamiltonian expanded at n-th order in the canonical operators.

A successful treatment could allow to give a more general description of these quantum spin models, valid in a larger subspace of the total Hilbert space, and thus with broader applicability.

Bibliography

[1] M. A. Nielsen and I. L. Chuang. *Quantum Computation and Quantum Information: 10th Anniversary Edition.* Cambridge University Press, 2011.

[2] A. Lerose, J. Marino, B. Žunkovič, A. Gambassi, and A. Silva. Chaotic dynamical ferromagnetic phase induced by nonequilibrium quantum fluctuations. *Phys. Rev. Lett.*, 2018.

[3] A. Lerose, B. Žunkovič, J. Marino, A. Gambassi, and A. Silva. Impact of nonequilibrium fluctuations on prethermal dynamical phase transitions in long-range interacting spin chains. *Phys. Rev. B*, 2019.

[4] P. Deffner and S. Campbell. Quantum speed limits: from Heisenberg's uncertainty principle to optimal quantum control. *J. Phys. A: Math. Theor.*, 2017.

[5] T. Caneva, M. Murphy, T. Calarco, R. Fazio, S. Montangero, V. Giovannetti, and G. Santoro. Optimal control at the quantum speed limit. *Physical review letters*, 2009.

[6] I. Walmsley and H. Rabitz. Quantum physics under control. *Physics Today*, 2003.

[7] T. Caneva, T. Calarco, and S. Montangero. Chopped random-basis quantum optimization. *Phys. Rev. A*, 2011.

[8] T. Caneva, A. Silva, R. Fazio, S. Lloyd, T. Calarco, and S. Montangero. Complexity of controlling quantum many-body dynamics. *Phys. Rev. A*, 2014.

[9] P. Doria, T. Calarco, and S. Montangero. Optimal control technique for many-body quantum dynamics. *Phys. Rev. Lett.*, 2011.

[10] H. Lipkin, N. Meshkov, and A. Glick. Validity of many-body approximation methods for a solvable model. *Nucl. Phys.*, 1965.

[11] S. Sachdev. *Quantum phase transitions*. Cambridge University Press, 2011.

[12] A. Das, K. Sengupta, D. Sen, and B. K. Chakrabarti. Infinite-range Ising ferromagnet in a time-dependent transverse magnetic field: Quench and ac dynamics near the quantum critical point. *Phys. Rev. B*, 2006.

[13] J. Larson. Circuit QED scheme for the realization of the Lipkin-Meshkov-Glick model. *EPL (Europhysics Letters)*, 2010.

[14] B. Sciolla and G. Biroli. Dynamical transitions and quantum quenches in mean-field models. *Journal of Statistical Mechanics: Theory and Experiment*, 2011.

[15] R. Schubert, R. O. Vallejos, and F. Toscano. How do wave packets spread? Time evolution on Ehrenfest time scales. *Journal of Physics A: Mathematical and Theoretical*, 2012.

[16] Y. Huang, T. Li, and Z. Yin. Symmetry-breaking dynamics of the finite-size Lipkin-Meshkov-Glick model near ground state. *Phys. Rev. A*, 2018.

[17] B. Žunkovič, A. Silva, and M. Fabrizio. Dynamical phase transitions and Loschmidt echo in the infinite-range XY model. *Philosophical Transactions of the Royal Society A: Mathematical, Physical and Engineering Sciences*, 2016.

[18] T. Caneva, T. Calarco, R. Fazio, G. E. Santoro, and S. Montangero. Speeding up critical system dynamics through optimized evolution. *Phys. Rev. A*, 2011.

[19] T. Caneva, R. Fazio, and G. Santoro. Adiabatic quantum dynamics of the Lipkin-Meshkov-Glick model. *Phys. Rev. B*, 2008.

[20] S. Campbell, G. De Chiara, M. Paternostro, G. M. Palma, and R. Fazio. Shortcut to adiabaticity in the Lipkin-Meshkov-Glick model. *Phys. Rev. Lett.*, 2015.

[21] R. Storn and K. Price. Differential evolution – A simple and efficient heuristic for global optimization over continuous spaces. *Journal of Global Optimization*, 1997.

[22] J. Ma, X. Wang, C. P. Sun, and F. Nori. Quantum spin squeezing. *Physics Reports*, 2010.

[23] A. Lerose and S. Pappalardi. Logarithmic growth of entanglement entropy in out-of-equilibrium long-range systems. 2018.

[24] M. Bukov, A. G. R. Day, D. Sels, P. Weinberg, A. Polkovnikov, and P. Mehta. Reinforcement learning in different phases of quantum control. *Phys. Rev. X*, 2018.

[25] A. Perelomov. *Generalized Coherent States and Their Applications*. Springer, 1986.

[26] M. Combescure and D. Robert. *Coherent States and Applications in Mathematical Physics*. Springer, 2012.

[27] J. Schliemann. Coherent quantum dynamics: What fluctuations can tell. *Phys. Rev. A*, 2015.

[28] G.H. Wannier. *Statistical Physics*. Dover Publications, 1987.